Regulation of *Hydra* Regeneration by Hippo Pathway effector YAP and Biomechanical forces

A thesis

submitted in the partial fulfilment of requirements

of the degree of

Doctor of Philosophy

By

MANU K UNNI

20113147

INDIAN INSTITUTE OF SCIENCE EDUCATION AND RESEARCH PUNE

2020

Dedicated to my mother and father for their unconditional sacrifices, love and support.

Declaration

I declare that this written submission represents my ideas in my own words and where others' ideas have been included, I have adequately cited and referenced the original sources. I also declare that I have adhered to all principles of academic honesty and integrity and have not misrepresented or fabricated or falsified any idea/data/fact/source in my submission. I understand that violation of the above will be cause for disciplinary action by the Institute and can also evoke penal action from the sources which have thus not been properly cited or from whom proper permission has not been taken when needed.

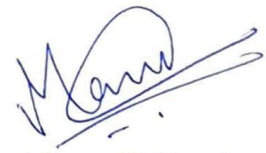

Manu K Unni
Roll No.: 20113147

Date: 06/03/2020

CERTIFICATE

Certified that the work incorporated in the thesis entitled "**Regulation of *Hydra* Regeneration by Hippo Pathway effector YAP and Biomechanical forces**" submitted by **Manu K Unni** was carried out by the candidate, under my supervision. The work presented here or any part of it has not been included in any other thesis submitted previously for the award of any degree or diploma from any other University or institution.

Prof. Sanjeev Galande
(Supervisor)

Date: 05 March 2020

Acknowledgements

Foremost, I would like to express my deepest gratitude to my supervisor, Prof. Sanjeev Galande, for being supportive, encouraging and motivating PhD mentor. His excitement for knowledge, science and life has been an inspiration to emulate. His patience, farsightedness and knowledge of doing science have been a constant source of education. I admire his ability to manage his time and responsibilities as a scientist and a common man meticulously. I am indebted to him for taking me from a place of self-doubt when I joined his lab to being a confident scientist who thinks nothing in science is impossible with a curious mind and the right will to find answers. I appreciate the freedom he has given me to pursue my own ideas and research without any boundaries. The fact that a good part of my PhD thesis is biomechanical study is a testament to his ability as a scientist who is fearless and confident in pursuing science, no matter where it leads to. Attention to detail, sense of urgency, a broader perspective about the research and collaborating with experts in fields rather than re-inventing the “wheel” are some of the important things I will take with me from him for my future endeavours. My time in the lab under his guidance has been truly edifying. I thank Sanjeev for the wonderful journey of PhD with all its ups and downs with him.

I would like to thank Dr Shivprasad Patil, who has been our collaborator for the biophysical studies, for sharing the interest in questions we were pursuing in our study. All the extensive discussions with him about how we approach the biomechanical problems by developing tools to address them helped me immensely in gaining a biophysical perspective towards my research. I admire his never-give-up attitude towards difficult problems and trying everything under the sun to tackle them.

I would like to thank Prof. Irit Sagi for taking keen interest in my research and giving me an opportunity to work in her laboratory at the Weizmann Institute of Science (WIS) in Israel for four months. My short stint in her laboratory was enough to inspire and convince me to continue my research as a postdoctoral fellow in her laboratory. I look forward to asking deeper questions about ECM regulation of tissue identity and function. I would like to thank Dr Inna Solomonov for being a wonderful mentor during my stint in WIS.

I would like to especially thank Dr PC Reddy (Mouli) for being an excellent mentor for me while I was taking my baby steps in the field of *Hydra* biology. His experimental and intellectual inputs have been invaluable for me in designing my study. I will miss our frequent deliberations on research problems, topics of mutual interest and personal problems. He has been a great support to me and I look forward to extend this camaraderie in the coming years.

I thank my RAC members, Dr LS Shashidhara and Dr Surendra Ghaskadbi (ARI, Pune) for their evaluations and invaluable suggestions. I would like to thank Dr Nagaraj Balasubramanian for helping me develop my interest in Cell-ECM interaction during my one year of research in his lab. I am grateful to Dr Suthirth Dey for convincing me to shift my research interest from plant biology to animal biology for my PhD (just for fun and experience). I am thankful to Dr Girish Ratnaparkhi as the Dean of Doctoral studies for keeping me on my toes and pursuading me to finish my PhD “faster”.

I would like to express my sincere thanks to IISER Pune for providing a healthy and excellent work atmosphere. I especially appreciate Prof. K.N. Ganesh and Prof. L.S. Shashidhara for being instrumental in creating such a stimulating ambience and enriching ecosystem and infrastructure at IISER Pune and especially the Biology Department. I would like to thank the current Director of IISER Pune, Dean Academics, Dean of Doctoral Studies and Chair of Biology Department for their extensive support during my tenure as a PhD student at IISER Pune. IISER Pune has helped me grow as a Scientist with an interdisciplinary outlook. Being in IISER Pune was not only scientifically enriching but also helped appreciate and develop my own taste in cultural and artistic nuances. Myriad of events hosted by SPICMACAY and many plays performed by SEA MINOR in IISER Pune will remain close to my heart. I would like to give a special mention to encouragement to sports and fitness in IISER Pune. I commend IISER Pune for developing a well-equipped gymnasium and a world-class Cricket ground. These have been extremely helpful to me when I felt the need to tap into my occasional sport and fitness drive. I am thankful to all the members of the Biohazard team (past and present) for giving me the happiness of being the part of the team to lift the IPL 2019 trophy.

I would like to thank UGC, EMBO, Infosys, DBT and IISER Pune for their generous funding at various stages during my PhD which ensured that I could sustain my research efforts without any financial crunch.

I am grateful to IISER Pune Biology, Chemistry and Physics departments for allowing me to access and use their resources. I am thankful to the entire IISER Pune administration and support staff for making my life during my PhD easier without worrying too much about things unrelated to my research. I would like to thank IISER Pune microscopy facility for providing state-of-art microscopy facilities. I would like to thank Dr Mahesh and Dr Sagar for their help with animal experiments. I would extend my heartfelt thanks especially Santosh, Piyush, Kalpesh, Mrinalini, Shabnam, Roopali, Vipradas sir, Vijay, Nilesh Dumbre, Tushar Kurulkar, Anil Jadhav, Sayalee & Kailash Kolhe for their help and support. I thank APT Testing and Research Pvt Ltd (National Toxicology Center) staffs for helping me with developing antibodies for my study. I wish to thank the support staff and electron microscopy staff of the Weizmann Institute of Science for all their help and support.

I would like to express my sincere thanks to all SG lab members (past and present) for all their support and help. I am lucky to have such a vibrant, critical, intelligent and friendly colleagues who have helped me grow as a person. The ‘unity in diversity’ is the motto of the lab where people studying different questions in different organisms work together as a unit to realise Sanjeev’s vision for research under the broad theme of epigenetic regulation. I am grateful to Suyash Naik, my first BS-MS mentee, for his contributions in developing the AFM technique to probe tissue stiffness in *Hydra*. He has made us all proud with his dedication to research and progress in his career. I wish him a highly successful career ahead. I am thankful to all the other trainees who have worked with me for their contributions- Jitesh Seth, Ameya Pore, Mrinmoy Pal, Rachel Paul, Gunjan Misri and Arkajyoti. I would like to especially thank rest of our Hydra Group (past and present) for being an amazing unit to help develop *Hydra* into a truly important model system to study various developmental processes- Mouli, Akhila, Aniruddh, Pallavi, Sudipta, Suyog, Indu & Neha.

I am thankful to the seniors in the SG laboratory for being so supportive and helpful with easing into a large lab like ours- Praveena, Kamal, Sunita, Rahul, Rini and

Rafeeq. They made a very joyful environment in the lab. I would like to acknowledge Praveena, Rafeeq, Rahul and Rini for their constant quizzing regarding the reasoning behind the experiments and techniques we routinely performed. Rafeeq and Rahul's energy and dedication to work were really overwhelming and inspirational. I cherish my long scientific discussions with Rafeeq over our common and not-so-common for others' topics. I extend my special thanks to Indu for being a good friend and for all the help she has given me over the years. I wish her successful postdoctoral research. I have been a troublemaker in the lab and have been notorious for my pranks. I am thankful to all the SG lab members for being sportive and patient about it; especially Sneha, Ankita, Jasmine, Ankitha, Rutika, Sapana, Akhila, Saurabh, Aniruddh, Ayush, Indu, Suyash, Greg and Rini. I would like to acknowledge the Postdoctoral fellows in our lab for their valuable suggestions and inputs- Dr Manjunath, Dr Ashwin, Dr Satya, Dr Ameya, Dr Poornima, Dr Vijay and Dr Ram. I would also like to thanks the rest of the SG lab members who have made my stay in the lab pleasant and joyful- Dr Sonam, Dr Anjali, Dr Farhat, Dr Smitha, Dr Sneha, Neha Oli, Priyanka, Soumitra, Ketakee, Nazneen, Keshav, Rahul Biradar, Devika, Prateek, Pavana, Aditi, Dr Amit, Dr Ajay and many more whom all I couldn't enlist here. I would also like to thank KK lab for their help and making our shared laboratory space enjoyable. I would especially thank Mukul and Abhishesk from KK lab for being good friends.

It gives me immense pleasure in thanking my dear friends Shrikanth, Mahendra, Sajilesh, Mikhail, Pallavi, Sneha, Trishna, Girish, Ruchira, Tushar, Aritro, Vidya and Rahul who made sure I had a real life outside IISER as well. I acknowledge all my teachers who have taught me different things to me at various stages of my life and instilling in me the values of patience, trust and knowledge which were instrumental in making me who I am today.

I am indebted to my loving family without whose support I wouldn't have been able to do my research. I am lucky to have their unconditional love and prayer. Above all, their faith and confidence in me have enabled me to do things which I never could have done without. I acknowledge my mother for all the sacrifices she has done for my upbringing. I owe my love for science and curiosity to my parents who always encouraged me to ask questions. I also acknowledge my father in being instrumental to drive my interest in science by giving me the right exposure at the right time which

included exsposing me to various science magazines, science toys and building science projects together etc. I am thankful to my loving brother for his support and being there for my parents when I was not around. My family is my strength and hope they (both present and future) will always keep me going for my future endeavours with all their blessings.

Manu K Unni

Table of Contents

Abstract

Hydra is a freshwater polyp belonging to the phylum Cnidaria. These polyps are known to exhibit tremendous regenerating potential. It is still unclear how the regenerating tissue is reorganized, how the complex interplay of signaling cascades required for generating positional information in regenerating tissue is produced and regulated. Specifically, the question of how biophysical forces govern the regeneration process by integrating early injury response with positional cues has been a subject of intense research in recent times in regenerative model organisms, including Zebrafish and Axolotl. Owing to the simple tissue organization and the well-characterized morphallactic regenerative biochemical signaling pathways, *Hydra* provides an ideal system for developing a model system to study biomechanical regulation. In this study, we employed the paradigm of head regeneration in *Hydra* to understand how tissue damage invokes changes in tissue mechanics and how the mechanical forces can affect the regenerative response. Hippo signalling is a well-known pathway for mechanotransduction in cells. In this study, we report for the first time the existence of a complete repertoire of the Hippo pathway core components in *Hydra.* By staining Hippo effector YAP during head regeneration, we report that mechanosensitive (YAP positive) cells migrate to the site of injury early during regeneration. We show that by disrupting the Hippo pathway by the perturbation of the interaction of YAP (a transcription co-activator) and its cognate transcription factor TEAD, we can accelerate the regeneration in *Hydra*. Further, scanning electron microscopy (SEM) based evaluation of the ultrastructure demonstrated an extensive fibrosis-like condition of the extracellular matrix (ECM) in regenerating tips of *Hydra* upon YAP-TEAD disruption.

We then characterized the role of ECM structure and tissue stiffness in regulating regeneration in *Hydra*. Towards this, using Atomic Force Microscopy (AFM) to measure the Young's modulus of *Hydra* body column, we show that tissue stiffness is tightly regulated during head regeneration. We also demonstrate that the fibrotic condition upon YAP-TEAD disruption causes a drastic increase in tissue stiffness. Using a combination of biochemical inhibition as well as ultrastructural studies using SEM, we show that tissue stiffness is a function of fibrillar collagen deposition and

cross-linking frequency in the ECM (referred to as mesoglea). Observations from this study argue in favor of the role of a hypothetical tissue stiffness threshold in the regulation of *Hydra* head regeneration. In support of this argument, perturbations leading to lowering the tissue stiffness during regeneration inhibit regeneration in *Hydra* while perturbation leading to an increase in tissue stiffness above the threshold lead to an enhanced regenerative response in *Hydra.*

Next, we focussed on understanding the alterations in gene expression patterns during regeneration and the role of YAP-TEAD interaction towards the same. Transcriptomic analysis of regenerating *Hydra* under inhibition of YAP-TEAD interaction revealed upregulation of pro-fibrotic genes and early activation of crucial developmental signalling pathways. More importantly, we find that β-catenin transcriptional targets such as Brachyury (*bra)* are upregulated earlier than the *wnt(s).* This study convincingly demonstrates that YAP is an important player in the regulation of regeneration in *Hydra*, having the capability of modulating fibrosis induced stiffness and integrating the resulting mechanical changes to the cross-talk with β-catenin to activate its potential as a head organizer for initiating the downstream regenerative programme needed for oral fate determination. Taken together, this study not only provides a therapeutic window to enhance the regenerative response in higher model systems without genetic modifications but also predicts an interesting prospect of β-catenin. Rather than the currently implicated WNT being the head organizer molecule, our study suggests that β -catenin acts as the head organizing factor which can be activated by a simultaneous WNT-independent mechanical stimulus and WNT-dependent signalling.

1 INTRODUCTION

1.1 HISTORY OF REGENERATION

Humans have been fascinated by the phenomenon of regeneration from ancient times. There was a mention about the regeneration of liver in Greek mythology when Prometheus was punished for bringing the gift of fire to humanity. His punishment entailed him being tied to a rock and his liver being fed upon every day by an eagle since his liver would grow back. However, the scientific community took an active interest in studying regeneration only in the early 18th century when French scientist René-Antoine Ferchault de Réaumur reported regeneration in crayfish and certain other arthropods. A few years later, Abraham Trembley discovered the regeneration in *Hydra* in 1744[1]. Later, Lazzaro Spallanzani carried out detailed regeneration studies in vertebrates such as newt and tadpoles and documented various internal and external factors affecting regeneration process. Regeneration studies later fell out of interest and were briefly renewed by Thomas Hunt in the late 19th century only to go out of favour again due to lack of tools to study the phenomenon. However, since last 40-50 years due to emergence of multiple model organisms such as *Hydra*, *Planaria*, *Drosophila*, *Xenopus*, Axolotls, Mice and availability of modern genetic analysis and modification tools have renewed and restored the interest of the scientific community in trying study regeneration at more closely. Thus, accelerating the understanding of underlying cellular and molecular mechanism involved in regeneration.

1.2 WHAT IS REGENERATION

Regeneration is the process of repair and restoration of lost or damaged cells, tissues or organs. There are different modes and strategies of regeneration which can be observed across phyla and is present in one or the other form in every organism. Regeneration potential varies according to the stage of the life cycle and also the age of the organism. This variability in regenerative potential is not only seen among different phyla or class but also among different tissues of the same organism has long puzzled the scientific community. Hence, essential questions in this field pertain to what is the biological and evolutionary reason for this diversity or

multi-faceted “ness”. The figure below depicts the underlying mechanism of regeneration in any given mode of regeneration. All the events depicted may or may not co-occur in a given organism.

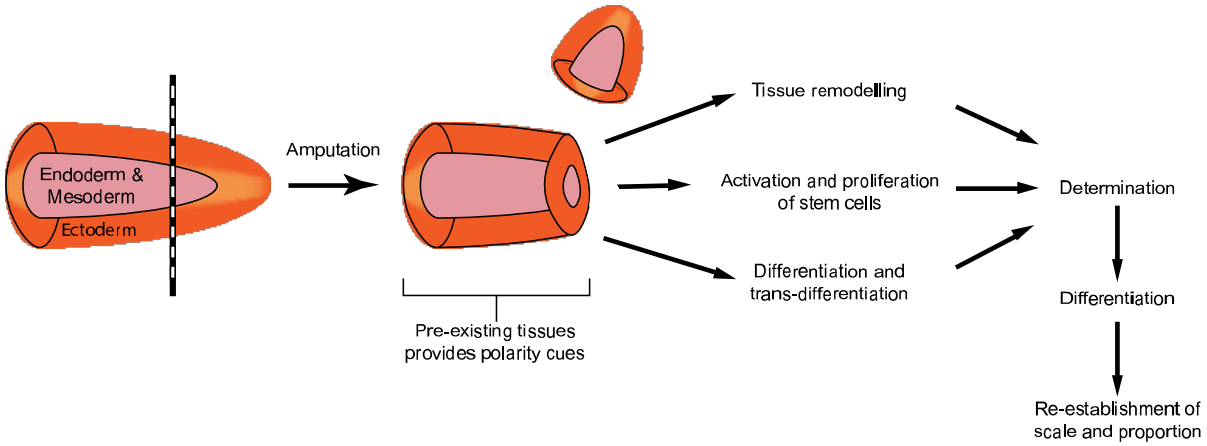

Figure 1.1: Basic mechanism of regeneration. After amputation, all the organisms undergo wound healing as the first stage of regeneration. Then, tissue polarity is set using pre-existing cues. This is then followed by three different paths, which may or may not occur in the same organism. This mainly involves tissue remodelling, trans-differentiation, de-differentiation and/or activation and proliferation of stem cells. After this, all of them usually culminates in re-establishment of the lost tissue or organ at the required scale and proportion. *(Adapted from Alvarado and Tsonis, 2006).*

Regeneration has various physiological roles in organisms too. It helps in maintaining cellular turnover in some animals, avoid predation or help in asexual propagation. The efficiency of an organism to regenerate is also dependent on its ability to maintain a specific pool of stem cells ready to respond to injury signals and replace the lost tissue by proliferation and differentiation. Hence organisms like *Hydra* and *Planaria* are well adept at regenerating lost tissue than other organisms such as *Human* or *mouse*. These observations indicate the probability of evolution of terminally differentiated cells required for achieving complexity in cell types but at the cost of regenerative capability. In these more complex organisms, the injury response often leads to scarring instead of complete replacement of lost tissue. Scarring is a process whereby an injury response includes heightened immune response followed by a rapid closure of the wound by keratinocytes. Recruitment of specific fibroblasts to the site follows which laydown fibrillar collagen for support and structure. In normal tissues, the collagen network is laid down in a reticulate, but during scarring, specific fibroblasts lay down collagens cross-linked in such a way

that they unidirectional and parallel[2]. Such a process leads to a rapid wound healing and fibrosis but with a stiffer yet weaker tissue structure.

1.3 WHY STUDY REGENERATION

Worldwide, approximately 20-50 million people get injured or disabled annually due to road accidents alone. In India alone, there are 20,000-25,000 annual cases of amputations. Concurrently, there is a need for about 10 million organ transplants annually worldwide, and out of this, presently only 10% requirement is met. Humans have a limited ability to regenerate their damaged or dysfunctional tissues. Acquiring the ability to regenerate has been a long-sought dream of humanity. A healthy human adult can only regenerate some organs like skin, liver and blood cells. Most of the natural attempt to regenerate tissue in humans leads to scarring which changes tissue characteristics irreversibly. The scarring is seen as a significant deterrent to perfect regeneration of tissues in most of the complex organisms.

Interestingly, it has been observed in many organisms in their neo-natal stages, including humans, that they can undergo regeneration in some tissues without any scarring. Human neonates have been reported to regenerate wounded skin and amputated phalanges without and scars. These raise the tantalising possibility that humans do have the necessary signalling networks to accomplish scar-free healing and possibly loses or blocks it in favour of attaining cellular complexity. Hence by studying various facets of regeneration will help unlock this missing link in our capability and understanding the phenomenon of regeneration in humans.

1.3.1 Problems and drawback of studying regeneration

Despite a plethora of attempts at studying regeneration, we are still a long way from completely understanding the process to the extent of having the ability to emulate scar-free healing or regeneration in humans. There are multiple reasons for this inability. Regeneration study is inherently a multi-disciplinary science. Hence, lacunae in knowledge present in fields required for studying regeneration will affect our ability to understand the process effectively. For example, lack of clear understanding of lineage differentiation of cells, need for more understanding of how cell-niche/microenvironment interaction regulates cell fate and function, need for

better bio-compatible biomaterials for supporting the tissue engineering, deeper understanding of mechano-regulation of cells etc.

1.3.2 Why study non-model organisms for regeneration

Owing to the ethical issues and the fact that not all tissues in neonates heal scar-free makes studying human embryos very difficult. Additionally, many of these problems mentioned above in studying regeneration arise due to the apparent complexity of the signalling processes involved in the regeneration of the mammalian model systems. Such problems can be alleviated by answering specific problems in a more minimalistic or simpler 'non-model' organisms where there are less redundancies or cross-talks in the pathways involved. On the same lines, researchers have been studying regeneration in organisms such as *Hydra, Planaria, Axolotls, Zebrafishes.* These studies have yielded many new insights into the regeneration process which wouldn't have been otherwise possible.

1.4 *HYDRA*

Among the 'non-model' organisms, *Hydra* is a very unique system to study regeneration. *Hydra* is a freshwater living organism and belongs to the class Hydrozoa of phylum Cnidaria[3, 4]. Cnidaria is a sister group to Bilateria and an early divergent phylum comprising multicellular animals with the tissue-level organization (Fig. 1.2 A). Members of the phylum are radially symmetrical and evolved with two germ layers. Animals from this phylum share bilaterian cell types such as neurons and muscular epithelial cells (Fig. 1.2 B). These properties have positioned the members of this phylum as favourite models to understand the molecular evolution determining organized body plan and evolution of cell types conserved in Bilateria.

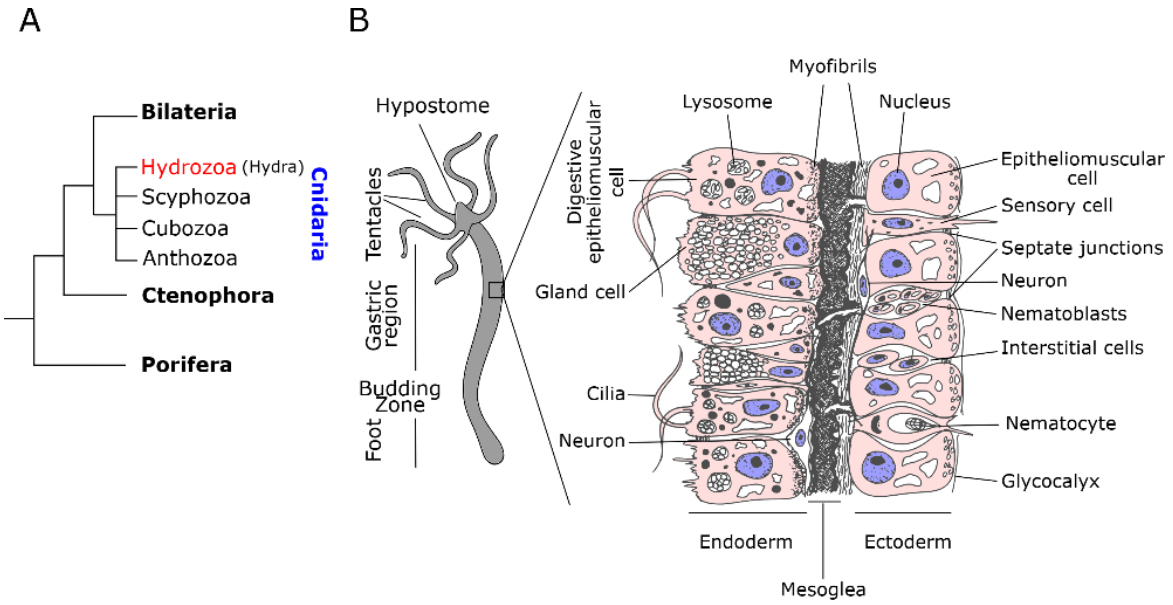

Figure 1.2: Phylogenetic position of *Hydra* and general morphology. A) Phylogenetic relation of basal metazoans and different classes of phylum Cnidaria with *Hydra* being a representative member of class Hydrozoa. **B)** The general body plan of *Hydra* (left) and histology cartoon depiction with the two germ layers and cell types typically seen in *Hydra*. (Reproduced from Reddy et al.,2019[5]).

Hydra is a diploblast possessing two layers of the cells which form a cylindrical body containing a gastric lumen. These polyps are among the earliest animals to have evolved a defined body plan and have an oral-aboral axis with the oral end consists of a dome-shaped hypostome (mouth) being surrounded by a ring of 5-6 tentacles which help them in feeding. The body column of a polyp can be divided into a gastric region, a budding region and a peduncle region. The aboral end of the polyp is called basal disk, which can secrete mucus that helps in the attachment of *Hydra* to various substrates[6]. As seen in Figure 1B, the cell layers are mainly constituted of epithelial cells with either ectodermal or endodermal stem cell origin. The epithelial cells have myofibrils at the base, due to which they are called as epitheliomuscular cells[7]. These myofibrils are oriented perpendicular to each other in ectoderm and endoderm. This organization of myofibrils helps in contraction or elongation of the polyp[8]. Endodermal cells are ciliated and have phagocytic capabilities while the ectodermal cells secrete a glycocalyx layer on the outermost side of the cells to protect the polyp from the environment[7]. Apart from epithelial cells, *Hydra* also possesses multipotent interstitial stem cells located in the interstitial spaces of epithelial cells. These stem cells differentiate into cells with unique functions such as gland cells, mucous cells, neuronal cells, nematocytes and gametes (oocytes or

sperms)[9]. The ectoderm and endoderm are divided by an acellular mesoglea which is essentially the extracellular matrix (ECM)[10].

1.5 Regeneration In *Hydra*

Hydra can regenerate missing body parts upon transverse or longitudinal amputation (Fig. 1.3 A). The *Hydra* polyps are also capable of regenerating from re-aggregated cells. These polyps, when dissociated into single cells, can reorganize and regenerate into a whole polyp when these cells are pelleted (Fig. 1.3 B). The cells reorganize into a lumen within first 12 h with ectodermal cells outside and endodermal cells facing inside the lumen[11, 12]. This reorganization (possibly) arises from differential cell adhesion between ectodermal and endodermal cells[11]. This process is followed by the establishment of head organizer *de novo* within 18-30 h (Figure 1.2 C)[13]. The first appearance of the head and tentacle structures can be seen by 48-72 h and finally, the whole adult *Hydra* body forms within 4 to 7 days[11].

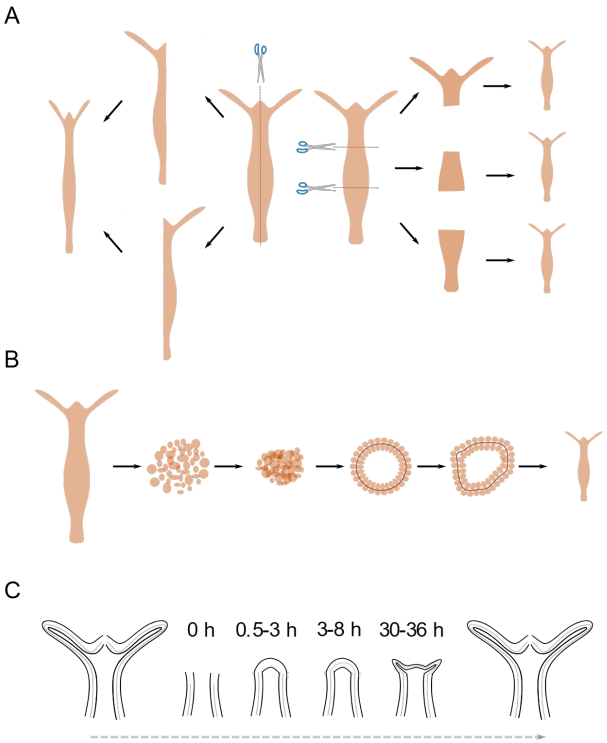

Figure 1.3: Regeneration capacity of *Hydra vulgaris.* The ability of *Hydra* to regenerate when dissected in various manners and the morphological changes observed are shown. **A)** *Hydra* can regenerate missing parts upon both transverse and longitudinal dissection in a morphallactic manner. **B)** *Hydra* can regenerate even after being dissociated into a single-cell suspension if the

cells are reaggregated and allowed to self-reorganize. **C)** Kinetics of gross morphological changes during *Hydra* head regeneration. (Reproduced from Reddy et al.,2019[5])

During regeneration, the site of injury responds by re-organization of the epithelial cells to close the wound within an hour. This is then followed by a lack of any gross morphological changes until 30 hrs post-amputation. After 30-36 h, small tentacle buds begin to emerge from the regenerating tip beginning the process of morphological differentiation of cells. The emergence of the tentacles happens over the next 24 h with the completion of the whole process taking place by 72 h, where the tentacles are mature enough to catch the prey. On the other hand, basal disk regeneration is completed within 30-36 h[6]. During regeneration wound healing is the initial step towards the morphological changes leading to major cellular reorganisation. This requires remodelling of ECM to facilitate tissue morphogenesis.

1.6 CELLULAR BASIS OF REGENERATION

Regeneration in animals can be either for homeostatic cell replacement like the replacement of blood cells or reparative replacement wherein a damaged tissue or organ needs to be regenerated. Regeneration can be broadly divided into two types:

a) Epimorphosis is a type of regeneration involving active cell proliferation for the completion of regeneration. This process can further be divided into two types, i.e., blastema-mediated or compensatory regeneration. In blastema-mediated regeneration, repair of lost tissue or organ proceeds by recruitment of either pre-existing progenitor cells in the vicinity of the injury or by de-differentiation of differentiated cells from the vicinity. These cells then start proliferating to form a mass of heterogeneous undifferentiated cells at the regenerating tip called a blastema. Once a specified number of cells are amassed, the cells in blastema start to differentiate and initiate the process of morphogenesis. This process then culminates with the restoration of the lost tissue either entirely or partially depending upon the organism, e.g. planaria, axolotls etc.[14]. In the compensatory regeneration, the regeneration proceeds without any blastema formation or requirement of stem cells. In this process, differentiated cells from the vicinity are recruited to the site of injury and

proliferate to replace the lost tissue. Liver regeneration is a prime example of compensatory regeneration[15].

b) Morphallaxis is a type of regeneration hallmarked by the absence of cellular proliferation. The existing tissue is re-patterned to replace the lost tissue. This kind of regeneration is frequently observed in lower invertebrate organisms such as *Hydra*[16, 17].

Epimorphic type of regeneration is the most prevalent type of regeneration across the animal kingdom. It would be wrong to assume dividing cells as the sole contributors towards the new tissue during regeneration. There exist possibilities of contribution from trans-differentiated and de-differentiated cells which might contribute to a new population of dividing and differentiating cells[18]. Hence to understand how regeneration process is regulated, it becomes important to dissect the origins of cells involved as a source of new cells required for regeneration upon specific injury signals. In planaria, multiple studies have shown that a continuously dividing population of cells called neoblasts contribute to the formation of new tissue[19]. These cells are clonal and pluripotent in nature; have the capability to rescue regeneration deficit planarians to regenerate with as few as 3-5 cells[20]. These clonogenic neoblasts are recruited to the site of injury where they proliferate into a mass of undifferentiated cells to form a blastema. The blastema cells then undergo a differentiation process for patterning the lost tissue[19]. In vertebrate systems, blastema formation doesn't consist entirely of one type of clonogenic pluripotent cells like the neoblasts. There seems to have a pre-determined heterogeneous group of cells having unipotent or multipotent capabilities. For example, in *Xenopus*, the muscle regeneration is solely dependent on the dormant population of satellite cells found adjacent to the muscle fibres[21]. These are the muscle stem cells which upon activation, differentiate into muscle fibres. In axolotls, it was shown using lineage-tracing experiments that muscular satellite cells and Schwann cells are found to be unipotent and were responsible for muscular and Schwann cells respectively; while, dermis cells of mesodermal origin contribute to a diverse repertoire of cartilage and connective tissues[22]. In the zebrafish caudal fin regeneration model, it was shown that most of the cell types required for regenerating the fin were derived from specific unipotent progenitors and the same is the case during the fin development during embryogenesis[23].

In *Hydra*, regeneration is manifested in two different modes depending on the region of amputation. Any amputation away from the mid-gastric region will exhibit a morphallactic mode of regeneration. In this mode, the wounded tissue undergoes wound healing by bringing together the ectodermal and endodermal cells which are initiated by the endodermal cells from the severed edge in a fashion similar to blastopore closure[24]. This is then followed by cellular re-arrangements and differentiation required for regeneration without any proliferation. It has also been reported that there is no involvement of interstitial stem cells or their derivatives towards the regeneration process and hence only requiring epithelial stem cells for the whole process[25]. On the other hand, it was reported that head regeneration after a mid-gastric cut proceeds through a process similar to the epimorphosis[26]. Upon amputation, there are detectable levels of activation of the apoptotic pathway in interstitial cells such as neurons, nematocytes etc. present near the area of injury. These cells start secreting Wnt3a in a yet unknown manner. These molecules of Wnt ligand then activate the Wnt signalling in nearby interstitial stem cells and induce them to do compensatory cell proliferation. This proliferation, however, does not form a very large mass of cells like in blastema. Simultaneously, the epithelial stem cells which are located at the apical end starts secreting Wnt3a and assume the role of head organizer after which follows the process of regeneration as seen in morphallactic regeneration[27].

Several studies have shown in *Hydra* that certain strains of *Hydra* do not exhibit any signs of ageing or senescence while other strains can be induced to senesce upon induction of gametes[28, 29]. The immortality in *Hydra* is attributed to the ability of *Hydra* to maintain a steady-state of shedding of cells and cell proliferation. The stem cells in the body column divide continuously either to replenish themselves or differentiate into specialized cells. The epithelial cells divide roughly every 3-4 days, and interstitial cells divide every 1.5 days[28]. These cells produce differentiated cells which are pushed to either end of the body column and are sloughed off. The differentiated cells proceed to move towards their destination, depending on the origin of the cells. They move to the basal disk if the cells originate from the peduncle region, the tentacles if they originate from the region just below the tentacle ring or are pushed to form new bud if the cells originate from the region above the budding region and below the tentacle ring. The cells moving towards their respective destinations have

a variable rate of movement depending on their position. Cells at the base of the tentacles take an average of 4 days to reach the tip and being pushed off. The cells at the base of the hypostome and at the peduncle reach their respective destination in 20 days. The cells in the body column require about 2-8 days to reach the budding zone and bud depending on their position (Fig. 4)[30]. In conclusion, it is evident that specific cell types play an important role in regeneration and tissue homeostasis.

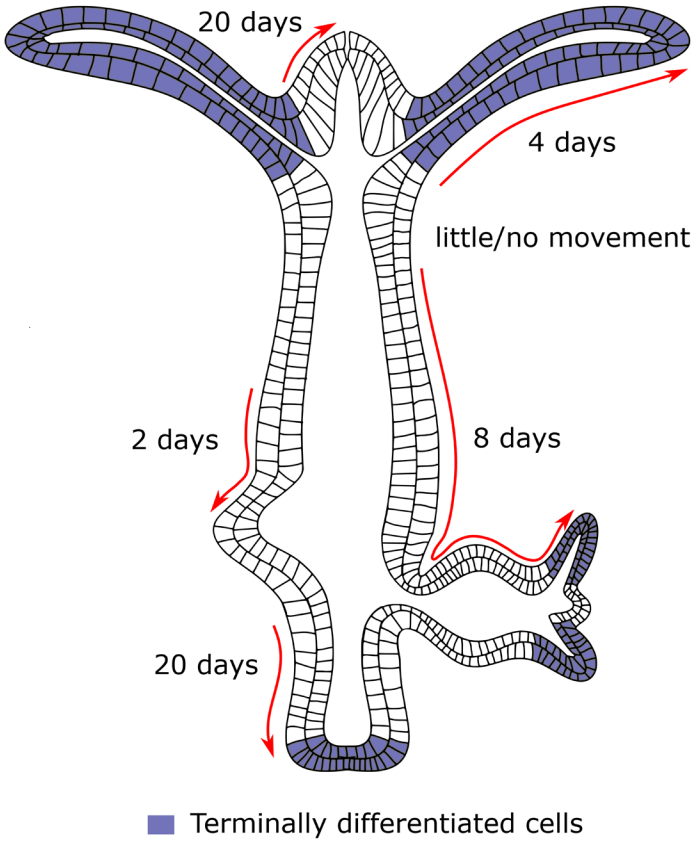

Figure 1.4: Cellular dynamics in *Hydra*. The various cell movements that take place during maintenance of the *Hydra* body plan are depicted here. Cells undergo continuous proliferation and movement in both directions along the oral-aboral axis. The empty cells denote proliferative cells, and the blue coloured cells are terminally differentiated. The number of days taken by the cells to reach their respective destinations such as buds or the hypostome and peduncle termini is shown. The arrows depict the direction of the cell movements. (Reproduced from Reddy et al., 2019 [5]).

1.7 SIGNALLING PATHWAYS INVOLVED IN *HYDRA* REGENERATION

Regeneration requires a concerted regulation of multiple cells and tissue types. For such a synergistic process to occur, there requires tightly regulated cell-

cell communication. There are eight developmentally essential signalling pathways known to exist in the metazoans - Wnt/Wingless (Wg), transforming growth factor-β (TGF-β)/BMPs, Notch, Receptor tyrosine kinase (RTK), Hedgehog (Hh), JAK-STAT [signal transducers and activators of transcription] pathway), nucleic acid receptor/hormone receptor-mediated signalling and Hippo pathway[31]. The molecular players of these pathways are spatio-temporally regulated for body axis establishment and symmetry breaking related function during embryonic development. Since regeneration involves morphogenesis to regain lost tissues, the pathways used to regulate cell-cell signalling during the embryonic development process are co-opted for the regeneration process.

In *Hydra*, Wnt signalling has been ascribed to contribute towards the head organizer function[32]. Wnt ligands are secreted by select cells and act as a function of their diffusion coefficient and ability of cells to express Wnt specific receptors on the cell membrane. This property of Wnt ligands hence is important for establishing anterio-posterior axis during organismal development in both embryos as well as newly developing buds. Similarly, Wnt signalling is crucial in regenerating amputated head in a *Hydra*[33]. Similar to Wnt ligands, ligands of TGF-β superfamily are also secreted molecules. TGF-β superfamily of signalling pathway contains many important players reported to be crucial in *Hydra* development. For example, BMP5-8 homolog in *Hydra* has been reported to be important for tentacle and foot formation during regeneration [34]. Nodal signalling has been shown to facilitate head organizer activity for new body axis to form a new bud from the parent *Hydra* body column by breaking the radial symmetry[35]. The TGF-β antagonisers have also been shown to be crucial for regulating head organizer function. Gremlin and Chordin-like proteins in *Hydra* have been shown to regulate head formation during regeneration and budding in *Hydra*[36, 37]. Members of the RTK family – VEGF and FGF have also been reported to be involved in regulating regeneration in *Hydra*[38]. The remaining two secretory/ long-range developmental pathways – JAK-SAT and Hedgehog signalling pathways are yet to be reported in *Hydra*.

The above-mentioned long-range morphogens are then further modulated and fine-tuned using other short-ranged signalling pathways. One among them is the Notch signalling which is a juxtacrine signalling system. The membrane-associated Notch ligands like Serrate/Jagged and Delta from one cell interact and associate with

the membrane-associated Notch receptors[39]. This module of signalling has been reported to be involved in head organizer activity, boundary formation and maintenance in *Hydra*. It has been shown that the Notch signalling is required for maintaining defined zone for Hypostome and tentacle zone possibly by using the lateral inhibition function through the balance of cis-trans interaction of Notch ligand and receptors[39, 40]. This boundary formation function has been indicated to modulate the ability of nearby cells to respond differently to the Wnt signalling, which comprise head organizer unit in *Hydra*. Similarly, another member of RTK signalling family, the Ephrin signalling system has also been reported to be involved in juxtacrine signalling during regeneration. Ephrin receptor HyEph1 has been reported to be upregulated later during regeneration (24 hpa) and suspected to aid Wnt and Notch signalling for boundary formation between the tentacles and the hypostome[41]. Another short-ranged pathway – The Hippo pathway is yet to be reported in *Hydra*.

The role of epigenetic cues and mechanical constraints in influencing the organismal development has recently gained traction among research communities. Mechanical forces can be transformed by cells into biochemical signals in a process called mechanotransduction[42]. Parameters like cell shape, ability to spread on the extracellular matrix and stiffness of the cell environment can directly govern cell differentiation and proliferation rate[43]. Recent experimental studies have begun to elucidate roles for mechanotransduction in regeneration and embryonic development, such as regulation of gene expression, pattern formation, and organogenesis[44-47]. In *Drosophila*, external mechanical stress-induced the key mesoderm determinant *twist*, whereas in zebrafish, mechanical stress-induced expression of brachyury, which is crucial for mesoderm development in all vertebrates[48]. Notably, in both organisms, this mechanically induced gene expression is dependent on β-catenin. In Nematostella, β-Catenin-dependent mechanism of mechanotransduction has also been reported to act through brachyury[49]. However, it is unclear till now how the mechanical changes are linked to Wnt signalling. One of the major player to emerge as this link is the Hippo pathway. Hippo pathway is a very important developmental pathway since it can modulate cellular and tissue morphology based on mechanical changes happening in the extracellular environment[50]. However, the role of the Hippo pathway in regulating the

cellular division makes it very difficult to study what their role is in the regenerative process since regeneration is linked to both cell differentiation and proliferation.

In this study, we have chosen *Hydra* to study the mechano-regulation in regeneration and how Hippo effector protein YAP acts as a mediator of change in mechanical forces and cellular response to amputation or injury. Head regeneration in *Hydra* exhibits the morphallactic form of regeneration and hence can be de-linked to the cell-proliferative properties of the Hippo pathway. This property, along with the ease of maintaining *Hydra* as well as its robust regenerative capability makes *Hydra* an ideal model system to be developed to undertake such a biomechanical study.

1.8 REFERENCES

1. Dinsmore, C.E. *A history of regeneration research: milestones in the evolution of a science*. (Cambridge University Press, 1991).
2. Ehrlich, H.P. & Krummel, T.M. Regulation of wound healing from a connective tissue perspective. *Wound repair and regeneration* **4**, 203-210 (1996).
3. Marques, A.C. & Collins, A.G. Cladistic analysis of Medusozoa and cnidarian evolution. *Invertebrate Biology* **123**, 23-42 (2004).
4. Campbell, R.D. A new species of Hydra (Cnidaria: Hydrozoa) from North America with comments on species clusters within the genus. *Zoological Journal of the Linnean Society* **91**, 253-263 (1987).
5. Reddy, P.C., Gungi, A. & Unni, M. Cellular and Molecular Mechanisms of Hydra Regeneration, in *Evo-Devo: Non-model Species in Cell and Developmental Biology* 259-290 (Springer, 2019).
6. Hoffmeister, S. & Schaller, H.C. A new biochemical marker for foot-specific cell differentiation in hydra. *Wilhelm Roux's archives of developmental biology* **194**, 453-461 (1985).
7. Hess, A., Cohen, A. & ROBSON, E.A. Observations on the structure of Hydra as seen with the electron and light microscopes. *Journal of Cell Science* **3**, 315-326 (1957).
8. Passano, L. & McCullough, C. Co-ordinating systems and behaviour in Hydra: I. Pacemaker system of the periodic contractions. *Journal of Experimental Biology* **41**, 643-664 (1964).
9. Campbell, R. & David, C.N. Cell Cycle Kinetics and Development of Hydra Attenuata: II. Interstitial Cells. *Journal of cell science* **16**, 349-358 (1974).
10. Sarras Jr, M.P. *et al.* Extracellular matrix (mesoglea) of Hydra vulgaris: III. Formation and function during morphogenesis of hydra cell aggregates. *Developmental biology* **157**, 383-398 (1993).
11. Technau, U. & Holstein, T.W. Cell sorting during the regeneration of Hydra from reaggregated cells. *Developmental biology* **151**, 117-127 (1992).
12. Gierer, A. *et al.* Regeneration of hydra from reaggregated cells. *Nature New Biology* **239**, 98-101 (1972).
13. Sato, M., Bode, H.R. & Sawada, Y. Patterning processes in aggregates of hydra cells visualized with the monoclonal antibody, Ts19. *Developmental biology* **141**, 412-420 (1990).
14. Alvarado, A.S. Planarian regeneration: its end is its beginning. *Cell* **124**, 241-245 (2006).
15. Michalopoulos, G.K. & DeFrances, M.C. Liver regeneration. *Science* **276**, 60-66 (1997).
16. Lenhoff, S.G., Lenhoff, H.M. & Trembley, A. *Hydra and the birth of experimental biology, 1744: Abraham Trembley's Mémoires concerning the polyps*. (Boxwood Pr, 1986).
17. Trembley, A. *Mémoires pour servir à l'histoire d'un genre de polypes d'eau douce, à bras en forme de cornes. Par A. Trembley*. (Chez Jean & Herman Verbeek, 1744).
18. Jopling, C., Boue, S. & Belmonte, J.C.I. Dedifferentiation, transdifferentiation and reprogramming: three routes to regeneration. *Nature reviews Molecular cell biology* **12**, 79 (2011).
19. Newmark, P.A. & Sanchez Alvarado, A. Bromodeoxyuridine specifically labels the regenerative stem cells of planarians. *Dev Biol* **220**, 142-153 (2000).
20. Wagner, D.E., Wang, I.E. & Reddien, P.W. Clonogenic neoblasts are pluripotent adult stem cells that underlie planarian regeneration. *Science* **332**, 811-816 (2011).
21. Le Grand, F. & Rudnicki, M.A. Skeletal muscle satellite cells and adult myogenesis. *Current opinion in cell biology* **19**, 628-633 (2007).
22. Kragl, M. *et al.* Cells keep a memory of their tissue origin during axolotl limb regeneration. *Nature* **460**, 60 (2009).

23. Tu, S. & Johnson, S.L. Fate restriction in the growing and regenerating zebrafish fin. *Developmental cell* **20**, 725-732 (2011).
24. Takaku, Y., Hariyama, T. & Fujisawa, T. Motility of endodermal epithelial cells plays a major role in reorganizing the two epithelial layers in Hydra. *Mechanisms of development* **122**, 109-122 (2005).
25. Sugiyama, T. & Fujisawa, T. Genetic analysis of developmental mechanisms in Hydra. II. Isolation and characterization of an interstitial cell-deficient strain. *Journal of cell science* **29**, 35-52 (1978).
26. Chera, S. *et al.* Apoptotic cells provide an unexpected source of Wnt3 signaling to drive hydra head regeneration. *Developmental cell* **17**, 279-289 (2009).
27. Galliot, B. & Chera, S. The Hydra model: disclosing an apoptosis-driven generator of Wnt-based regeneration. *Trends in cell biology* **20**, 514-523 (2010).
28. Martínez, D.E. & Bridge, D. Hydra, the everlasting embryo, confronts aging. *International Journal of Developmental Biology* **56**, 479-487 (2012).
29. Kaliszewicz, A. Sex ratio patterns and trade-off between sexual and asexual reproduction in the brown hydra. *Freshwater Science* **37**, 551-561 (2018).
30. Campbell, R.D. Tissue dynamics of steady state growth in Hydra littoralis. II. Patterns of tissue movement. *Journal of Morphology* **121**, 19-28 (1967).
31. Barolo, S. & Posakony, J.W. Three habits of highly effective signaling pathways: principles of transcriptional control by developmental cell signaling. *Genes & development* **16**, 1167-1181 (2002).
32. Hobmayer, B. *et al.* WNT signalling molecules act in axis formation in the diploblastic metazoan Hydra. *Nature* **407**, 186 (2000).
33. Bode, H.R. Head regeneration in Hydra. *Developmental dynamics: an official publication of the American Association of Anatomists* **226**, 225-236 (2003).
34. Reinhardt, B., Broun, M., Blitz, I.L. & Bode, H.R. HyBMP5-8b, a BMP5-8 orthologue, acts during axial patterning and tentacle formation in hydra. *Developmental biology* **267**, 43-59 (2004).
35. Watanabe, H. *et al.* Nodal signalling determines biradial asymmetry in Hydra. *Nature* **515**, 112 (2014).
36. Fujisawa, T. Hydra is joining the bandwagon. (2006).
37. Rentzsch, F., Guder, C., Vocke, D., Hobmayer, B. & Holstein, T.W. An ancient chordin-like gene in organizer formation of Hydra. *Proceedings of the National Academy of Sciences* **104**, 3249-3254 (2007).
38. Krishnapati, L.-S. & Ghaskadbi, S. Identification and characterization of VEGF and FGF from Hydra. *International Journal of Developmental Biology* **57**, 897-906 (2014).
39. Sprinzak, D. *et al.* Cis-interactions between Notch and Delta generate mutually exclusive signalling states. *Nature* **465**, 86 (2010).
40. Münder, S. *et al.* Notch-signalling is required for head regeneration and tentacle patterning in Hydra. *Developmental biology* **383**, 146-157 (2013).
41. Tischer, S., Reineck, M., Söding, J., Münder, S. & Böttger, A. Eph receptors and ephrin class B ligands are expressed at tissue boundaries in Hydra vulgaris. *International Journal of Developmental Biology* **57**, 759-765 (2013).
42. Orr, A.W., Helmke, B.P., Blackman, B.R. & Schwartz, M.A. Mechanisms of mechanotransduction. *Developmental cell* **10**, 11-20 (2006).
43. Dupont, S. *et al.* Role of YAP/TAZ in mechanotransduction. *Nature* **474**, 179 (2011).
44. Leckband, D.E., le Duc, Q., Wang, N. & de Rooij, J. Mechanotransduction at cadherin-mediated adhesions. *Current opinion in cell biology* **23**, 523-530 (2011).
45. Shi, Z.-D. & Tarbell, J.M. Fluid flow mechanotransduction in vascular smooth muscle cells and fibroblasts. *Annals of biomedical engineering* **39**, 1608-1619 (2011).

46. Huang, C. & Ogawa, R. Mechanotransduction in bone repair and regeneration. *The FASEB Journal* **24**, 3625-3632 (2010).
47. Leucht, P., Kim, J.-B., Currey, J.A., Brunski, J. & Helms, J.A. FAK-Mediated mechanotransduction in skeletal regeneration. *PLoS One* **2**, e390 (2007).
48. Brunet, T. *et al.* Evolutionary conservation of early mesoderm specification by mechanotransduction in Bilateria. *Nature communications* **4**, 1-15 (2013).
49. Pukhlyakova, E., Aman, A.J., Elsayad, K. & Technau, U. β-Catenin–dependent mechanotransduction dates back to the common ancestor of Cnidaria and Bilateria. *Proceedings of the National Academy of Sciences* **115**, 6231-6236 (2018).
50. Dupont, S. Role of YAP/TAZ in cell-matrix adhesion-mediated signalling and mechanotransduction. *Experimental cell research* **343**, 42-53 (2016).

2 CHARACTERIZATION OF THE ROLE OF HIPPO EFFECTOR YAP IN *HYDRA* REGENERATION

2.1 INTRODUCTION

Hippo Pathway and its Role in Mechanotransduction

Hippo signalling pathway is a kinase-based pathway which has been implicated in promoting cell death, inhibiting cell proliferation, cell differentiation, tissue regeneration, and Regulating Organ size. It was first described and reported in *Drosophila* while screening for tumour suppressor genes in 1995[1]. However, it was only in 2005 when Yorkie, a transcription co-activator, was linked to Hippo signalling, and the importance of the Hippo pathway in regulating transcriptional landscape was truly realised. Since then, the Hippo signalling pathway has been in actively researched upon uncovering its various facets in cellular signalling and regulation. The core components of Hippo characterized in *Drosophila* consists of Ser/Thr kinases- Hippo (Hpo) and Warts (Wts); and their adapter proteins- Salvador (Sav) and Mats. In mammalians, the equivalent set of factors is named as- Mst, Lats, Sav and Mob, respectively.

It has been reported that in mammals and *Drosophila* that MST/HIPPO undergoes auto-activation upon homo-dimerization (Figure 2.1)[2]. This dimer formation requires a single Hippo molecule to bind to the SARAH domain of SAV (a scaffolding protein) which then forms a hetero-tetrameric complex to bring together two MST/HIPPO[3]. This leads to the dimerization of MST/HIPPO and undergoes auto-activation to regulate downstream interactors, including LATS. In humans, MOB1 binds to LATS at the MOB-binding domain, recruits LATS1 to the cell membrane and forms a complex with the MST1/2 dimer. LATS1 T1079 is phosphorylated by MST1/2 to allow auto-phosphorylation of T-loop at LATS S909 required for the kinase activity of LATS[4]. T35 residue in MOB1a of human has been reported to be phosphorylated by MST1/2 and is required for binding to LATS[5]. S127 and S381 phosphorylation by LATS has been extensively reported to be essential for YAP localization and stability in mammals[6]. The hippo signalling culminates with

inactivation of Yorkie (YAP/TAZ), a transcriptional co-activator. Phosphorylation of S127 has found to be essential for cytoplasmic retention of YAP and sequestration through 14-3-3 protein. While phosphorylation of S381 by LATS primes YAP to be phosphorylated at the downstream phosphodegron motif by CK1-ɣ. The activity of Yorkie (Yki) is regulated by its phosphorylation.

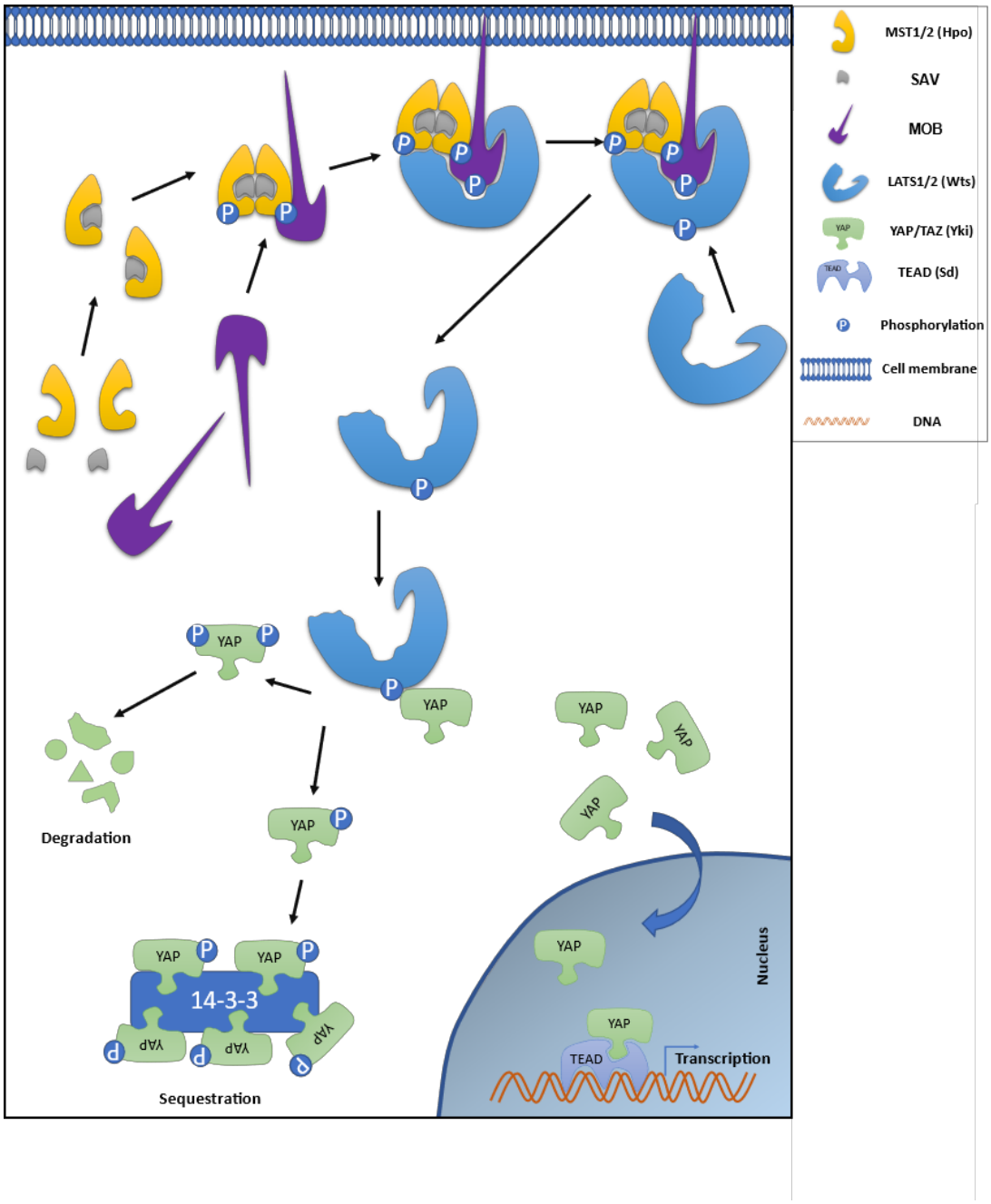

Figure 2.1: Hippo signalling pathway. This figure schematically depicts how the core components of the Hippo pathway regulate YAP activity through a cascade of kinases. The activation of MST1/2 but various specific cues causes MST1/2 to be free to heterodimerize with SAV. Hetero-tetrameric MST-SAV complex is formed causing an auto-phosphorylation of MST1/2 which in-turn acts as a scaffold for recruitment of MOB to the tetrameric complex at the cell membrane. The MOB is

phosphorylated by the MST1/2 and allows MOB to recruit LATS1/2 to the complex. The LATS1/2 is then phosphorylated and activated by MST1/2. The active form of LATS1/2 is now able to regulate the YAP activity by phosphorylating it. The YAP phosphorylation leads either cytoplasmic sequestration or degradation. An unphosphorylated YAP can shuttle across into the nucleus and act as transcription co-activator for TEAD.

The active-unphosphorylated form localizes to the nucleus and is then known to regulate a variety of cellular processes by binding to transcription factors including TEAD, SMAD, RUNX etc. Since the pathway was first discovered in *Drosophila,* it has been extensively studied and characterized in this model organism. The core components and homologs of the pathway in *Drosophila* are named differently and hence they been represented in Figure 2.2 to draw parallel from the mammalian system.

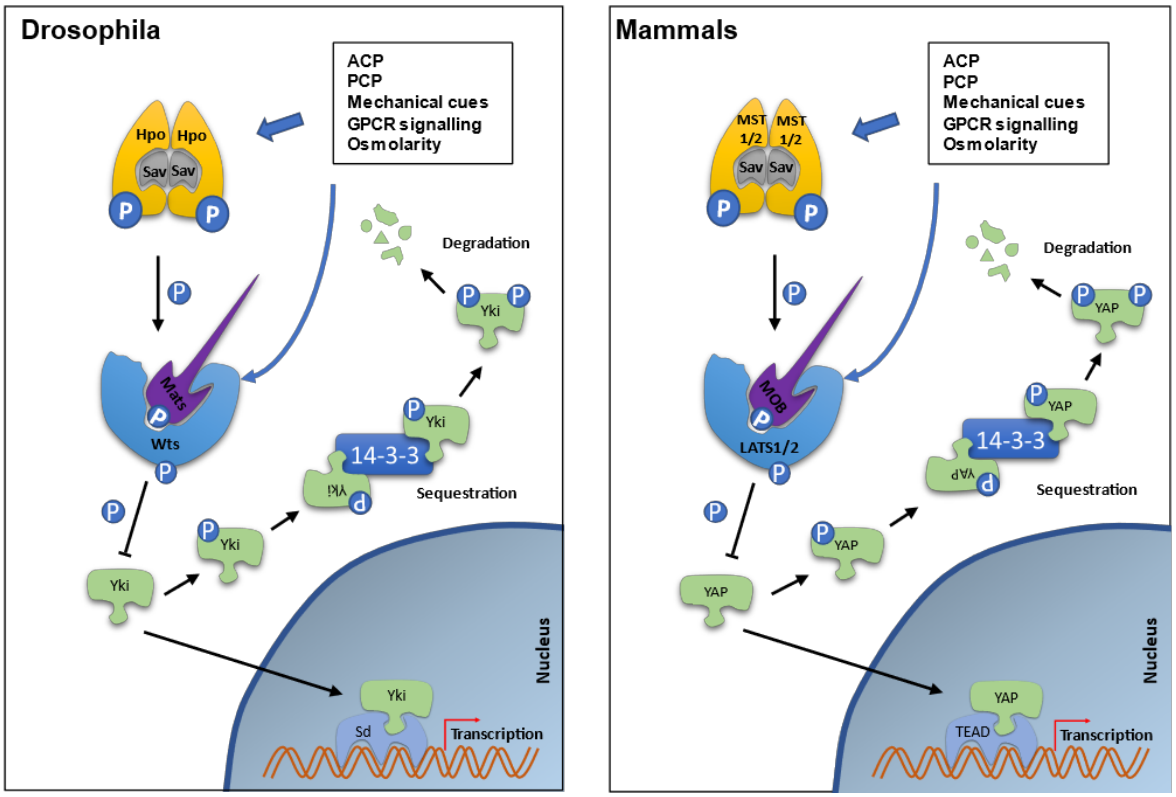

Figure 2.2: The Hippo pathway in *Drosophila* and mammals. This figure shows a schematic comparison of the Hippo pathway phosphorylation cascade and its effect on YAP/Yki activity in *Drosophila* and mammals. The left panel is represented by names of Hippo pathways components of *Drosophila* while the right panel represents the names of the mammalian counterparts.

Hippo signalling is involved in Stem cell differentiation, self-renewal and expansion. It has also been implicated in tissue regeneration. YAP and TAZ have

been reported to regulate embryonic stem cell self-renewal in response to TGFβ/BMP signalling[7]. YAP is inactivated during mouse embryonic stem cell differentiation and activated in induced pluripotent stem cells (iPSCs)[8]. The same study also goes on to report that YAP/TEAD directly binds to the promoter region of many genes which are known to be important in the regulation of stem cells. In *Drosophila* mid-gut, YAP is restricted to the intestinal stem cells. Under normal resting conditions, YAP is localized in the cytoplasm. Under injury, YAP is activated and transported to the nucleus[9]. In a recent study of mice heart development, it was shown that the Hippo Pathway Inhibits Wnt Signaling to restrain cardiomyocyte proliferation and heart size[10]. The same group also showed that Yap interacts with β-catenin on Sox2 and Snai2 genes. In invertebrates, Demircan et al. showed that Hippo pathway in *Macrostomum lignano* regulates tissue homeostasis and its disruption causes tissue outgrowths and aberrant organ size to shape ratio during regeneration[11].

Increasing evidence from recent studies suggests that the Hippo pathway is regulated by mechanical cues (Figure 2.3). YAP/TAZ has been shown to be regulated by cell geometry, with active YAP/TAZ present in cells that have undergone cell spreading, and inactive YAP/TAZ found in round and detached cells [12]. The same group also showed that YAP/TAZ could respond to the stiffness of the ECM, with active YAP in cells seeded on stiff surfaces, and inactive YAP/TAZ in cells seeded on soft surfaces. These studies increasingly pointed out that rearrangement of the actin cytoskeleton in response to different mechanical cues is associated with changes in the YAP/TAZ activity. Depletion of actin-capping protein, which inhibits actin polymerization, resulted in Yki activation and tissue outgrowth[13]. Zhao et al. showed in 2012 that RhoA strongly enhanced YAP/TAZ activity with CDC42 and Rac also showing the same effect but with less potency. Dupont et al. also showed that YAP/TAZ could sense cellular tension. Another report related to the aforementioned study of the role of collagen VI in muscle regeneration showed that YAP plays a crucial role in muscle satellite cell fate. Hence, it is evident that YAP/TAZ seems to be a function of mechanotransduction for cells and is involved in regulating various genes accordingly. A schematic illustration shown in Figure 2.3 summarizes the mechanical cues regulating the Hippo pathway.

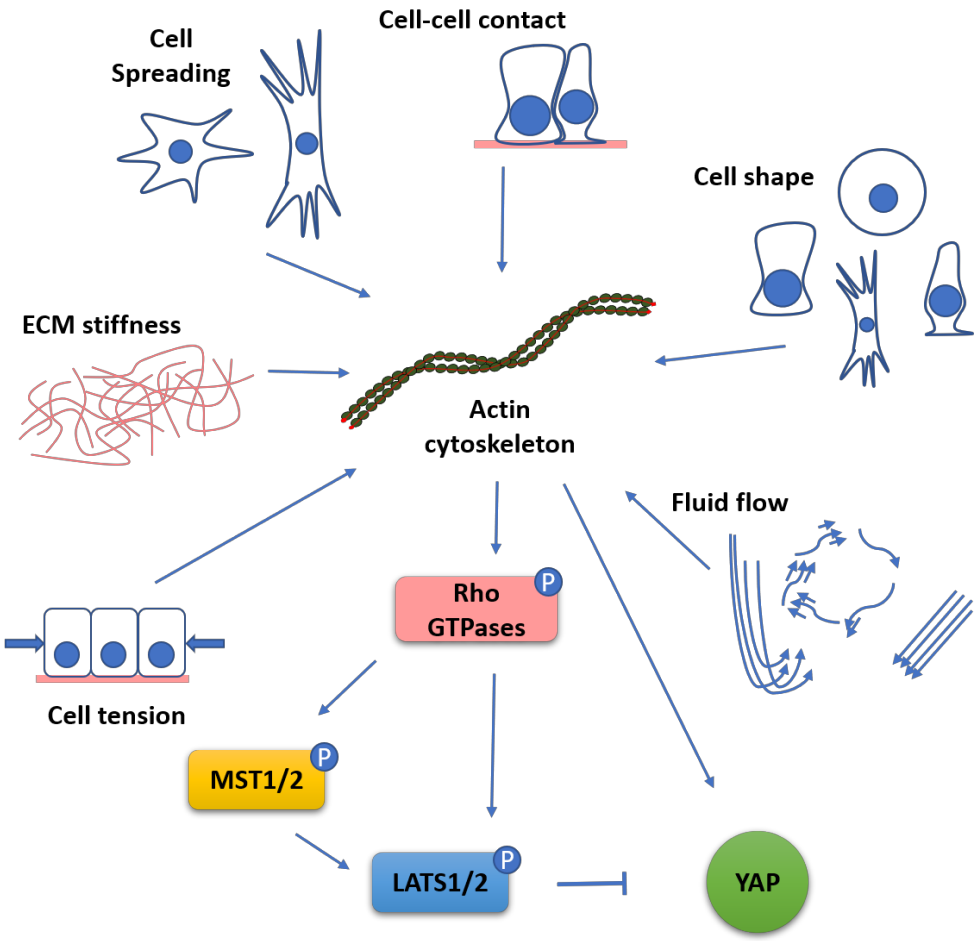

Figure 2.3: Regulation of Hippo signalling by mechanical cues. The figure shows different mechanical cues like cell-cell contact, cell shape changes, fluid flow pattern changes, cellular tension, ECM stiffness differential and cell spreading regulates Actin cytoskeleton dynamics. These changes, in turn, can directly or indirectly regulate YAP activity by regulating various effectors like the Rho GTPase among other small GTPases. These GTPases are known to regulate the activity of YAP regulators- MST1/2 and LATS1/2

There has been a paucity of literature to date about Hippo signalling in lower organisms. Role of Hippo signalling in highly regenerative lower organisms like *Hydra* is unknown. It is, therefore, of immediate interest to study the role of Hippo signalling in the backdrop of changing ECM composition during regeneration from amputated regions. Since the Hippo pathway has been shown to transduce changes in ECM in a more complex organism, it is quite possible that it might play an important role in lower organisms. Hence, it is pertinent to characterize the homologs of core Hippo pathway components in *Hydra* and probe their role during regeneration in *Hydra*. A recent study has characterized the core components of the Hippo

pathway in *Nematostella*[14], suggesting that this pathway has fairly conserved ancient origin during the evolution of multicellular organisms.

2.2 MATERIALS AND METHODS

2.2.1 Animals and culture conditions

Hydra polyps (*Hydra* sp. 'Ind-Pune') kindly gifted by the Ghaskadbi laboratory were cultured and clonal cultures were propagated in crystallizing bowls with *Hydra* medium (Horibata et al., 2004) at a constant temperature of 18±1°C and 12 hours light/dark cycle.

Cultures were fed daily with freshly hatched *Artemia salina* and washed 6–8 hrs after feeding. Prior to RNA isolation, the animals were starved for at least 48 hrs to avoid contamination of the preparations with Artemia nucleic acids.

Hatching of Artemia cysts - Half a teaspoon of Artemia cysts was added per 1 L of artificial seawater (3.2 g rock salt in distilled water) left to hydrate for an hour and incubated overnight at room temperature with aeration. Freshly hatched larvae were collected and washed with *Hydra* medium before use for feeding.

2.2.2 Identification of Hippo pathway homologs in *Hydra*

Hydra magnipapillata genome draft comprising 82.5% of 1.05 Gbp sequenced genome available as Refseq was initially used for identifying Hippo Pathway core components[15]. It was found that the assembly was incomplete and we were unable to fish out any homologs. An in-house transcriptome assembly generated in the Galande laboratory[16] was therefore used for the present study. To further improve the assembly, the in-house transcriptome was merged with the NCBI RefSeq to generate a Hybrid assembly. The hybrid assembly was found to be 99.6 % complete as compared to 95.7% exhibited by NCBI RefSeq[16]. Using Stand-alone NCBI BLAST program, hits of homologs of Hippo pathway core components were identified[17]. To confirm the hits, Reverse BLAST was performed. Finding a hit of a homolog in different phyla or species would confirm the homolog status. To further confirm, the amino acid sequences of these homologs were searched in HMMER for affirmation based on the hits returned[18]. Once the homologs were identified, further analyzed for domain organization by SMART[19]. After manual evaluation of the domain organization, the domain architecture was constructed to scale using DOG 2.0 software[20].

2.2.3 Molecular phylogenetic trees

Alignments and molecular phylogenetic trees of the protein sequences were carried out using MEGA 6.0 software[21]. MUSCLE algorithm was used for amino acid sequence alignment[22]. Phylogenetic trees were computed with a minimum evolution method by using the Jones-Taylor-Thornton (JTT) model for amino acid substitution [23]. ME method was selected because of its speed and minimum errors in tree topologies. A bootstrap test for all trees was conducted with 10,000 replicates. All the trees were validated by the maximum likelihood method using JTT amino acid substitution model and 1000 bootstraps in PhyML3.0[24].

2.2.4 Total RNA extraction

Total RNA from 48 hrs starved *Hydra* was extracted using TRIzol (Invitrogen) as per manufacturer's protocol[25]. Fifty *Hydra* polyps were homogenized in 1 ml of TRIzol/ TRI reagent. To the homogenate, 200 ul of chloroform was added, mixed well and centrifuged at 12000 rpm for 15 min at 4° C. Aqueous phase was collected and the previous step was repeated. 2/3rd volume of isopropanol was added to the aqueous phase collected and after incubation at -20° C for 30 min, RNA was precipitated by centrifugation at 12000 rpm for 15 min at 4° C. The precipitate was washed with 70% ethanol, air-dried and dissolved in RNase-free water.

2.2.5 Agarose gel electrophoresis:

DNA was resolved, visualized and analyzed on 1% agarose gel (or based on the size of the DNA being run). Agarose gel is prepared by mixing 1% Agarose type II in 0.5X TBE buffer and heated until it is completely dissolved. After melting, for visualization of DNA, ethidium bromide was added to the final concentration of 0.5 µg/ml and poured in appropriate casts (BioRAD) with suitable combs. DNA mixed with xylene cyanol FF and orange G were loaded in the gel and electrophoresis was carried out in 0.5X TBE buffer at 70-80 V till the dye front reaches 3/4th of the gel. DNA was visualized under a UV transilluminator and the image was captured using Syngene Gel Doc system or band of interest was excised using a sterile blade for further processing.

2.2.6 cDNA synthesis

First-strand of cDNA was synthesized from total *Hydra* RNA using ImProm-II reverse transcription system (Promega)/ Applied Biosystem High Capacity cDNA Reverse Transcription Kit (Thermo Scientific). Reverse transcription reactions were performed according to the manufacturer's instructions (Tables 2.1 and 2.2).

Table 2.1- cDNA synthesis reaction with ImProm-II reverse transcription system (Promega)

Component	Volume
ImProm-II™ Reaction 5X Buffer	4 µl
dNTP Mix	2 µl
$MgCl_2$, 25 mM	1.6 µl
ImProm-II reverse transcriptase	1 µl
RNase inhibitor	0.5 µl
Nuclease-Free Water	5.9 µl
RNA+Primers (oligo dT)	1-4 µl (1-2 µg)+1µl =5 µl
Total volume	20 µl

Table 2.2- Applied Biosystem High Capacity cDNA Reverse Transcription Kit (Thermo Scientific)

Component	Volume
10× RT Buffer	2 µl
25× dNTP Mix (100 mM)	0.8 µl
10× RT Random Primers	2 µl
MultiScribe™ Reverse Transcriptase	1 µL
RNase inhibitor	1 µl
Nuclease-Free Water	5.9 µl
RNA+Primers (oligo dT)	1 - 5 µl (1-2 µg)
Total volume	20 µl

Reaction conditions:

ImProm-II reverse transcription system (Promega) - Initially, primer-template mixture was denatured at 70°C for 5 min and chilled on ice. Denatured primer-template was added to the reaction mixture and reaction was carried out by annealing at 25°C for 5 min, reverse transcription at 42°C for 60 min and final inactivation at 72°C for 15 min.

Applied Biosystem High Capacity cDNA Reverse Transcription Kit (Thermo Scientific) - Initially, the primer-template mixture was denatured at 70°C for 5 min

and chilled on ice. Denatured primer-template was added to the reaction mixture and reaction was carried out by annealing at 25°C for 10 min, reverse transcription at 37°C for 120 min and final inactivation at 85°C for 5 min.

2.2.7 Polymerase chain reaction

Polymerase chain reaction[26] was used to amplify different fragments and/or complete genes. Reaction mixtures and conditions used are given in the tables below. Elongation time for standard PCR reaction was calculated as 1 kb/min.

Table 2.3 – PCR reaction and programme

Component	Volume
10X Reaction buffer	5 µl
PCR Nucleotide mix, 10mM	1 µl
MgCl2, 25mM	5 µl
Forward primer (100 µM)	0.5 µl
Reverse primer (100 µM)	0.5 µl
Taq DNA polymerase (3u/µl)	0.35 µl
Template DNA	variable (<0.5µg)
Nuclease-Free Water	Variable
Final volume	50 µl

Programme	Temperature	Time	Cycles
Initial Denaturation	94°C	5 min	1
Denaturation	94°C	10 s	25-40
Annealing	(Primer Tm)	30 s	
Elongation	72°C	1min	
Final Elongation	72°C	10 mins	1
Cooling	4°C	unlimited	

2.2.8 Cloning of identified genes

Preparation of competent cells:

A single colony of *E. coli* DH5α was inoculated in 5 ml LB medium and incubated overnight at 37°C. The following morning, primary culture (1:100) was inoculated in 250 ml of LB medium with 10 mM $MgCl_2$ and incubated at 37°C until an OD of ~0.5 was obtained. After cooling the culture on ice for 15 min, cells were collected by

centrifugation at 4500 rpm for 10 min at 4°C. The pellet was resuspended in 30 ml of TFBI and incubated on ice for 60-90 min. Resuspended cells were centrifuged at 4500 rpm for 5 min at 4°C, the supernatant was decanted, and the cell pellet was resuspended in 2 ml of TFBII (ice-cold). The final cell suspension was stored as 50/100 ml aliquots in sterile microfuge tubes at -70°C.

Ligation:

The PCR products were ligated into pGEM-T Easy vector using pGEM-T Easy vector systems or TOPO TA/ Blunt vector (Thermo Scientific). The ligation reaction was carried out as per the manufacturer's protocol. A molar ratio of 3:1 of PCR product: vector was used.

Transformation:

The transformation was carried out by using chemically competent *E. coli* DH5α cells as per standard protocol[27]. The ligation reaction was added to 50 µl of thawed competent cells and incubated for 30 min on ice. Heat shock was given to cells for 90 sec at 42°C and cooled on ice for 2 min. 950 µl of LB medium was added and incubated for 45 min at 37°C with shaking. 50 to 100 µl of transformation cell suspension was plated out on LB Ampicillin plates and incubated overnight at 37°C. Recombinant colonies were screened for the expected size of the insert.

Screening for recombinant colonies:

Colonies were screened for the correct insert size by performing colony PCR. Here, each colony was picked into 10 µl PCR reaction mixture, and one vector-specific primer (generally SP6 and T7) and other gene-specific primer were used for amplification and orientation confirmation. Colonies with the right size of inserts were grown for plasmid extraction and preparation of glycerol stocks.

Plasmid purification:

Plasmids were extracted by a modified alkaline-SDS lysis method using the GenElute plasmid miniprep kit (Sigma) according to the manufacturer's protocol. Bacterial cells harbouring recombinant plasmids were cultured in 5 ml LB medium and harvested for plasmid preparation.

2.2.9 Whole-mount *in situ* hybridisation for localisation of transcripts

Preparation of template DNA:

TOPO plasmids (TOPO TA/ TOPO Blunt) with the gene of interest (partial/complete) were used for the preparation of template DNA. The gene of interest was PCR amplified in sense and anti-sense direction using SP6/T7 primer and a gene-specific primer. This strategy ensured confirmation of the orientation of the gene, preparation of separate set of templates for sense and anti-sense probes and also a larger amount of template for *in vitro* transcription as compared to usage of linearized plamid. The amplicons were loaded on a 1% agarose gel. The amplicons were cut and eluted from the gel, and the eluant was used as the template for *in vitro* transcription.

***In vitro* transcription:**

In vitro transcription reaction was performed using the DIG RNA labelling kit (Roche) as per instructions in the product information. For a 20 µl reaction, 1 µg of linear DNA was used as the template, 2 µl of 10X NTP labelling mixture, 2 µl of 10X transcription buffer, 1 µl of Protector RNase inhibitor and 2 µl of SP6/T7 RNA polymerase were added. After mixing the reaction mixture gently, it was incubated for 2 hrs at 37° C, and the reaction was continued with an addition of RNase-free DNase to digest the template DNA for 15 more minutes and stopped by the addition of 2 µl of 0.2M EDTA. DIG-labelled RNA was precipitated with 2.5 µl of 4 M LiCl and ice-cold absolute ethanol by overnight incubation at -20° C followed by centrifugation at 10000 rpm for 15 min at 4° C. The pellet was given a wash in 70% ethanol, air-dried and dissolved in nuclease-free distilled water. Alternatively, the probes were purified using Invitrogen™ MEGAclear™ Transcription Clean-Up Kit (ThermoFisher) using the procedure as given in the product manual.

Checking labelling efficiency of the riboprobes:

For checking DIG-labelling efficiency, the following procedure was carried out: 2 µl of the reaction product was denatured in RNA loading buffer and separated on 1% denaturing agarose gel electrophoresis. DIG-labelled RNA was transferred on to a

positively charged nylon membrane by capillary transfer with 10X SSC overnight. The blotted RNA was UV-cross linked for 90 sec on each side and equilibrated in buffer I for 5-10 min. In order to block the non-specific sites, the blot was incubated in buffer II for 30 min at room temperature with shaking. Blocking solution was replaced with buffer II containing AP labelled anti-DIG antibody (1:5000 dilution) and further incubated at room temperature for 30 min. After removing the antibody solution, the blot was equilibrated in buffer III, replaced with a colour substrate for AP and allowed to develop in the dark. Once bands of the desired intensity appear, the developing reaction was stopped by removing the detection solution and by the addition of autoclaved distilled water. After washing with autoclaved distilled water, the blot was stored in 2XSSC at 4° C. A rough estimation of labelled RNA was done by comparing the intensity with control DIG-labelled RNA.

2.2.8.4 *In situ* hybridization:

Whole-mount *in situ* hybridization (WISH) technique used for the study of gene expression pattern was modified from[28]. *Hydra* polyps were starved at least for one day before fixation. Animals were relaxed in 2% urethane for 1-2 min and fixed in 4% paraformaldehyde (in 1XPBS) overnight at 4° C or 1 hr at RT and stored at -20° C after washing in methanol. Animals were rehydrated to PBT by ethanol (alternatively methanol can be used)/PBT gradients [100% Methanol -3 washes, 5 min each; 75% methanol+ 25% PBT- one wash for 10 min; 50% methanol+ 50% PBT- one wash for 10 min; 25% methanol+75% PBT- one wash for 10 min and 100% PBT- 3 washes, each wash for 10 min]. Animals were permeabilized with 10 µg/ml proteinase K at room temperature for 15 min to facilitate the diffusion of the probe into the cells. The animals were treated with 1X Glycine solution to stop the Proteinase K reaction followed by 3 washes in PBT (each wash for 10 min). Proteinase K treatment exposes NH_2^+ of tissue surface proteins which may result in non-specific binding of riboprobes. To neutralize amine groups, TEA (pH 7.8; 10 min each) wash was given to the animals - treated once with TEA+0.25% for 5 min followed by TEA + 0.50% acetic for 5 min. After three washes in PBT (10 min each), animals were re-fixed in 4% paraformaldehyde overnight at 4° C. Fixed animals were washed thrice with PBT (10 min each), twice with 2XSSC (10 min each) and heated to 70° C for 15 min in 2XSSC to inactivate endogenous alkaline phosphatase. *Hydra* polyps were

equilibrated to prehybridization buffer, for which the animals were washed in pre-warmed hybridization solution/2X SSC (1:1) for 10 min at hybridization temperature followed by a wash in 100% prewarmed hybridization solution for 10 min at the hybridization temperature. Blocking was carried out with pre-warmed hybridization buffer (hybridization solution with 0.2 mg/ml of tRNA) for 2 hrs at the hybridization temperature. Hybridization was carried out by the addition of DIG-labelled riboprobes at the same temperature for 18-60 hrs. Animals were transferred back to 2X SSC using hybridization solution and 2X SSC gradients at the hybridization temperature [100% Hybridization solution for 10 min, 75% Hybridization solution + 25% 2X SSC for 10 min, 50% Hybridization solution+50% 2X SSC for 10 min, 25% Hybridization solution + 75% 2X SSC for 10 min and 100% 2X SSC for 10 min]. Animals were washed twice in 2X SSC + 0.1% CHAPS (30 min each) at hybridization temperature to remove unbound and non-specifically bound riboprobes.

The hybridized probe was detected as follows: The initial two washes of MAB-T were given at room temperature (10 min each) followed by a long wash for 1 hr. The non-specific protein binding sites were blocked by incubating the animals in blocking solution (80% MAB-T + 20% Foetal Bovine Serum) for 3-4 hrs at 4°C. Blocking solution was replaced by alkaline phosphatase-conjugated anti DIG-antibody (1: 3000 dilution in blocking solution) and incubated overnight at 4°C. Unbound and non-specifically bound antibody were removed by giving eight washes in MAB-T (20 min each). Animals were equilibrated in alkaline phosphatase detection buffer NTMT (pH 9.5) for 5 min, followed by incubation in NTMT + levamisole for 5 min. NTMT + levamisole solution was replaced with BMP substrate solution and allowed to develop in the dark. Once animals develop colour, the reaction was stopped by washing in methanol and were stored in methanol at -20° C. Stained animals were observed under incident light with ZEISS AxioZoom.V16 apotome microscope.

2.2.10 Cryosectioning of WISH stained *Hydra* samples

The stained polyps were rehydrated to PBS gradually through PBS: methanol gradient (25%, 50%, 75% and 100 % wash each for 10 mins). These polyps were then shifted to a 30 % sucrose solution by gradually taking it through 10 % and 20 % for 30 mins each. The polyps were left in 30 % sucrose overnight. These polyps

were then embedded in 10 % PVP (polyvinyl pyrrolidone) by making cubes of PVP (1 x 1 x 2 cm^3) made from aluminium foil cast. The embedded polyps were then sectioned (25 µm) using Leica CM1950 – Cryostat. The sectioned ribbons were then collected on a glass slide and covered and sealed under a coverslip. The sectioned ribbons were then photographed under ZEISS Axio Zoom V16 apotome microscope.

2.2.11 In-silico identification of Hvul_YAP expressing cells in *Hydra*

Single Cell Portal is a web-based tool made available by Broad Institute for visualization of results from a recent study published on the molecular signature of various cell types in *Hydra* at the different spectrum of cell states obtained by sequencing transcriptomes of approximately 25,000 single *Hydra* cells using Drop-seq[29]. "Juliano aepLRv2" specific id for Hvul_YAP was obtained by BLAST from www.research.nhgri.nih.gov/Hydra/sequenceserver/. The ID obtained was "t14163aep|YAP1_ORYLA". This ID was used as a query for obtaining expression profiles of Ectodermal, Endodermal, Interstitial and Neuronal cell types.

2.2.12 In-house antibody generation against Hvul_YAP and Hvul_TEAD

The Hippo pathway is a kinase activity cascade-based pathway, and hence a study undertaking regulation of the same requires experiments to analyse the protein regulation of these components. Antibodies needed to be generated against Hippo pathway proteins for an in-depth understanding of the regulation of pathway in *Hydra*. An initial strategy of expressing full-length proteins did not succeed (expressed proteins were insoluble and aggregating), specific peptides were used as antigen for immunization. Peptide design was done using Web-based "The immune epitope database" (IEDB)[30, 31]. The peptides were designed using the following algorithms:

1) Bepipred Linear Epitope Prediction

2) Kolaskar & Tongaonkar Antigenicity

3) Chou & Fasman Beta-Turn Prediction

4) Parker Hydrophilicity Prediction

5) Emini Surface Accessibility Prediction

6) Karplus & Schulz Flexibility Prediction

Each full protein sequences were run in all the above predictions, and only the peptide regions which overlapped in most of them were chosen. Two peptides were designed for Hvul_YAP and Hvul_TEAD– one from C-terminal region and another from N-terminal region based on their ease of accessibility to antibodies. A cysteine residue was added to the N-terminal of all the peptides for allowing coupling with Sulfo-link columns. Following were the peptide sequences finalized for each of the Hippo pathway components:

Hvul_Hpo N-terminal: CIMQQCDSPYV (67-76)
Hvul_Mob1 N-terminal: CDHCTSESCPV (77-86)
Hvul_SAV N-terminal: CYPKDNKIPSDEI (62-73)
Hvul_LATS1 C-terminal: CVSVPNSDANKS (1040-1050)
Hvul_YAP
N-term: CLPASFFRPPPSL (49-60)
C-term: CLSPNNKPNA (376-384)
Hvul_TEAD
N-terminal: CSNTDPEQMAS (13-22)
C-Terminal: CKVETEYPRYE (361-370)

Since YAP is the effector to the Hippo pathway regulation, it was decided that this study will focus on YAP-TEAD signalling axis. To enable the same, peptide-specific polyclonal antibodies were generated against Hvul_YAP and Hvul_TEAD in Rabbits. For the injections, peptides were first conjugated with the carrier protein- keyhole limpet hemocyanin (KLH) using Pierce Imject Activated Immunogen Conjugation Kit (Product Number 77611) to increase the antigenicity of the peptides. Two mg KLH per 2 mg peptide was used for the preparation. The solution was then dialyzed to wash away unconjugated peptides and then filter sterilized with 0.2-micron syringe filters. These were then quantified using BCA and then frozen at -20 °C until required. 2-3-month-old rabbits were selected for immunization. The first injection to the rabbit was done with 200 µg coupled peptide-KLH. The coupled peptides were then mixed with Freund's complete adjuvant (1:1 by total volume) in a total volume of 1ml (500 µl adjuvant + coupled peptide + NFW). The mix was then emulsified using a syringe and then injected into the rabbit using a 25-gauge needle as follows:

• 0.5 ml of the injection mix into six sites intradermally on the back.

• 0.3 ml into two sites intramuscularly (thigh).

• 0.2 ml into two sites subcutaneously in the neck region.

Subsequently, booster injections of 100 µg protein emulsified with Freund's incomplete adjuvant (1:1 by total volume) were given at intervals of 28 days. About 20 ml of blood was removed from the rabbit pinna ten days after each boost.

The blood was then allowed to coagulate for 2 hours at room temperature and stored overnight at 4°C. The following day, the serum was separated from the blood by centrifugation at 3500 rpm for 15 mins. The supernatant was collected as serum and filtered through a 0.2 µm syringe filter. The serum was then affinity purified. Affinity purification column was prepared by coupling peptides used for immunization to Sulfolink columns. Since these peptides contained cystine in the N-terminals, a free sulfhydryl group could be generated using a reducing agent like Tris(2-carboxyethyl)phosphine (TCEP). These peptides can then be coupled to the column using Thermo Scientific SulfoLink Immobilization Kit for Peptides (Cat no. 44999). The exact protocol for peptide coupling and affinity purification was followed as given in the kit.

2.2.13 Protein lysate preparation, SDS PAGE and Western Blotting

Protein lysate for Western blots and Immunoprecipitation (IP) was prepared by collecting the requisite number of polyps (100 polyps per experiment for Western blotting and 2000 polyps per experiment for nuclear isolation needed for IP). Polyps were collected and lysed in RIPA lysis buffer (150 mM NaCl, 50 mM Tris-Cl, pH 7.5, 5 mM EDTA, 0.5 % NP-40, 1 mM Sodium orthovanadate, 0.1 mM PMSF & 0.1 % SDS) for preparing lysate for western blot. For the co-IP experiment, the nuclear fraction was prepared by suspending *Hydra* in ice-cold Wash buffer 1 (0.25 % Triton-X, 10 mM EDTA, 0.5 mM EGTA, 10 mM HEPES (pH 7.5), 1mM PMSF& 1mM DTT) with PIC. The suspension was incubated on ice for 5 mins. The polyps were aspirated in 200 µl pipette multiple times to dissociate the cells and release the nucleus. The nuclear pellet was made by spinning down the suspension at 1000 x g for 5 mins at 4°C. These pellets were then washed with Wash buffer 2 (0.2 M NaCl, 1 mM EDTA, 0.5 mM EGTA, 10 mM HEPES (pH 7.5), 1mM PMSF& 1mM DTT) with

PIC on ice and the nuclear pellet was made by spinning it again. This pellet was then lysed in IP buffer 1(10 mM HEPES pH 7.9, 300 mM NaCl, 0.2 % NP 40, 20 % Glycerol & 0.1 % EDTA). The antibodies needed for the experiment were coupled to Dynabeads using the Invitrogen Dynabeads Coupling Kit. The lysate was then used for binding to the antibody-coupled Dynabeads for IP. The beads were incubated in the lysate for overnight at 4°C. IP buffer 2 (10 mM HEPES pH 7.9, 400 mM NaCl, 0.2 % NP 40, 20 % Glycerol & 0.1 % EDTA) was used for washing the beads. The protein was finally eluted using 100 mM glycine pH 2.5.

2.2.14 Immunofluorescence staining

Immunofluorescence assay was performed as per the protocol given by Takaku et. al., 2014 [32]. *Hydra* polyps were starved at least for one day before fixation. Animals were relaxed in 2% urethane for 1-2 min and fixed in 4% paraformaldehyde (in 1XPBS) overnight at 4° C or 1 hr at RT. 1:100 concentration of primary antibody was used for anti-Hvul_YAP and anti-Hvul_TEAD antibodies. 1:100 concentration of Invitrogen Alexa-conjugated secondary antibodies were used throughout. Invitrogen Alexa 488 or 568 conjugated Phalloidin was used for this study. DAPI was used for nuclear staining throughout the study.

2.2.15 *Clytia hemisperica* specific CheYki antibody

Since in-house developed Hvul_YAP antibody didn't work for IFA for *Hydra.* A recently published paper reported the presence of Yorkie (YAP/Yki) in *Clytia hemispherica* and producing polyclonal antibody specific to CheYki in rabbit against the peptide FNRRTTWDDPRKAHS[33]. This antibody along with the pre-immune serum was kindly gifted by Dr Michaël Manuel (Sorbonne Universités, Université Pierre et Marie Curie (UPMC), Institut de Biologie Paris-Seine (IBPS) CNRS) to us. The antibody was validated by Western blot and Immunofluorescence.

2.2.16 *Hydra* regeneration assay

Multiple experiments in this work use *Hydra* regeneration paradigm as a model for studying the regulatory roles of the various aspects. Regeneration assay was done by taking the requisite number of regularly fed polyps. These polyps will then be decapitated (all the experiment in this study used head amputation model) and allowed to regenerate for the required amount of time. Most of the experiments in

this study use early regenerative time points involving a subset of following time points: 0, 0.5, 1, 2, 4, 8, 16 and 24 hrs post-amputation (hpa). For 0 and 0.5 hpa time points, if the number of polyps to be amputated is large, then the amputation is done on ice to slow down metabolism of *Hydra* to effectively synchronize the regenerative or wound healing process of all the decapitated polyps.

2.2.17 Verteporfin treatment assay

Verteporfin (Vp) was procured from Sigma (SML0534) and dissolved in DMSO. A 2 mM stock was prepared and kept in 50 µl aliquots at -20 °C for long-term storage in the dark. The vial was thawed for 30 minutes in dark before use. For the assay, the polyps were treated with 5 µM Vp in *Hydra* medium and the same volume of DMSO in *Hydra* medium as vehicle control. For regeneration assay, the polyps were pre-treated with Vp for 12 prior to decapitation and fresh Vp was added post-amputation. The Vp solution was replaced every 24 hrs. For the budding assay, the non-budding polyps were collected and incubated in Vp. The Vp solution was replaced every 24 hrs and reading for number buds were taken every 24 hrs. Every step of Vp treatment assay was performed in the dark.

2.3 Results and Discussion

2.3.1 Prediction and analysis of core Hippo pathway homologs in *Hydra vulgaris*

Core Hippo pathway homologs – *Hippo*/MST, MOB, LATS, SAV, YAP and TEAD were identified from in-house *Hydra* transcriptome using NCBI stand-alone BLAST. In mammals, *Hippo*, MOB, LATS and YAP have 2 paralogs each while TEAD has 4 paralogs. SAV, on the other hand, have no reported paralogs. The occurrence of these paralogs has been attributed to Whole-genome duplication event correlated to certain fish species[34]. Therefore, any species evolved earlier to fishes do not contain paralogs as reported for Hippo pathway genes. Conforming to these studies, *Hydra* consists of only one gene was identified for each of the core Hippo pathway components. Since this is the first report of the Hippo pathway in *Hydra*, they were named as follows: Hvul_Hpo, Hvul_MOB, Hvul_LATS, Hvul_SAV, Hvul_YAP and Hvul_TEAD. The homologs were analysed and curated using the methods described in the Methods section. The nucleotide and peptide sequences of the confirmed Hippo pathway homologs in *Hydra* are enlisted in the appendix (4.2 & 4.3)

A detailed domain analysis using SMART website for the amino acid sequence of Hippo pathway homologs revealed highly conserved domain organization of the proteins analysed which indicated a fully functional pathway consisting of these core components (Figure 2.4 A). Hvul_Hpo domain analysis revealed conserved N-terminal Protein kinase domain (PKinase Domain) and a C-terminal SARAH (Salvador-RASSF-Hippo) domain. Presence of these domains indicates the conserved regulation of activation of Hvul_Hpo kinase activity. The Hvul_SAV also can be seen to have conserved the SARAH domain required for orchestrating the reported scaffolding activity. Hvul_LATS domain architecture indicates conservation of the hydrophobic motif (Motif: AFYEF**T**FRHFFDDGG) (a 37.5% hydrophobicity confirmed using web-based peptide analysis tool at www.peptide2.com/N_peptide_hydrophobicity_hydrophilicity.php) containing the Threonine residue (T993) required for activation of LATS by HIPPO phosphorylation. The MOB binding motif is highly conserved in Hvul_LATS as compared to the human and mouse (Figure 2.4 B). The auto-activation T-loop (near S909) of Hvul_LATS is 100 % conserved (Motif: AH**S**LVGTPNYIAPEVL) near S830. Hvul_MOB is highly

conserved (83-84 % identity) as compared to any other components of Hippo pathway homologs in *Hydra* indicating highly conserved function. The same site as reported for Human MOB is also highly conserved in Hvul_MOB at T35 (Motif: LLKHAEA**T**LGSGNLR). Hvul_YAP domain analysis revealed that it had a conserved TEAD-Binding Domain (TBD) and two WW domain. A serine phosphorylation prediction for YAP protein sequence was performed using GPS 2.1 web-based tool [35]. Based on GPS prediction and manual curation, Hvul_YAP is predicted to have LATS phosphorylation site at S74 (motif: PIHTRAR**S**LPSNIGQ) and S277 (motif: YTAYMN**S**SVLGRGSS) homologous to the S127 (motif: PQHVRAH**S**SPASLQL) and S381 (motif: SDPFLN**S**GTYHSRDES). Similar to mammals, a phosphodegron motif was identified immediately downstream to the S381 site FFDSLQA**S**NVDLDIL which could be phosphorylated by CK1-ɣ at S344 of Hvul_YAP. These analyses indicated that the Hippo pathway effector protein YAP was well equipped to regulation from the LATS and CK1-ɣ and with its defined TEAD binding domain and WW domain, it could interact with transcription factor TEAD and other reported PPXY domain-containing proteins. Upon determining the nucleotide percent identity with other reported model organisms used for studying the Hippo pathway, we find that *Hydra* had higher percent identity with humans than *Drosophila* (Figure 2.4 C). Hvul_HPO shows about 60 % identity with human and 56 % identity with *Drosophila.* Hvul_SAV is comparatively less conserved with a 24 % identity with human and 22 % identity with *Drosophila*. Hvul_MOB is highly conserved across the animal phyla with about 84 % identity with human and 83 % identity with *Drosophila.* Hvul_LATS has about 41.6 % identity with human and 42 % identity with *Drosophila.* Hvul_YAP shows 34.6 % identity with human and 34 % identity with *Drosophila.* Hvul_TEAD exhibits about 65 % identity with human and 59 % identity with *Drosophila*. Molecular phylogenetic analysis revealed that these genes reported in vertebrates have a closer evolutionary relationship to *Hydra* homologs than that of *Drosophila* (Figure 2.4 D). Certain organisms including *C. elegans* and *Drosophila* have been known to diverge a lot from their common ancestors of the metazoans.

2.3.2 Confirmation of core Hippo pathway component transcripts

To confirm the presence of predicted Hippo pathway components, we amplified the genes from the cDNA prepared from *Hydra vulgaris* Ind-Pune strain total RNA (Table 2.4) (Section 2.2.4-7). The amplicon size was confirmed and cloned into TOPO TA/

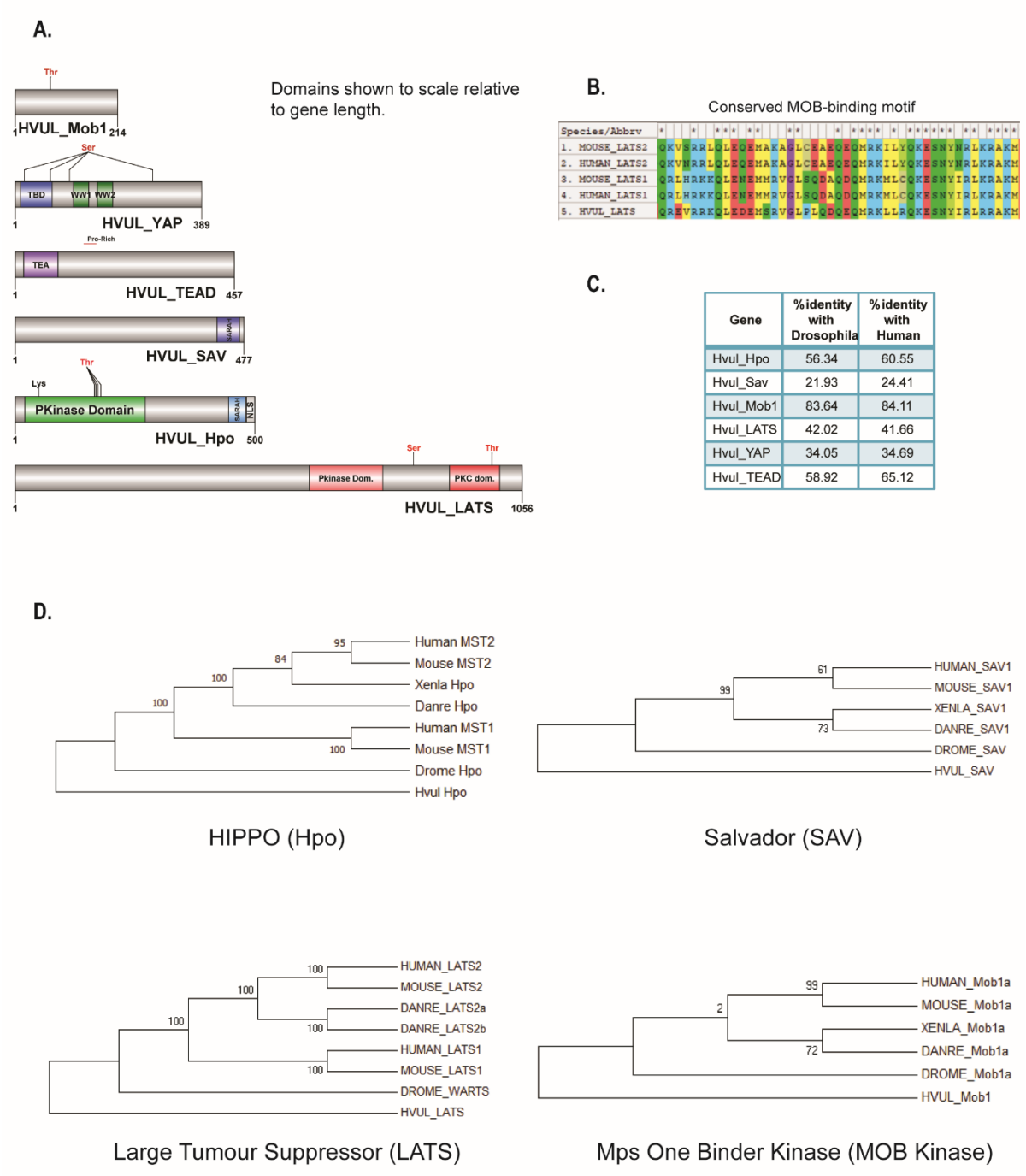

Figure 2.4: Hippo Pathway homologs in *Hydra*. A. Domain architecture of the homologs as visualized using DOG 2.0. **B**. Multiple sequence alignment of Hvul_LATS at the MOB Binding domain with other species indicating high conservation. **C**. Depicts the percent identity of *Hydra* homolog with Drosophila and Human. **D**. Molecular phylogenetic tree of individual Hippo pathway homologs.

Blunt vector, sequenced and verified (Section 2.2.8) (Figure 2.5). Hvul_Hpo was amplified at 1503 bp and cloned into in the 3' to 5' direction of TOPO TA vector (See Appendix 3.3). Hvul_Sav was amplified at 1434 bp and cloned into in the 5' to 3' direction of TOPO TA vector. Hvul_LATS was amplified at 1360 bp and cloned into in the 3' to 5' direction of TOPO Blunt vector. Hvul_Mob was amplified at 645 bp and cloned into in the 5' to 3' direction of TOPO TA vector. Two such clones were obtained (See Appendix 3.3). Hvul_YAP was amplified at 1170 bp and two clones were obtained with both 5' to 3' and 3' to 5' direction of TOPO TA vector. Hvul_TEAD was amplified at 1356 bp and cloned into in the 5' to 3' direction of TOPO TA vector. The presence of the predicted transcripts ensures the reliability of predicted gene models and their functional involvement in *Hydra*.

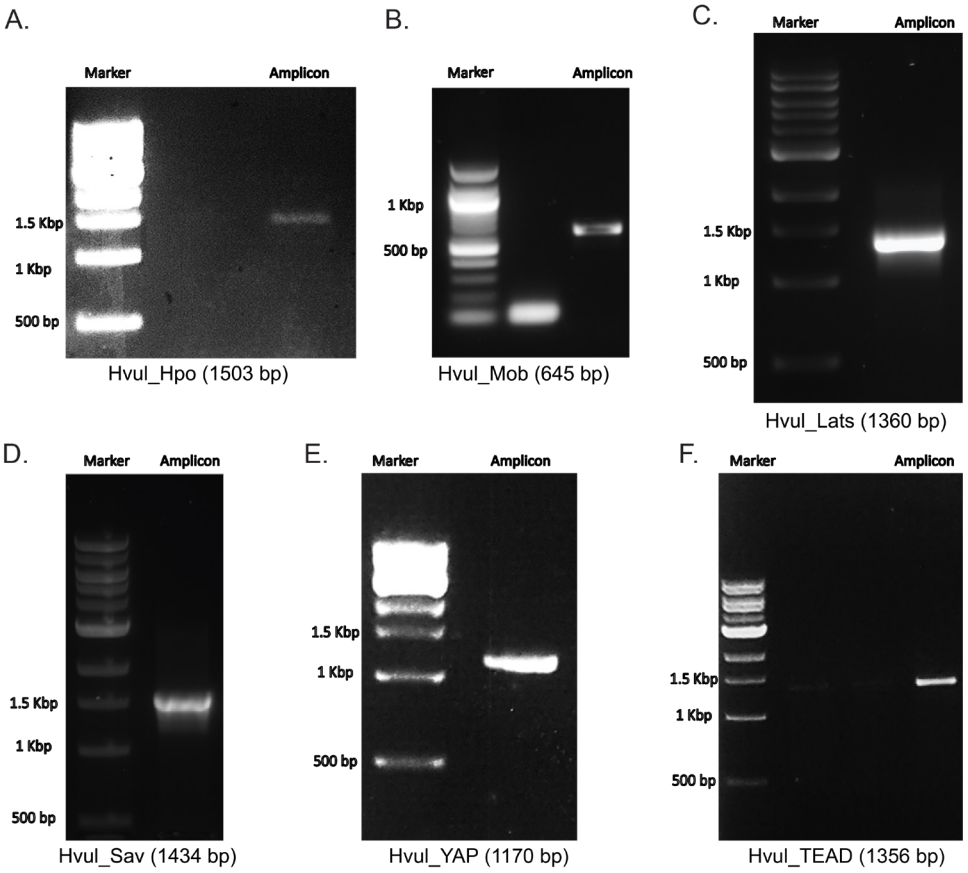

Figure 2.5: Validation of the Hippo Pathway homologs in *Hydra* by PCR mediated amplification using the predicted sequence. A. Hvul_Hpo was amplified at 1503 bp. **B**. Hvul_Mob was amplified at 645 bp.**C**. Hvul_LATS was amplified at 1170 bp. **D**. Hvul_SAV was amplified at 1434 bp. **E.** Hvul_YAP was amplified at 1170 bp. **F.** Hvul_TEAD was amplified at 1356 bp.

2.3.3 Expression pattern of Hvul_YAP gene

This study mainly focuses on Hvul_YAP expression and regulation in *Hydra*. An in-depth analysis of YAP expression will be done in this section. The expression pattern of Hvul_YAP in *Hydra* polyp was studied by whole-mount *in situ* hybridization (WISH) (Described in Section 2.2.10). The staining pattern observed from the whole polyp indicates low-level expression throughout the body with higher expression at the tentacle base and tip of new bud (Figure 2.6 A.i). A closer look indicates that the expression is stronger in the endodermal cells as compared to the ectodermal cells (Figure 2.6 A.ii - iv). YAP expression in the early stages of bud development indicates its role in budding. Higher YAP expression at the region of high mechanical stress such as the tentacle base, early budding tip and mature bud-parent polyp boundary indicates a probable ancient mechano-sensory role of YAP in *Hydra*. Cryosectioning of these polyps was done to have a closer look at the types of cells expressing YAP (Section 2.2.11). The images of these sections revealed cells in doublets, quadruplets and groups of cells among other stained cells indicating cells of interstitial stem cell origin, plausibly nematoblast and nests of nematoblasts (Figure 2.6 B.i). *In-Silico* Analysis of YAP expression using Single Cell Portal (Section 2.2.12) was in line with the observation from WISH results. There was a low-level expression of YAP in almost all cell types of *Hydra* (Figure 2.6 B.ii-v). Few cell types like i_n_ec2 which indicate ectodermal cells co-expressing neuronal markers; i_nb5 (nematoblast cells), i_nem (nematocytes); head and tentacle region-specific endodermal cell showed marginally higher expression compared to other cell types. Such an expression pattern indicates a ubiquitous requirement of YAP for regulatory roles and a possible protein level regulation for a finer activity related regulation as reported in more complex model systems.

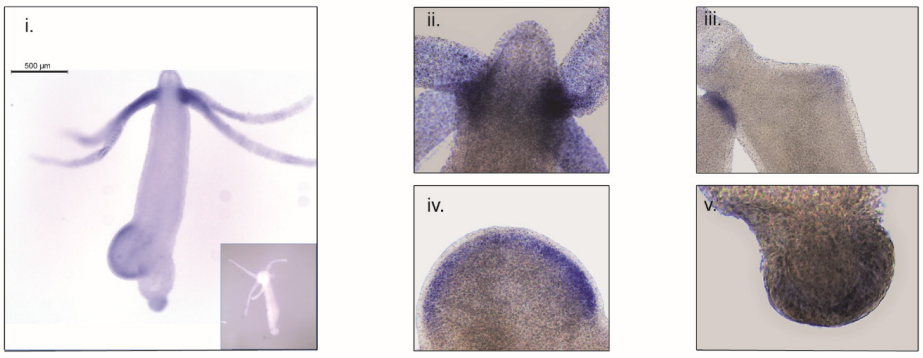

Figure 2.6: Hvul_YAP expression analysis in *Hydra*. Whole-mount *in situ* hybridization of Hvul_YAP expression at **i)** Region across the polyp (inset shows polyp probed with sense RNA probe). **ii)** Head, **iii)** early bud/bud foot, **iv)** mid-stage bud, **v)** basal disk.

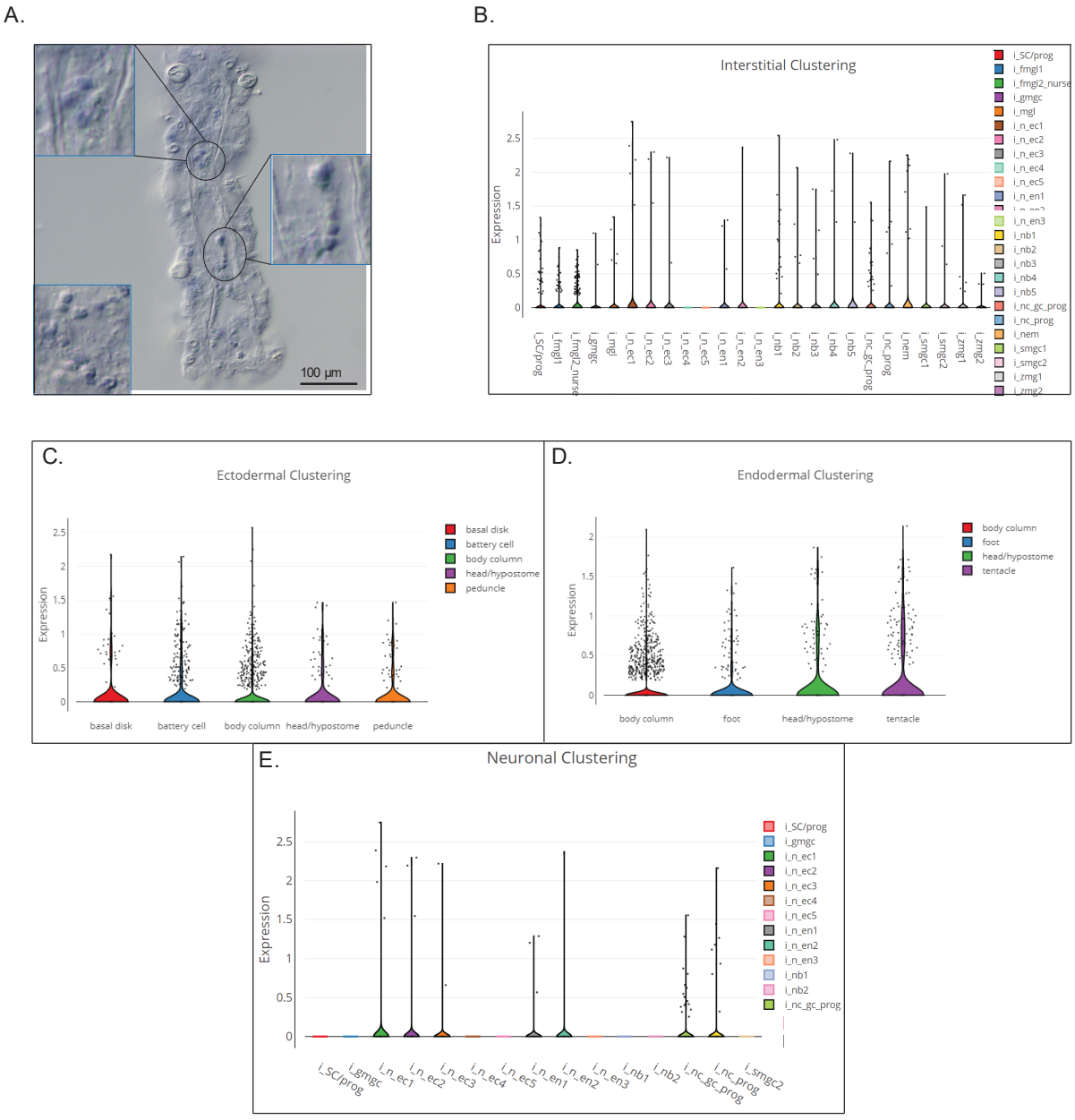

Figure 2.7: Hvul_YAP expression analysis in *Hydra*. Cell-type analysis of YAP expressing cells in *Hydra*. For visualizing cells stained by RNA WISH, the whole polyps stained using WISH were cryosectioned into 25 µm and imaged under apotome. **A.** Cryosection of YAP WISH at tentacle showing specific cell-type expression. B-E. Cell clustering of YAP expressing cells was generated using Single Cell Portal[29].**B.** Interstitial cell clustering, **C.** Ectodermal cell clustering, **D.** Endodermal cell clustering & **E.** Neuronal cell clustering of Hvul_YAP expressing cells. Cluster Label Abbreviation Key: bat: battery cell, bd: basal disk, db: doublet cluster, ec: ectoderm, ecEP: ectodermal epithelial cell, en: endoderm, enEP: endodermal epithelial cell, fmgl: female germ-line, gc: gland cell, gmgc: granular mucous gland cell, i: cell of the interstitial lineage, id: integration doublet, mgl: male

germline, mp: multiplet, nb: nematoblast, n: neuronal cell, nem: nematocyte, pd: suspected phagocytosis doublet, prog: progenitor, SC: stem cell, smgc: spumous mucous gland cell, tent: tentacle, zmg: zymogen gland cell.

2.3.4 Expression pattern of Hvul_Hpo and Hvul_MOB genes

An RNA WISH study of Hvul_Hpo showed expression throughout the gastric region (Figure 2.7). No expression was observed at the differentiated zones of Hypostome, tentacle or basal disk which might indicate a role in stem-cell maintenance or differentiation but not in terminally differentiated cells. There is a slight reduction in expression at the budding zone and early buds which might indicate the antagonistic role of Hpo towards YAP activity in areas of high mechanical stress as reported in other organisms. Hpo expression can also be seen at mature bud-parent polyp boundary indicating a fine-tuning of regulation Hippo pathway-dependent during bud detachment. Hvul_MOB expression showed a similar pattern to that of Hvul_YAP with a distinct down-regulation at the basal disk region of both adult and budding *Hydra* (Figure 2.7). Hvul_SAV expression reflected the expression pattern of Hvul_Hpo indicating similar role. It can also be noted that there is marked reduction in expression at the budding region, early and late buds, unlike the Hvul_Hpo.

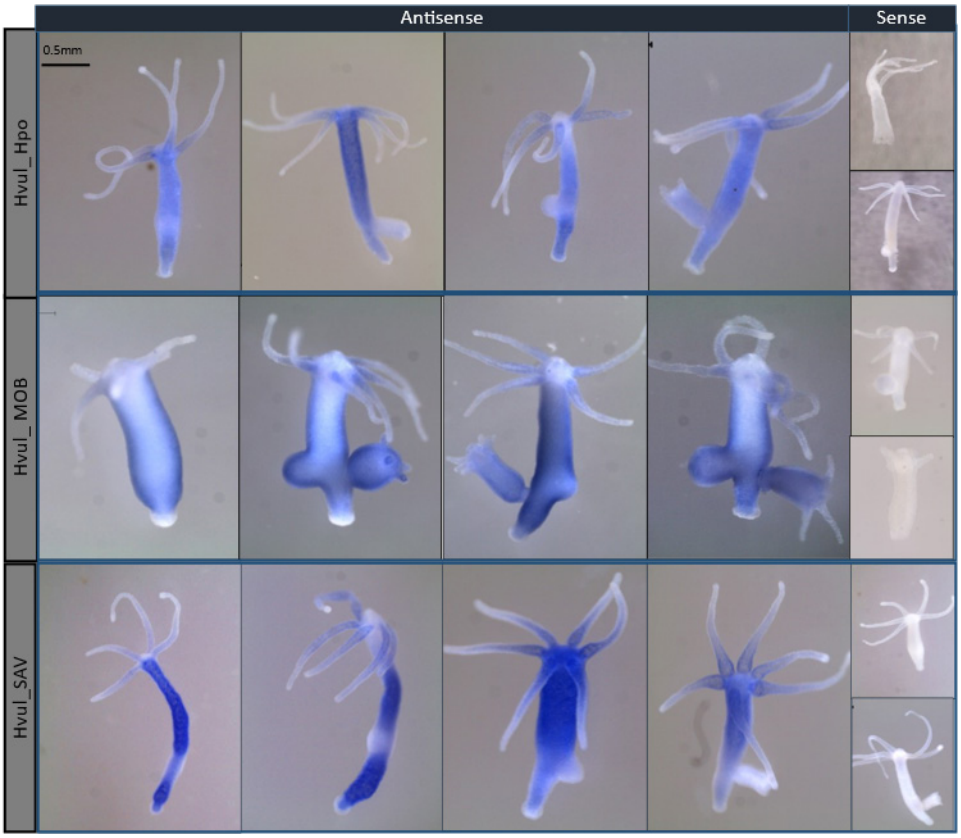

Figure 2.7*: Hvul*_Hpo, *Hvul*_MOB and *Hvul*_SAV expression analysis in *Hydra.* Whole-mount *in situ* hybridization of Hvul_Hpo (Top), Hvul_MOB (middle) and Hvul_SAV (bottom)expression for the whole polyp. The small images on the right indicate negative controls probed with sense RNA probe.

2.3.5 Generation of antibodies against Hvul_YAP and Hvul_TEAD

Since no antibodies were reported to be generated against *Hydra* homologs previously, we had to generate antibodies *in-house*. To generate the antibodies, we designed two peptides corresponding to the N & C terminal region of proteins of interest because these regions are considered to be comparatively more accessible. Four rabbits were immunized with N-terminal specific Hvul_YAP, N-terminal specific Hvul_TEAD, C-terminal specific Hvul_YAP & C-terminal specific Hvul_TEAD respectively. Among these, C-terminal specific Hvul_TEAD immunized rabbit died unexpectedly after the first booster. Rest of all the rabbits were immunized with a total of 17 boosters before terminating the experiment. Out of the three, C-terminal Hvul_YAP immunized rabbit did not generate any immunogenicity to Hvul_YAP. N-terminal specific Hvul_YAP & N-terminal specific Hvul_TEAD immunized Rabbits generated specific polyclonal antibodies against their immunogen. Western blotting of *Hydra* lysate was performed to test the specificity of the antibodies generated. N-terminal specific Hvul_YAP antibody was able to detect Hvul_YAP in total *Hydra* lysate at about 40 KDa (Figure 2.8 A) while N-terminal specific Hvul_TEAD antibody was able to detect Hvul_TEAD in total *Hydra* lysate at about 48 KDa (Figure 2.8 B i.). The expected molecular weights for Hvul_YAP and Hvul_TEAD is 42 KDa and 50 KDa respectively. Immunofluorescence assay (IFA) was performed for both the antibodies. Anti-Hvul_YAP antibodies did not produce any signals in IFA. Anti-Hvul_TEAD antibodies worked for IFA and were able to produce expected expression patterns. The TEAD positive cells were observed throughout the body of the *Hydra* polyp (Figure 2.8 B ii.). A closer look at 100X magnification confirmed nuclear localization of the transcription factor TEAD.

2.3.6 Cross-reactivity of *Clytia hemispherica* specific CheYki antibody with Hvul_YAP *Hydra*

The CheYki antibody was immunized using a peptide from the WW1 region of CheYorkie. The CheYki peptide sequence was extracted from the **Mar**ine **I**nvertebrate **M**odel Data**ba**se (MARIMBA) and aligned using CLUSTAL. The full protein alignment showed just a 39.36 % identity. However, a peptide-specific

(immunogen) alignment gave a 66% similarity and a 60 % identity which raised the probability of cross-reactivity of this antibody against Hvul_YAP (Figure 2.9 A). To test the same, a western blot was run using CheYki antibody or pre-immune serum

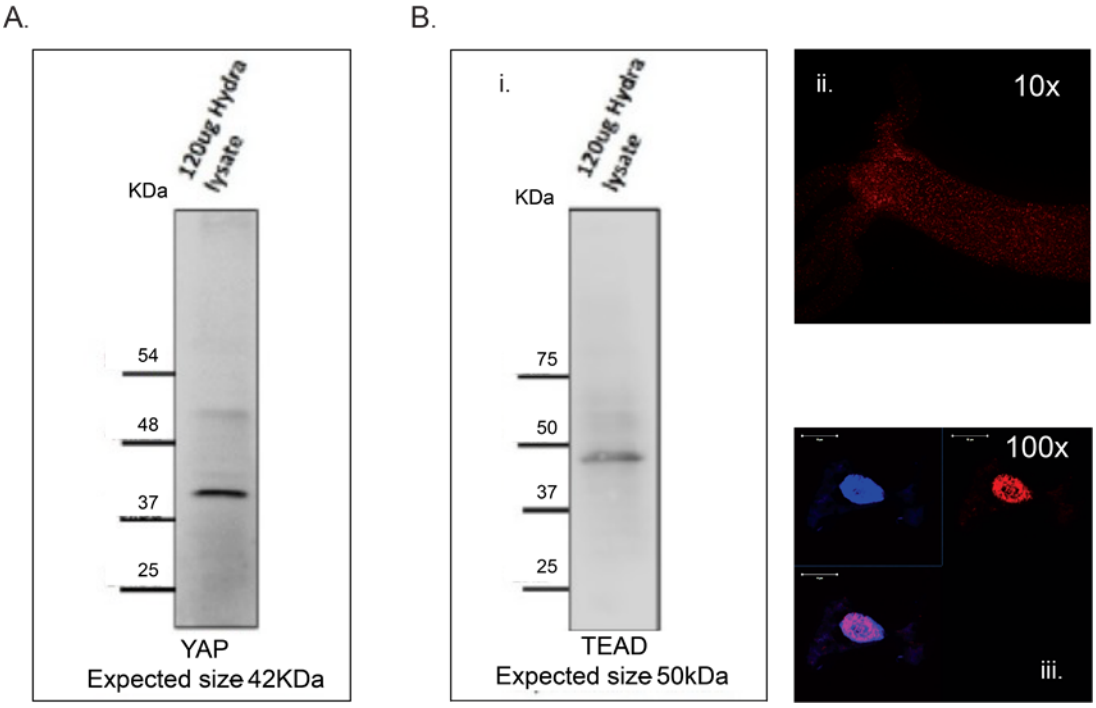

Figure 2.8*:* Western blotting and Immunofluorescence assay of in-house generated antibodies. A. Western blot of *Hydra* lysate (120 µg) probed with anti-Hvul_YAP showing a band at about 40 KDa and **B.** i. with anti-Hvul_TEAD showing a band at about 48 KDa. **B.** ii. Immunofluorescence assay of whole *Hydra* polyps using anti-Hvul_TEAD antibody at 10x magnification. **B.** iii. Immunofluorescence assay using the anti-Hvul_TEAD antibody of macerated cells at 100x. Red: YAP & Blue: Nucleus. (Magenta indicates merged image)

as the primary antibody. Unfortunately, the CheYki failed to give a specific signal against Hvul_YAP as against the negative control of pre-immune serum. The inability of the antibody to work for western blot might stem from the fact that the proteins are in denatured form and hence lose their 3D structural features. An immunofluorescence assay, on the other hand, yielded a robust signal for CheYki antibody as compared to the negative control (Figure 2.9 B) In IFA, the protein structure is retained. It may be hypothesized that the CheYki antibody may be structure-specific and not exactly sequence-specific. A careful examination revealed prominently nuclear-localization of the signal. Cytoplasmic localization was not apparent and maybe too diffused to be detectable by IFA. Examination of localization of YAP expressing cells (YAP positive cells from here onwards), shows a pattern similar to what we found in YAP ISH (Figure 2.9 C). There was more or less

expression throughout the body. The sub-hypostomal region encompassing the tentacle ring or the base of the tentacle had high expression similar to that seen in ISH but the number of YAP positive cells drops soon into the tentacle zone. Unlike the pattern of transcripts seen in the ISH for basal disk, the YAP positive cells are very sparse in the region. The body column is uniformly interspersed with YAP positive cells. The YAP positive cells are almost exclusively seen in groups (Figure 2.10). There were specific patterns of these groups which looked similar to the ones seen in cryosections of ISH samples. Since the IFA staining was mostly nuclear, it is difficult to ascertain the cellular morphology. A careful analysis of cells expressing YAP based on the staining intensity and intercellular distance, as seen in IFA indicates different subsets of cells. Based on the YAP expression intensity, there seem to be cells having High expression (Blue arrow), medium expression (yellow arrow) and low expression (green arrow). Based on the cellular clustering, cell types can be divided into cells which are duplets or quadruplets (orange arrows) which may be interstitial stem cell undergoing first and second mitotic division. There are also clusters of cells which are arranged into a linear file whose identity is difficult to judge (red arrows). Yellow arrows indicate clusters of cells which looks like part of a nest of nematoblasts. These nest cells are typically arranged into 8-16 cell-clusters. As can be noticed here, these clusters are not completely YAP positive, and only a subset are expressing YAP. This may indicate that these cells are expressing only at certain stages of nematoblast differentiation. Such similar clusters can be observed even in the high-level YAP expressing cells (blue arrows) indicating a yet different subset of nematoblast cells. A different population of cells show extra-nuclear staining (white arrow). These stains might be non-specific since they are localized in cysts similar to that seen in desmonemes and stenoteles. These results suggest that at least some of the YAP positive cells have interstitial cell origin and a detailed IFA study of individual cells made from dissociated cells separated by FACS is required for a thorough investigation into identifying the full gamut of cell-types.

2.3.7 YAP expressing cells are early responders to head amputation

YAP IFA performed on decapitated polyps shed light on the participation of YAP positive cells during early regeneration (Figure 2.11). YAP positivecells can be observed occupying the site of injury within one hour of amputation. These cells increase in density as time progresses until 4 hours post-amputation (hpa). Since

wound healing takes approximately 1-2 hpa, the YAP positive cells may migrate along with the epithelial cells during the wound-healing phase. An increase in density might be caused by either further migration of the YAP positive cells from the body column or by division from the pre-existing cells at the site of injury. The interesting observation to note is that the population of YAP positive cells at the site of injury

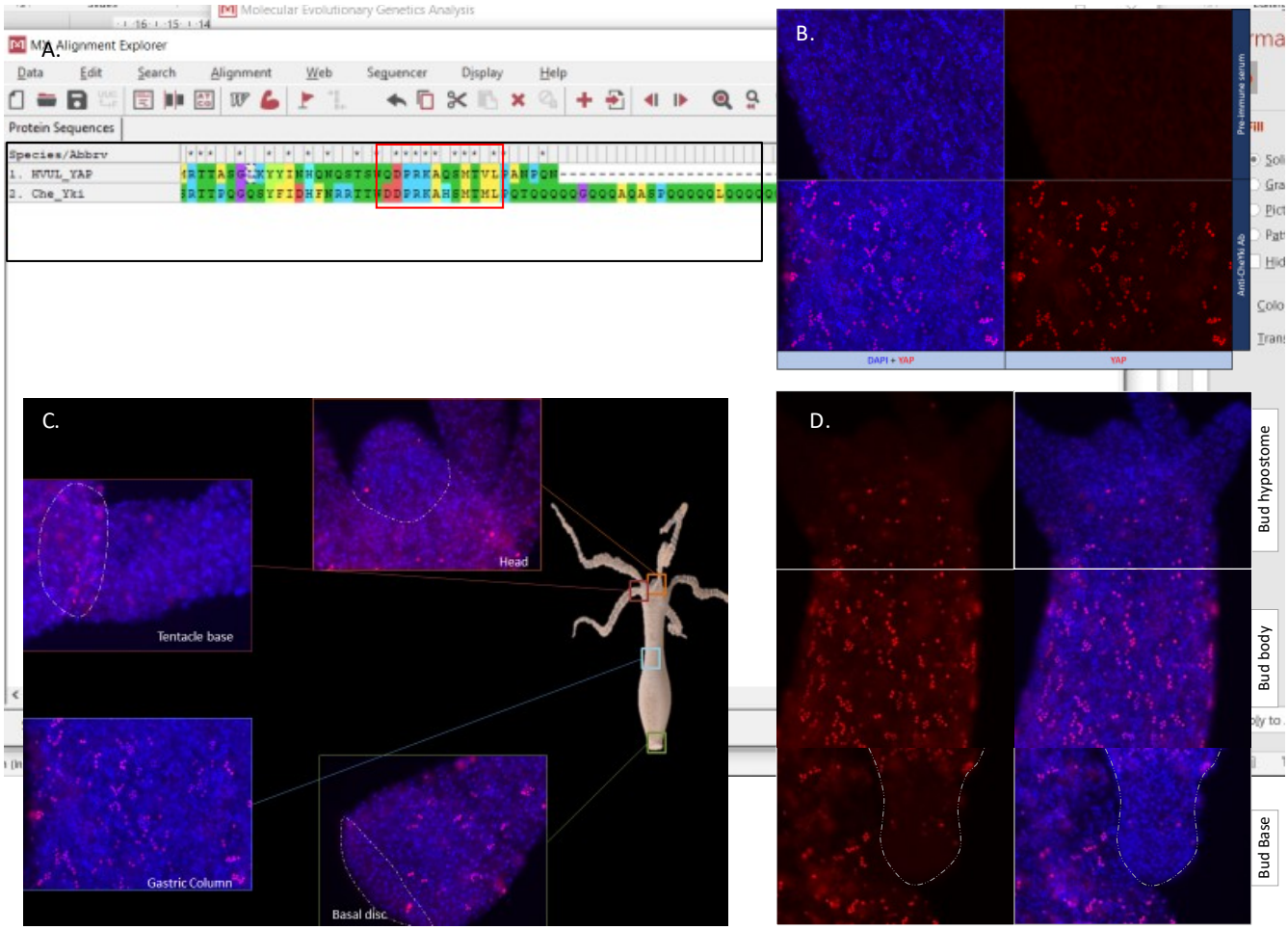

Figure 2.9*:* Immunofluorescence assay of the CheYki antibody. A. Alignment of Hvul_YAP and CheYki protein primary sequences (red box indicate the immunogen peptide used). **B.** IFA of CheYki antibody showing staining pattern of Hvul_YAP against the negative control (pre-immune serum). **C.** Localization of YAP positive cells throughout the adult polyp. **D.** Localization of YAP positive cells at the hypostome, body column and Basal region of mature bud in *Hydra* (dotted line indicates bud-parent boundary).

until 4 hpa is similar to the population seen in the body column of Hydra (green arrows). This changes after 8 hpa as the YAP positive cells at the distal-most region

of regenerating tip assumes a new cell-type characteristic. These cells stop being clustered or paired. They can now be seen as individual cells arranged arbitrarily at the tip. Since YAP is a known mechanotransducers, these cells are either differentiated from the cells migrated from the body column or are cells assuming a new phenotype in response to the mechanical change in the cellular environment

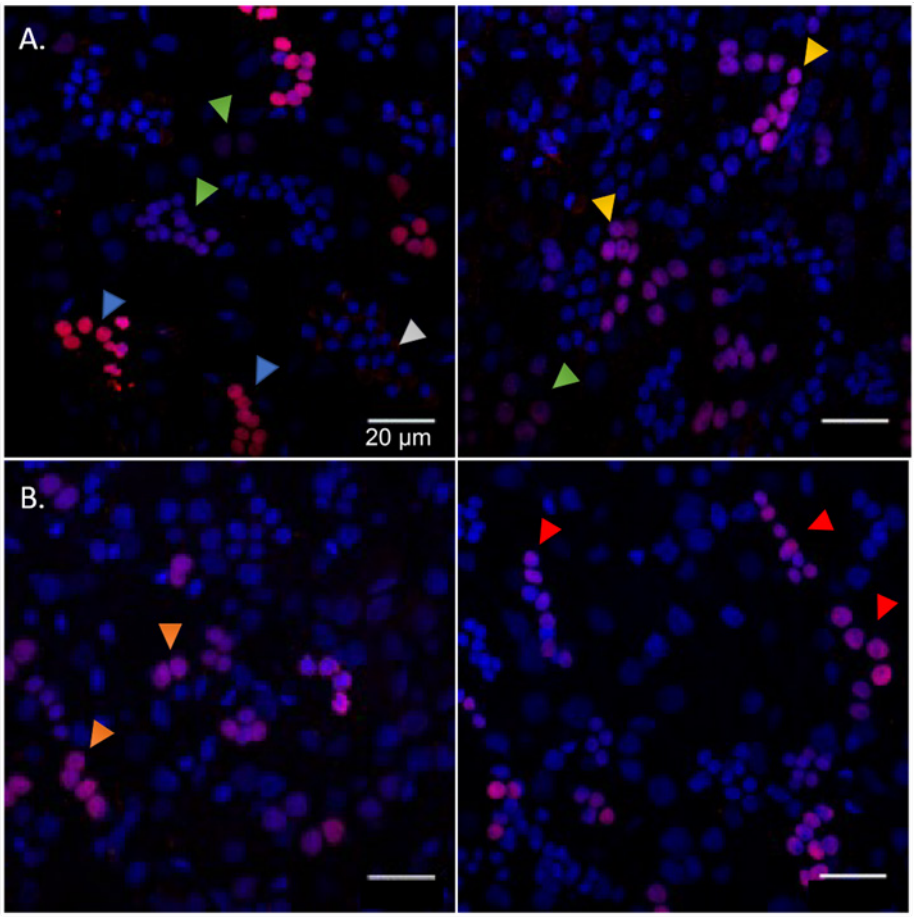

Figure 2.10: Types of YAP expressing cells. Immunofluorescence assay using the anti-Hvul_YAP antibody of macerated cells at 60X. A. This panel shows cell types based on signal intensity or YAP expression level in cells. Blue arrow represents cells with high YAP expression, yellow arrow represents cells with medium YAP expression, cells with a green arrow represents low YAP expression. White arrow indicates extra-nuclear staining in nematocysts. B. This panel shows cell types based on the cellular arrangement. Orange arrows represent cells with duplet or quadruplet arrangement and red arrow represents cells arranged linearly. Red: YAP & Blue: Nucleus (Magenta indicates merged image). Immunofluorescence assay using the anti- Hvul_YAP antibody of macerated cells at 60X. (Scale bar: 20 µm)

due to lack of ECM and physical disruption of cells. The dynamics of YAP positive cells in the regenerating tips indicate that they are recruited to the site of injury early

during the regeneration and are probably early responders of mechanical changes caused due to amputation.

2.3.8 Verteporfin is an effective inhibitor of YAP-TEAD interaction in *Hydra*

Verteporfin (Vp) is a benzoporphyrin derivative small inhibitor generically known as Visudyne. It was originally used for photodynamic therapies in Ophthalmologic sciences[36]. It was later found as a potent inhibitor for YAP-TEAD interaction without photoactivation[37]. The mode of action of Vp is represented in the schematic diagram

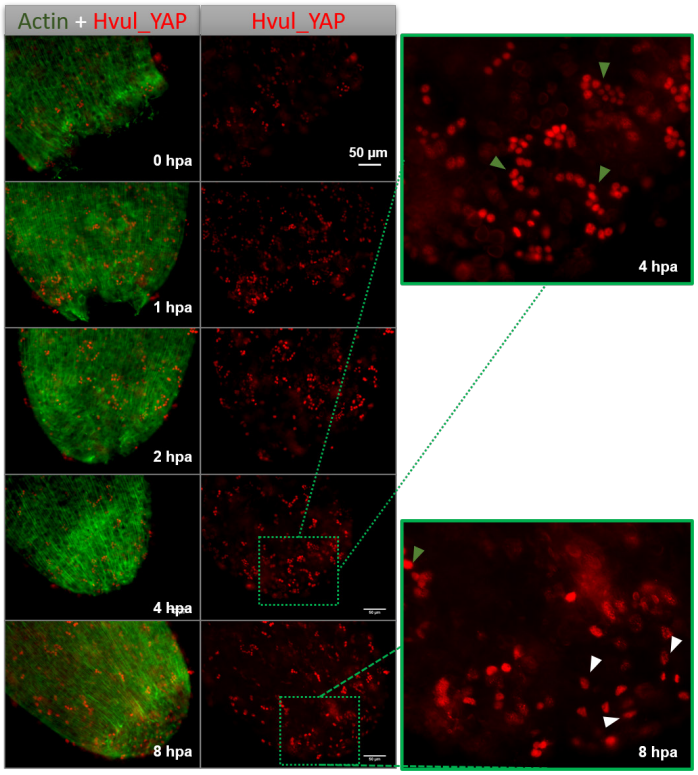

Figure 2.11: YAP positive cells are recruited early to the regenerating tip. Immunofluorescence assay using the anti-Hvul_YAP antibody for head regenerating *Hydra* showing recruitment of YAP positivecells to the regenerating tip. The density of YAP positive cells can be seen increasing at the site of injury from 1 hr post-amputation (1 hpa). White arrows indicated in the zoomed-in image shows the generation of a new type of YAP expressing cells at the regenerating tip by 8 hpa as compared to cell population seen away from the tip or previous time points. (green arrows) Red: YAP & Green: Actin.

shown below indicating disruption of YAP-TEAD interaction by binding of Vp to YAP and preventing it from interacting with TEAD (Figure 2.12). This drug is extensively used for inhibiting Hippo pathway signalling axis in mouse and human cell lines for studying the role of the Hippo pathway in cell and cancer biology. Since the YAP-TEAD interaction domain in *Hydra* and Human are conserved, we tried to assay whether Vp could inhibit Hvul_YAP-Hvul_TEAD interaction as well. We performed a dose response assay to test the optimum dosage of Vp to be administered to *Hydra*

polyps before which it becomes lethal to the animals (Figure 2.13). It was found that a concentration of 5 µM, all the polyps remained healthy and responsive to stimuli (touch and light) but were having a notably reduced flexibility as compared to normal polyps. A concentration of 10 µM and above were lethal to the polyps within 24 hrs of treatment. Therefore, five µM concentration of Vp was used for treating the polyps for the study. A co-Immunoprecipitation of YAP was performed using TEAD antibody to check for a change in YAP-TEAD interaction in *Hydra* upon 3hrs of Vp treatment in adult polyps (Figure 2.14 A). For better results, nuclear lysate from 2000

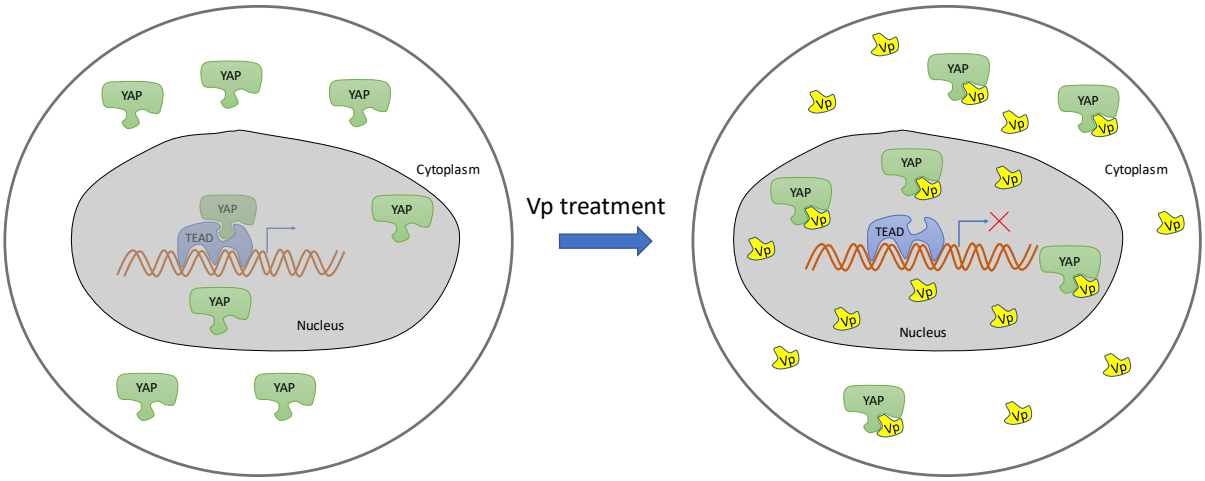

Figure 2.12: Schematic representation of the action of Verteporfin (Vp) on YAP-TEAD interaction. The Hippo effector protein YAP (transcription co-factor) and the transcription factor TEAD interaction in the nucleus is disrupted by Vp by binding to the TEAD-binding domain of YAP. This disrupts transcription of target genes of TEAD.

Vp treated and DMSO treated polyps each was used for the assay. A slight reduction in the amount of YAP pulled down by TEAD was observed by checking the immunoprecipitated proteins on western blot (Figure 2.14 B). Densitometric analysis was done for the same to confirm the visual difference (Figure 2.14 C). It indicated that there was about a 60% drop in the amount of YAP co-immunoprecipitated upon Vp treatment as compared to the DMSO treated. This result indicates that Vp treatment has an inhibitory effect to Hvul_YAP-Hvul_TEAD interaction in *Hydra* as well and can be used for modulating or disrupting the YAP co-transcriptional activity in *Hydra*.

2.3.9 Verteporfin treatment accelerates *Hydra* head regeneration

Regeneration assay was performed to observe the effects of Vp treatment on the regenerative ability of Hydra. The assay was performed as shown in the schematic below (Figure 2.15 A). Accelerated regeneration dynamics were observed in these animals (Figure 2.15 B). Tentacles can be seen growing in the Vp treated polyps at 36 hpa while in control polyps, polyps take about 48-55 hrs to start growing the tentacles. Examination of the regeneration assay by plotting the number of *Hydra* with newly emerged tentacles confirms that control polyps start making most of the tentacle buds after 48 hpa while there is a linear increase of number new buds from

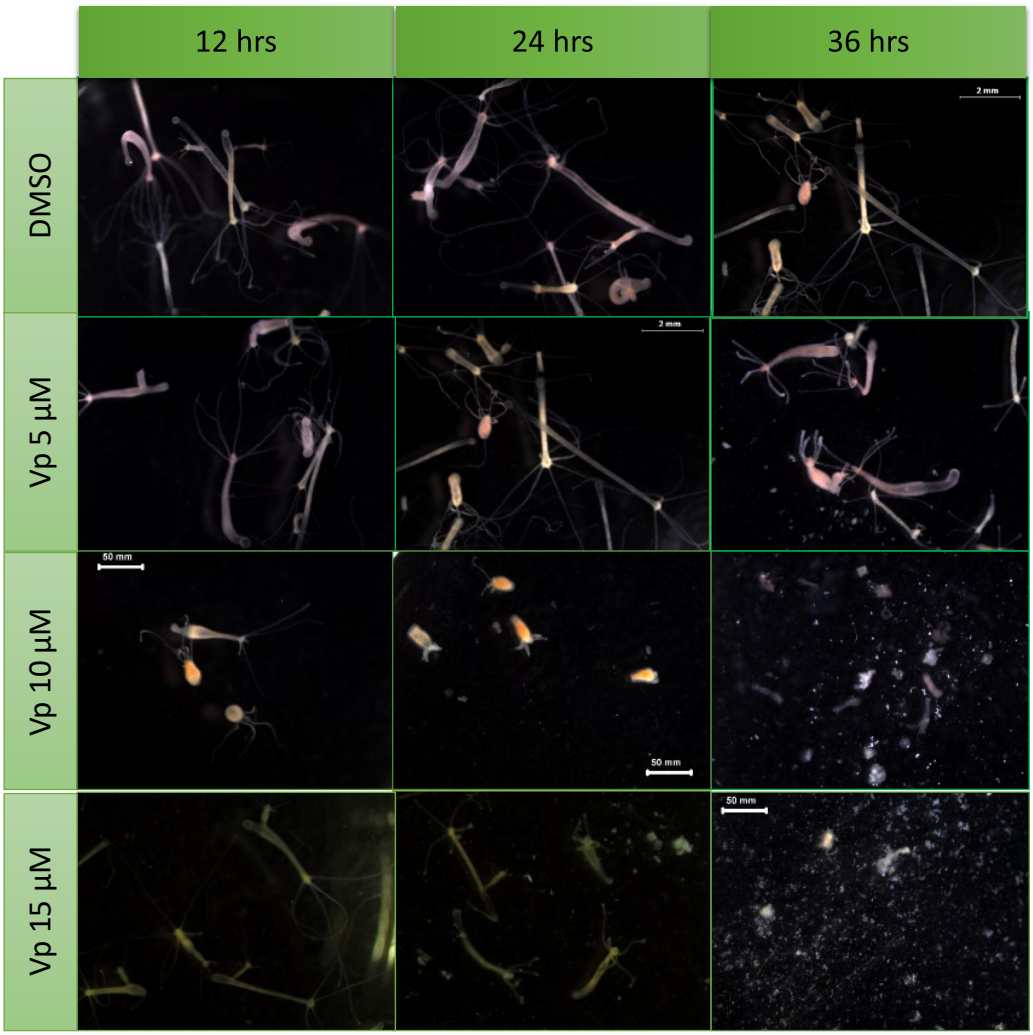

Figure 2.13: Vp dose response assay shows that a concentration of 5 µM is the optimal concentration for treatment on *Hydra* polyps. Effect of Vp treatment on polyps were studied for a concentration of 5 µM, 10 µM and 15 µM. A concentration of 10 µM and above has deleterious effect on Hydra polyps by 24 hours of treatment.

36 hpa in Vp treated polyps and hence giving a jumpstart (Figure 2.16 A).A closer look at the number of *Hydra* with a given number of tentacles (1, 2, 3 & 4 nos.) on a time points clearly indicates that more polyps show three or more tentacles from 36 hpa in Vp treated *Hydra* as compared to control (Figure 2.16 B). This indicates an acceleration in the growth rate of new tentacle due to Vp treatment. These observations hence indicate that VP treatment caused YAP-TEAD interaction inhibition cause accelerated regeneration in *Hydra*. Such an observation seems counter-intuitive since YAP-TEAD signalling is known to be pro-regenerative in more complex organisms like the Zebrafish species *Danio rerio* [38, 39]. One way to reconcile this would be the fact that regeneration in *Hydra* is morphallactic and hence might have a different regulatory network in place to control regeneration without cell proliferation.

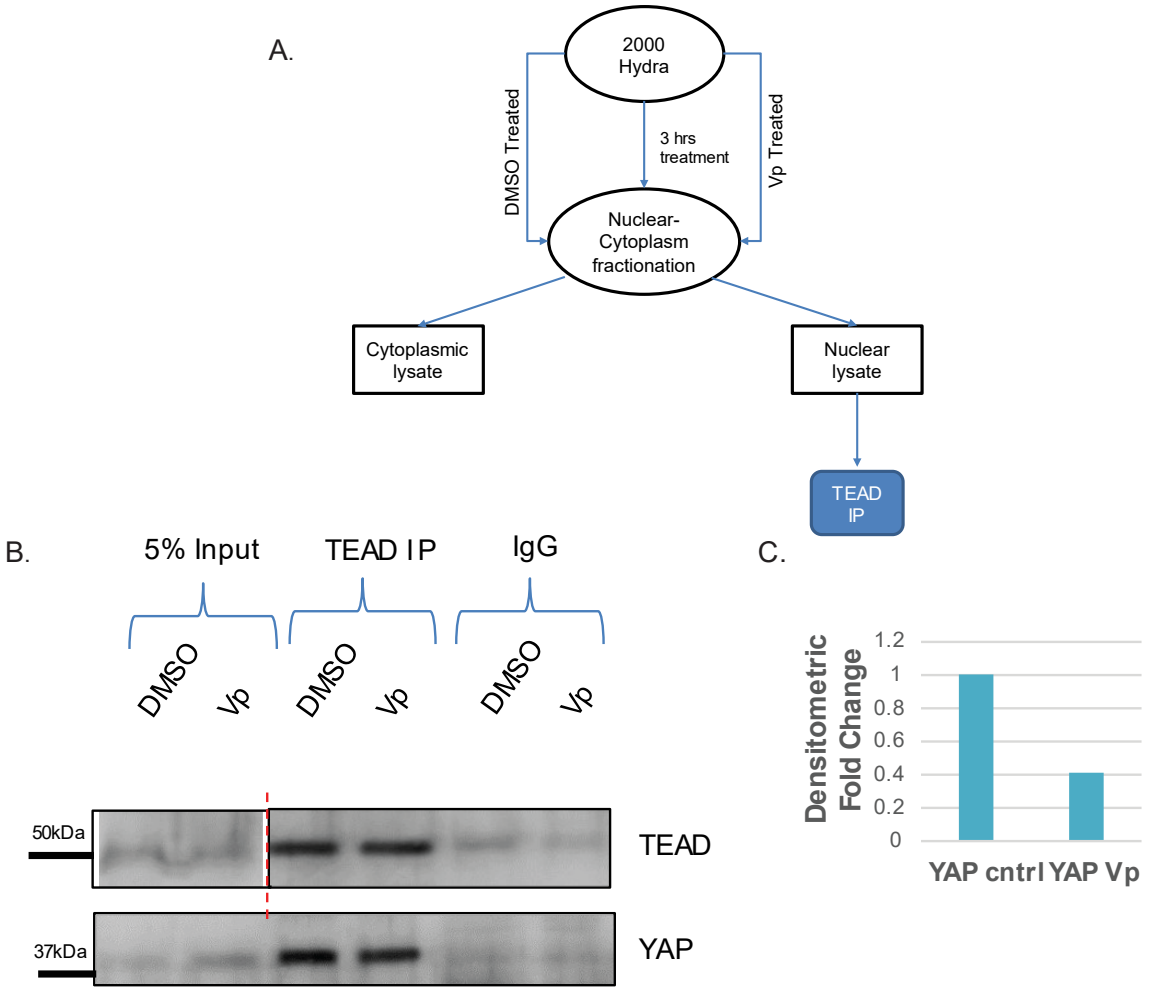

Figure 2.14: Hvul_YAP-Hvul_TEAD interaction is disrupted by Vp in *Hydra*. A) A schematic representation of the experimental set-up of co-IP of YAP using TEAD antibody. **B)** Western blot of TEAD IP of nuclear lysate of Vp treated *Hydra* shows a slight decrease in co-IP of YAP (lower blot)

compared to the DMSO treated *Hydra*. **C)** Densitometry of the western blot clearly shows a 60 % decrease in YAP-TEAD interaction normalized to the TEAD intensities in *Hydra* after Vp treatment (N = 1 & n = 2000).

It is possible that in *Hydra* this signalling pathway controls some kind of a checkpoint which may be in place before the actual regenerative process is initiated. Another possibility is the availability of YAP to now interact with other transcription factors like Runx and SMADs due to the stoichiometric shift produced due to inability of YAP to bind TEAD.

2.3.10 Verteporfin treatment increases the rate of budding in *Hydra*

A budding assay was performed to assay the effects of Vp on budding. Vp treatment leads to increase in the average number of buds per polyps (total number of buds from a set of 48 polyps were calculated and then divided by 48 to obtain the value)

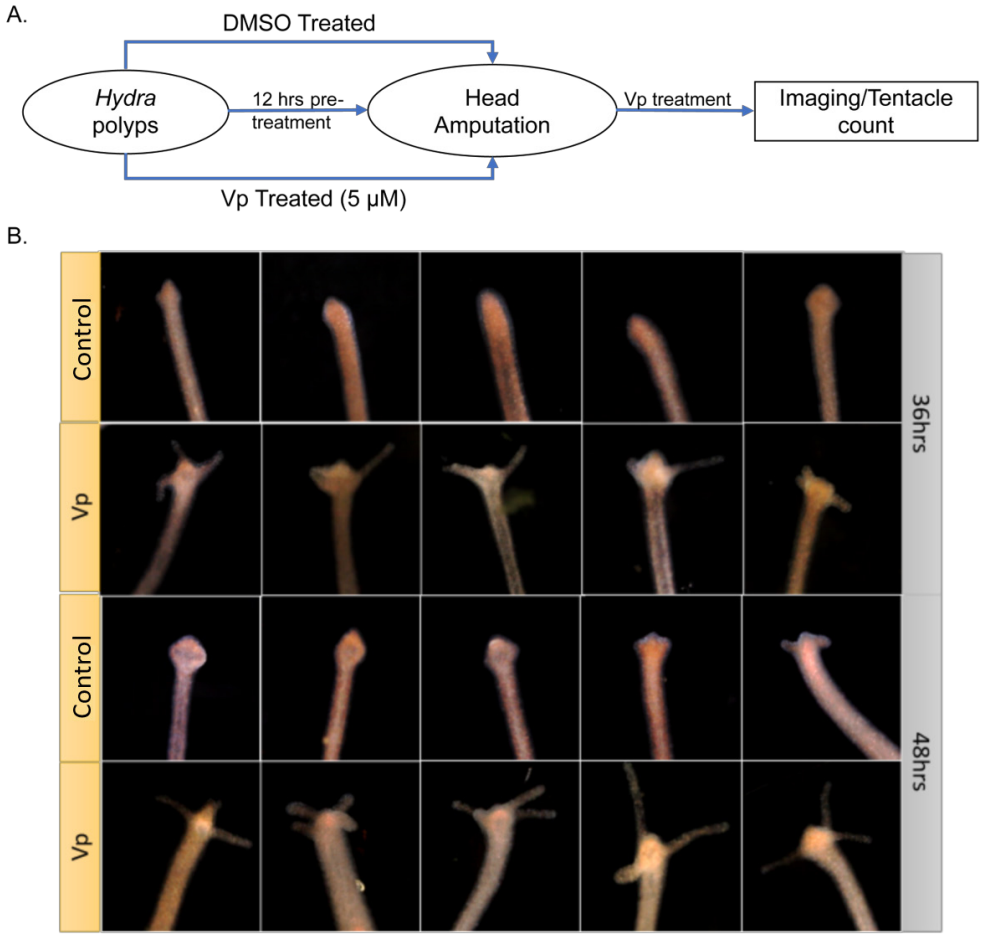

Figure 2.15: Vp treatment causes accelerated regeneration dynamics in *Hydra*. A) A schematic representation of the experimental set-up for the Vp regeneration assay. **B)** image panels showing stages of regeneration in Vp treated and DMSO treated polyps (5 polyps represented) at 36 hrs and 48 hrs post-amputation.

(Figure 2.17 A). To confirm whether this was an effect due to increased rate of bud detachment and not new budding, an assay was performed to quantitate the cumulative number of fallen buds (detached). As can be seen from the graph below, the detachment rate didn't change drastically (Figure 2.17 B). These observations indicate that Vp treatment causes the polyps to produce more new buds than the control. Since the budding rate is indicative of the rate of cell proliferation and maintenance of steady-state[40], Vp treatment is also indicative of increased cell proliferation.

A.

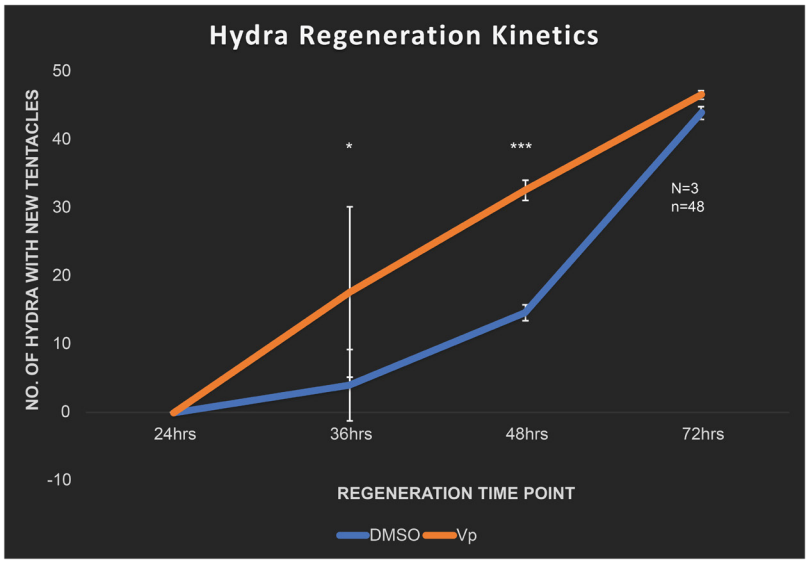

B.

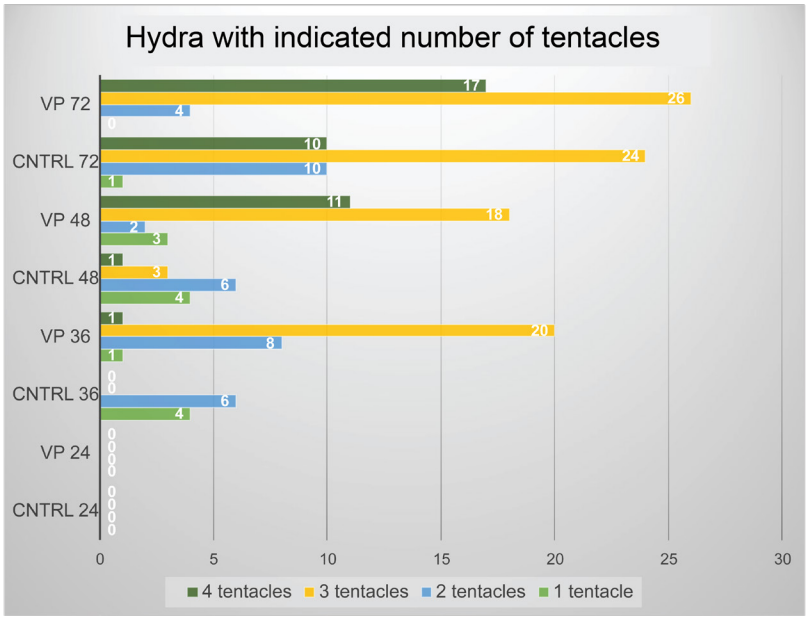

Figure 2.16: Regeneration kinetics of Vp treated *Hydra*. A) This graph indicates kinetics of number *Hydra* with new tentacles from 24-72 hpa in DMSO (blue) vs Vp (orange) treated polyps. N = 3, n =

48 **B)** This graph indicates the number of *Hydra* with the indicated number of tentacles (1, 2, 3 or 4) at a given time point (24, 36, 48 or 72 hpa). Number of experiments (N) = 1, Number of experiments (n) = 48.

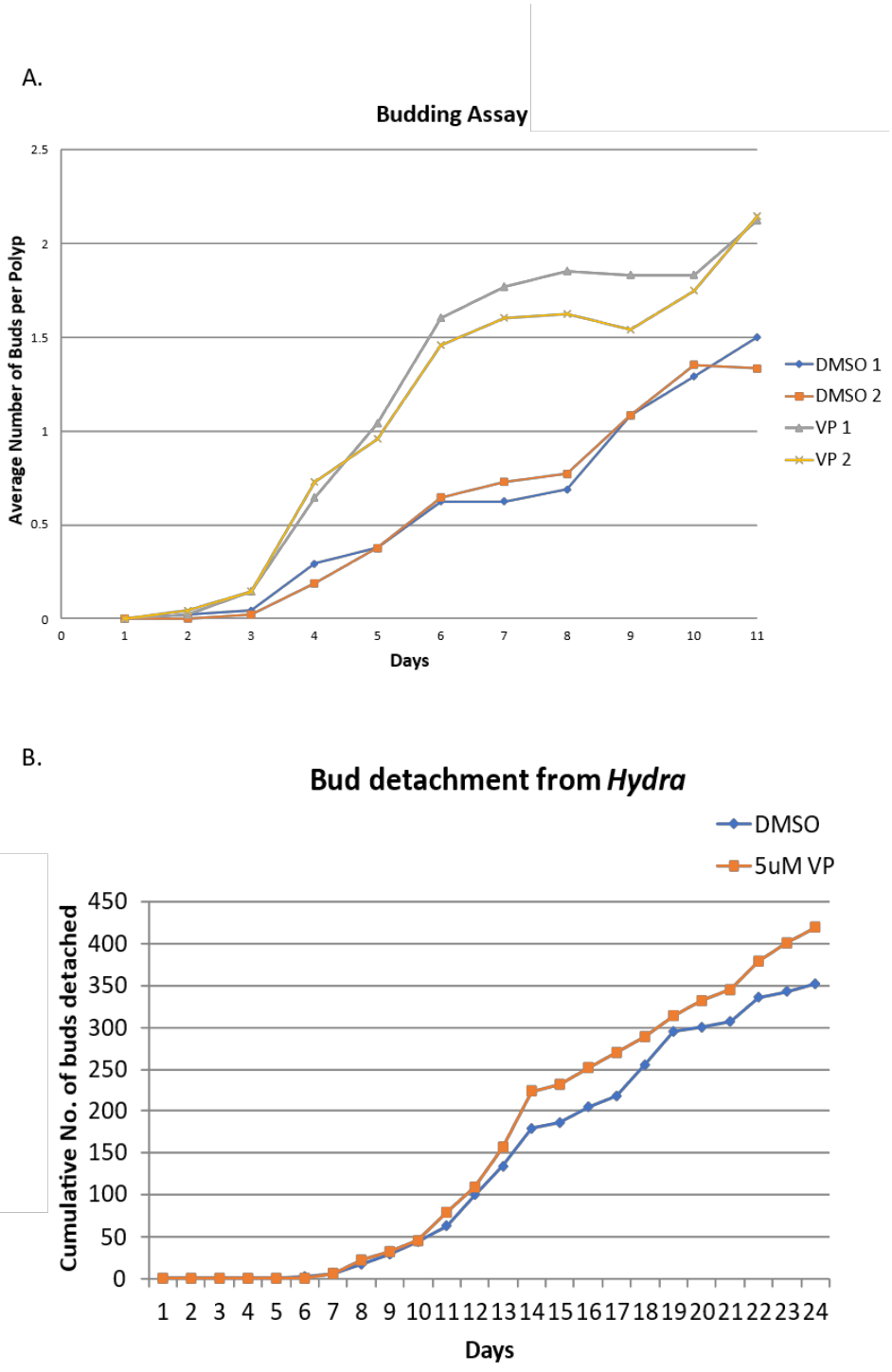

Figure 2.17: Vp treatment causes increased budding rate in *Hydra*. A) This graph indicates kinetics of 2 sets of experiments showing the average number of buds per *Hydra* in DMSO treated vs Vp treated polyps. Number of experiments (N) = 2, Number of polyps per experiement (n) = 48. **B)** This graph indicates the rate of bud detachment in DMSO treated vs Vp treated polyps.Number of experiments (N) = 1, Number of experiments (n) = 48.

.

2.3.11 Verteporfin treatment accelerates Actin dynamics during *Hydra* head regeneration

To understand how early Vp treatment has an effect on regeneration, actin dynamics around early wound healing and re-establishment of trans-cellular actomyosin bundles (myoneme) were examined. F-Actin dynamics in *Hydra* head regeneration was studied by fluorescently staining actin using Alexa 568-conjugated Phalloidin. The wound healing of decapitated *Hydra* can be equated blastopore closure where 'actin cables' surround the gap in tissue and the associated actomyosin contraction leas to closing the wound. Upon Vp treatment, it can be clearly seen that actin-assisted wound closure is at its completion by 0.5 hpa while control polyps take about an hour to do so (Figure 2.18). As can be seen from the figure, the myoneme structures at the wound are broken down in response to injury and it takes about 8-12 hrs for these trans-cellular actomyosin bundles to be reformed. In Vp treated polyps, it is can be seen formed between 1-3 hrs. These observations indicate that

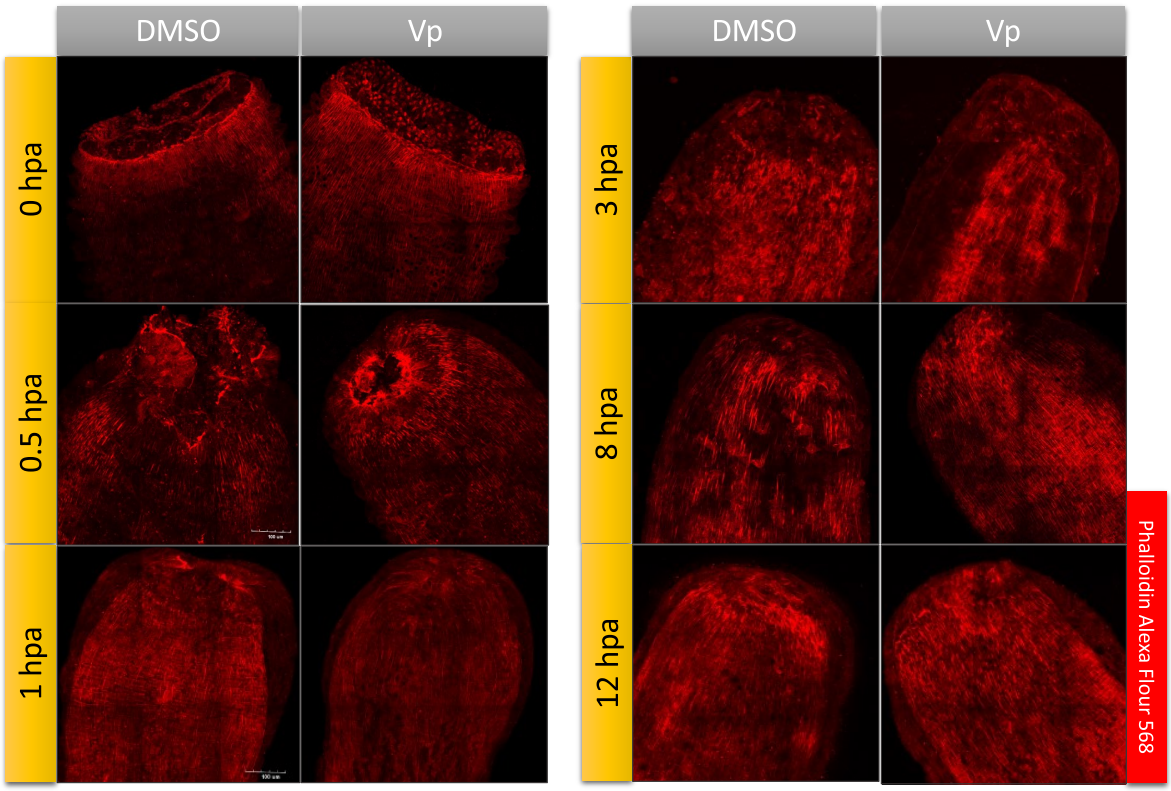

Figure 2.18: Vp treatment leads to faster actin-assisted wound healing and myoneme establishment in *Hydra*. The regeneration time course assay for actin dynamics was performed by staining the fixed polyps at different time points using Phalloidin. The figure shows that actin dynamics is faster in Vp treated polyps. Vp treated polyps shows faster wound closure than the

DMSO treated polyps. The re-formation of myonemes can also be seen to occur earlier in Vp treated animal. Red: Actin

the effects of Vp are not just on cell proliferation and regeneration specific, it also has an effect on wound healing and actin dynamics very early during regeneration.

2.3.12 Vp causes an increase in recruitment of the number of YAP positive cells at the site of injury

Since the Vp treatment caused an accelerated regeneration and wound healing dynamics, the effect of the same on dynamics of YAP positive cell recruitment to the site of injury was assayed by IFA. This assay showed that Vp treated polyps had higher and brighter YAP positive cells being recruited to the regenerating tip (Figure 2.19). A careful examination indicates an increase in YAP positive cell numbers within 1 hpa. Such an increase indicates that inhibition by Vp doesn't affect the YAP nuclear localization or the ability of these cells to migrate or proliferate in response to injury and mechanical changes.

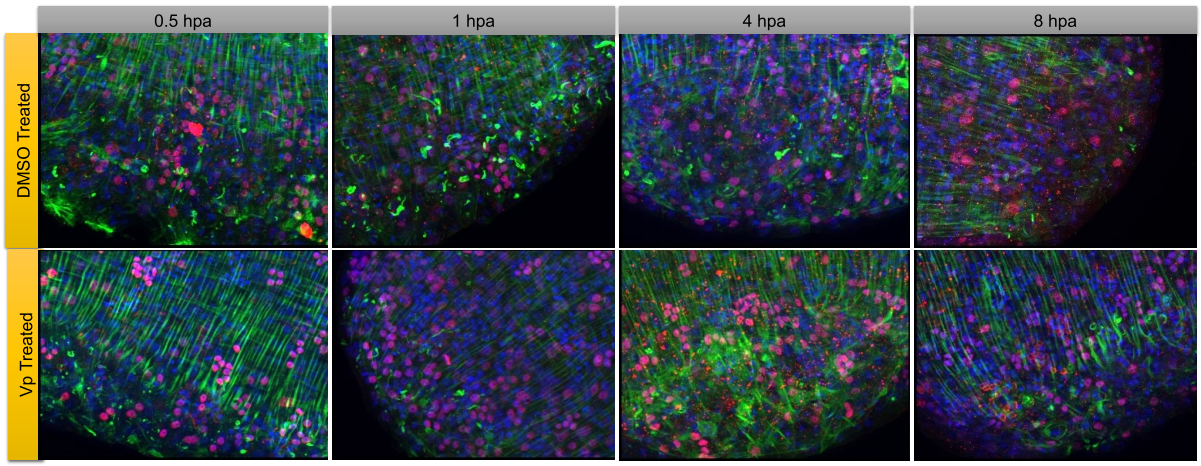

Figure 2.19: Vp treatment causes rapid accumulation of YAP positive cells at the site of injury. Immunofluorescence assay using the anti-Hvul_YAP antibody for head regenerating *Hydra* in Control (DMSO) and (Vp treated) state showing increased recruitment of YAP positive cells to the regenerating tip upon Vp treatment. Higher number of cells can be seen as early as 1 hours post amputation in Vp treated regenerating tips. Red: YAP, Green: Actin & Blue: Nucleus.

2.4 CONCLUSION

Detailed characterization of the Hippo pathway and its components in pre-bilaterians has not been reported to date. There have been few studies reporting the presence of Hippo homologs in these primitive organisms. *Capsaspora owczarzaki,* a single-celled eukaryote is the primitive-most organism predicted to have a complete set of functional core Hippo pathway homologs indicative of a holozoan origin of the functional pathway[41]. Another study confirmed the presence of Yki in a Ctenophore species: *Pleurobrachia pileus* and a Cnidarian species *Clytia hemispherica*[33]. They showed indirectly that the role of Yki in these animals are conserved for the regulation of cell proliferation and growth. In this study, we have for the first time reported and confirmed a complete set of core Hippo pathway components in *Hydra vulgaris* by bioinformatic analysis and cloning. We have also made functional antibodies against Hvul_YAP and Hvul_TEAD which can be used for studying protein-level regulation of these proteins in various context. By performing IFA against Hvul_YAP, we have for the first time reported early recruitment of YAP positive cells to injured tissue in a morphallactic regenerative model system. Using YAP-TEAD inhibitor- Verteporfin, we show that disruption of TEAD transcription activity causes acceleration of regenerative kinetics in amputated polyps. Our observation that Vp treatment accelerates budding rate in *Hydra* indirectly affirms the conserved role of the Hippo pathway in cell proliferation in *Hydra*. The effect of Vp treatment can also alter actin dynamics during head regeneration causing an accelerated wound healing in these polyps. Although, at this point it is difficult to establish a cause or effect link to the accelerated wound-healing observation. A more detailed study involving YAP-GFP transgenic and a CRISPR based *Hydra* transgenic with inducible YAP deletion-mutant incapable of TEAD interaction would be required to shed light on the exact nature of these observations.

2.5 REFERENCES

1. Xu, T., Wang, W., Zhang, S., Stewart, R.A. & Yu, W. Identifying tumor suppressors in genetic mosaics: the Drosophila lats gene encodes a putative protein kinase. *Development* **121**, 1053-1063 (1995).
2. Ni, L. *et al.* Structural basis for autoactivation of human Mst2 kinase and its regulation by RASSF5. *Structure* **21**, 1757-1768 (2013).
3. Deng, Y., Matsui, Y., Zhang, Y. & Lai, Z.-C. Hippo activation through homodimerization and membrane association for growth inhibition and organ size control. *Developmental biology* **375**, 152-159 (2013).
4. Hergovich, A., Schmitz, D. & Hemmings, B.A. The human tumour suppressor LATS1 is activated by human MOB1 at the membrane. *Biochemical and biophysical research communications* **345**, 50-58 (2006).
5. Praskova, M., Xia, F. & Avruch, J. MOBKL1A/MOBKL1B phosphorylation by MST1 and MST2 inhibits cell proliferation. *Current Biology* **18**, 311-321 (2008).
6. Zhao, B., Li, L., Tumaneng, K., Wang, C.-Y. & Guan, K.-L. A coordinated phosphorylation by Lats and CK1 regulates YAP stability through SCFβ-TRCP. *Genes & development* **24**, 72-85 (2010).
7. Varelas, X. *et al.* TAZ controls Smad nucleocytoplasmic shuttling and regulates human embryonic stem-cell self-renewal. *Nat Cell Biol* **10**, 837-848 (2008).
8. Lian, I. *et al.* The role of YAP transcription coactivator in regulating stem cell self-renewal and differentiation. *Genes & development* **24**, 1106-1118 (2010).
9. Karpowicz, P., Perez, J. & Perrimon, N. The Hippo tumor suppressor pathway regulates intestinal stem cell regeneration. *Development* **137**, 4135-4145 (2010).
10. Heallen, T. *et al.* Hippo pathway inhibits Wnt signaling to restrain cardiomyocyte proliferation and heart size. *Science* **332**, 458-461 (2011).
11. Demircan, T. & Berezikov, E. The Hippo pathway regulates stem cells during homeostasis and regeneration of the flatworm Macrostomum lignano. *Stem Cells and Development* **22**, 2174-2185 (2013).
12. Dupont, S. *et al.* Role of YAP/TAZ in mechanotransduction. *Nature* **474**, 179-183 (2011).
13. Fernandez, B.G. *et al.* Actin-Capping Protein and the Hippo pathway regulate F-actin and tissue growth in Drosophila. *Development* **138**, 2337-2346 (2011).
14. Hilman, D. & Gat, U. The evolutionary history of YAP and the hippo/YAP pathway. *Molecular biology and evolution* **28**, 2403-2417 (2011).
15. Chapman, J.A. *et al.* The dynamic genome of Hydra. *Nature* **464**, 592-596 (2010).
16. Reddy, P.C. *et al.* Molecular signature of an ancient organizer regulated by Wnt/β-catenin signalling during primary body axis patterning in Hydra. *Communications Biology* **2**, 1-11 (2019).
17. Madden, T. The BLAST sequence analysis tool, in *The NCBI Handbook [Internet]. 2nd edition* (National Center for Biotechnology Information (US), 2013).
18. Potter, S.C. *et al.* HMMER web server: 2018 update. *Nucleic acids research* **46**, W200-W204 (2018).
19. Letunic, I. *et al.* Recent improvements to the SMART domain-based sequence annotation resource. *Nucleic acids research* **30**, 242-244 (2002).
20. Ren, J. *et al.* DOG 1.0: illustrator of protein domain structures. *Cell research* **19**, 271 (2009).
21. Tamura, K., Stecher, G., Peterson, D., Filipski, A. & Kumar, S. MEGA6: molecular evolutionary genetics analysis version 6.0. *Molecular biology and evolution* **30**, 2725-2729 (2013).
22. Edgar, R.C. MUSCLE: multiple sequence alignment with high accuracy and high throughput. *Nucleic acids research* **32**, 1792-1797 (2004).

23. Jones, D.T., Taylor, W.R. & Thornton, J.M. The rapid generation of mutation data matrices from protein sequences. *Bioinformatics* **8**, 275-282 (1992).
24. Guindon, S. & Gascuel, O. A simple, fast, and accurate algorithm to estimate large phylogenies by maximum likelihood. *Systematic biology* **52**, 696-704 (2003).
25. Chomczynski, P. A reagent for the single-step simultaneous isolation of RNA, DNA and proteins from cell and tissue samples. *Biotechniques* **15**, 532-534, 536-537 (1993).
26. Saiki, R.K. *et al.* Enzymatic amplification of beta-globin genomic sequences and restriction site analysis for diagnosis of sickle cell anemia. *Science* **230**, 1350-1354 (1985).
27. Sambrook, J., Fritsch, E.F. & Maniatis, T. *Molecular cloning: a laboratory manual*. (Cold spring harbor laboratory press, 1989).
28. Corbo, J.C., Erives, A., Di Gregorio, A., Chang, A. & Levine, M. Dorsoventral patterning of the vertebrate neural tube is conserved in a protochordate. *Development* **124**, 2335-2344 (1997).
29. Siebert, S. *et al.* Stem cell differentiation trajectories in Hydra resolved at single-cell resolution. *Science* **365**, eaav9314 (2019).
30. Yang, X. & Yu, X. An introduction to epitope prediction methods and software. *Reviews in medical virology* **19**, 77-96 (2009).
31. Vita, R. *et al.* The immune epitope database (IEDB) 3.0. *Nucleic acids research* **43**, D405-D412 (2014).
32. Takaku, Y. *et al.* Innexin gap junctions in nerve cells coordinate spontaneous contractile behavior in Hydra polyps. *Scientific reports* **4**, 3573 (2014).
33. Coste, A., Jager, M., Chambon, J.-P. & Manuel, M. Comparative study of Hippo pathway genes in cellular conveyor belts of a ctenophore and a cnidarian. *EvoDevo* **7**, 4 (2016).
34. Chen, Y. *et al.* The Hippo pathway origin and its oncogenic alteration in evolution. *bioRxiv*, 837500 (2019).
35. Xue, Y. *et al.* GPS 2.1: enhanced prediction of kinase-specific phosphorylation sites with an algorithm of motif length selection. *Protein Engineering, Design & Selection* **24**, 255-260 (2010).
36. Bressler, N.M. & Bressler, S.B. Photodynamic therapy with verteporfin (Visudyne): impact on ophthalmology and visual sciences. *Investigative ophthalmology & visual science* **41**, 624-628 (2000).
37. Brodowska, K. *et al.* The clinically used photosensitizer Verteporfin (VP) inhibits YAP-TEAD and human retinoblastoma cell growth in vitro without light activation. *Experimental eye research* **124**, 67-73 (2014).
38. Xin, M. *et al.* Hippo pathway effector Yap promotes cardiac regeneration. *Proceedings of the National Academy of Sciences* **110**, 13839-13844 (2013).
39. Hayashi, S. *et al.* Transcriptional regulators in the Hippo signaling pathway control organ growth in Xenopus tadpole tail regeneration. *Developmental biology* **396**, 31-41 (2014).
40. Campbell, R.D. Tissue dynamics of steady state growth in Hydra littoralis: I. Patterns of cell division. *Developmental biology* **15**, 487-502 (1967).
41. Reddy, P.C., Gungi, A. & Unni, M. Cellular and Molecular Mechanisms of Hydra Regeneration, in *Evo-Devo: Non-model Species in Cell and Developmental Biology* 259-290 (Springer, 2019).

3. CHARACTERIZATION OF THE ROLE OF ECM STRUCTURE AND TISSUE STIFFNESS IN REGULATING REGENERATION IN *HYDRA*

3.1. INTRODUCTION

Role of ECM in morphogenesis and regeneration

The extracellular matrix (ECM) in animals has been shown to contribute towards diverse functions including cell-adhesion, mechanical support, cell-signalling, and scaffolding for other extracellular molecules. The transition of unicellular organisms to multicellular organisms requires ECM as a conduit for the integration of various information between cells to function together. Recent studies have shown that the basic 'Toolkit' required to form the basal membrane coincided with the emergence of multicellularity. ECM components are encoded in eukaryotes as early as the unicellular choanoflagellate *Monosiga brevicollis*. More recently, it was reported that a unicellular organism named *Ministeria vibrans* belonging to a filozoan clade of filasterea which diverged earlier to Choanozoa contains a gene similar to collagen IV [1]. This premetazoan origin of collagen type IV indicates that it is possibly the most primitive form of collagens and possibly other components of ECM evolved from this. Earliest phylum reported to have a complete functional set of ECM components and related proteins is in Cnidaria. The fact that ECM components expanded their repertoire from phylum Cnidaria onwards indicates their eumetazoan specific functions. Hence, studying cnidarian ECM can shed light on the role of ECM components in the organization of the body plans of early multicellular organisms.

ECM has been reported to play a crucial role in regulating cell fate and tissue morphology in multiple organisms. The chemical and physical properties of ECM can influence cell behaviour and fate (Figure 3.1). It was reported that solely by varying the stiffness properties ECM, the differentiation fate of mesenchymal stem cells could be altered[2]. The regulation of cell fate by ECM occurs as a function of its interaction with ECM specific cell receptors such as integrins which in turn transmit the information either through chemical signal transduction or mechanically through force distribution via actomyosin networks[3]. ECMs can also regulate tissue morphogenesis by controlling and sequestering morphogenic ligands, including

BMP[4]. These capabilities of ECM can, therefore, make them an important player in 'sculpting' an organism during embryogenesis. A recent study showed that during *Drosophila* embryogenesis, ECM components in the basement membrane are differentially deposited to form a morphogen-like gradient during tissue elongation [5]. This creates an anisotropic resistance to isotropic tissue expansion and hence helps in shaping organs by creating a mechanical imbalance. Another study in sea urchins showed how spatio-temporal incorporation of the hygroscopic chondroitin sulphate proteoglycan causes swelling of ECM which creates hydrostatic pressure for folding of the epithelial sheet during embryonic invagination[6]. The branching morphogenesis in mice salivary gland has been shown to be regulated by fibronectin deposition which signals the tightly packed epithelial cells to lose the E-cadherin contacts and help in the conversion of cell-cell adhesions to cell-matrix adhesions[7].

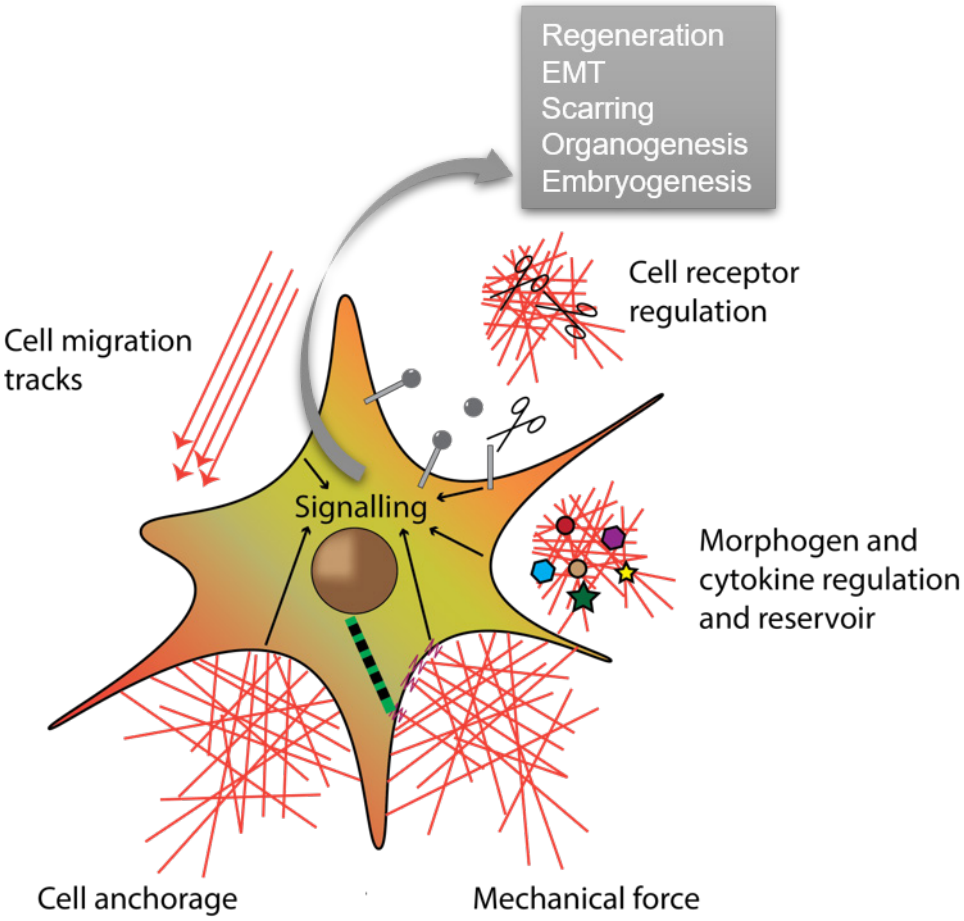

Figure 3.1: Role of ECM in regulating tissue morphogenesis. The figure illustrates how different functions of ECM (depicted in red lines) related effects can alter tissue behaviour required for regeneration, epithelial-to-mesenchymal transition (EMT), scarring, organogenesis or embryogenesis

through signal transduction. Cell-ECM adhesion is required for anchorage dependent pathways. The mechanical properties of ECM will cause mechanotransduction effected through actomyosin (green rod with black striations) regulation. Various morphogens and cytokines (represented as circles, hexagons and stars) like BMP, WNT etc. can be stored and regulated in ECM by controlling its diffusion and accessibility to cellular recptors. ECM also contains various MMPs (represented as scissors) capable of regulating ECM and cell receptor availability by cleaving the extracellular domain of the receptors. ECM is also acts as a track to help in cellular migration.

In mammalian systems, ECM has been reported to be crucial for regeneration and sustaining cell proliferation and differentiation post-injury. Mammals possess very limited potency to regenerate their lost or injured tissues. Skeletal muscles are among the few tissues that mammals can regenerate, and it was found that upon muscle degeneration, it leaves behind a hull of basement membrane ECM which acts as a scaffold to facilitate myofiber fusion[8]. In mammals, early stages of skeletal muscle regeneration are associated with downregulation of laminin and collagen type I to facilitate de-differentiation of satellite cells to form myoblasts[9]. Fibronectin, Hyaluronic acid and Tenascin-C are shown to be up-regulated during the same period. Another study showed that by altering the ECM stiffness of a three-day old mouse, it was possible to restore the ability to regenerate heart which is lost after day 1[10]. Certain species of mammals are reported to have an astonishing capability to regenerate. For example, the African spiny mouse (*Acomys* sp.) which can loose and regenerate up to 60% of its dorsal surface including hair, follicle, skin, sweat glands etc. Here, It was shown that laminin and collagen type I molecules are down-regulated while the cells de-differentiate and later upregulated during cellular differentiation[11]. Another study which looked at the regeneration of skeletal muscle of tibialis anterior in *Acomys* found that it has higher collagen type VI in the regenerating tissue as compared to *Mus* sp.[12]. This difference renders a softer biomechanical property to the *Acomys* tissue which is believed to be important to achieve a faster, scar-free regeneration with higher macrophage infiltration, low expression of inflammatory and fibrotic genes at the site of injury. A recent study has demonstrated that fibronectin in the niche was necessary for maintaining a functional muscular stem cell population capable of regenerating lost muscular tissue. The reconstitution of fibronectin levels in aged stem cell niche is enough to remobilize and restore functional muscular stem cells[13].

In axolotls, skeletal muscle regeneration follows similar regulation of collagen type I, laminins, fibronectin, hyaluronic acid and tenascin-C as in mammals in the early phase of regeneration to allow de-differentiation of satellite cells[14-16]. In *Xenopus* tadpoles, it has been reported that Hyaluronic acid plays an important role in the regeneration of tailbud after amputation[16]. An adequate level of hyaluronic acid in the regenerating tail bud is required for sustaining mesenchymal cell proliferation.

Studies in zebrafish also indicate a similar role of ECM in regeneration. Fin regeneration studies indicate an early upregulation of fibronectin, hyaluronic acid and tenascin-C, which seems to be a conserved mechanism across different organisms in the vertebrates[16]. Additionally, Hapln1a, hyaluronan and proteoglycan aggrecan are also upregulated during the process. On the other hand, laminin levels do not show any appreciable changes during fin regeneration in zebrafish. Fibronectin is necessary for heart regeneration and is shown to be expressed by epicardial cells. The cardiomyocytes start to express itgb3 receptors which can respond to the presence of fibronectin at the site of injury for a successful heart regeneration[17]. A study on the caudal fin regeneration indicates a crucial role of collagen type IV and specific matrix remodellers from the MMP and TIMP family of proteins[18].

Regulation of ECM during *Hydra* regeneration

ECM in cnidarians are arranged discretely sandwiched between the two germ layers. Since they were initially noted as a gelatinous noncellular layer and found between the germ layers, they were termed as mesoglea. *Hydra* mesoglea is 0.5 - 2 µm thick depending upon its position in the body. The mesoglea is a trilaminar structure dividing the two epithelia[19]. The epithelial cells are in direct contact with the basal lamina which sandwiches a thick central layer of interstitial matrix. The mesoglea also has trans-mesogleal pores which enable inter-epithelial cellular interactions via cell processes running through them[20]. ECM secretory dynamics have been studied using the *Hydra* regeneration model. It is known that post-amputation there is a retraction of mesoglea, and its restoration is required for initiation of regeneration[21]. Post-amputation, loss of ECM is followed by sealing of wound which causes direct contact of ectoderm and endoderm cells, leading to change of morphology of these cells from being cuboidal or columnar to flattened (Figure 3.2)[20, 21]. During regeneration, within 3 hours, all the components of ECM are actively transcribed by

their respective cells and then by 7 hours components of the basal lamina - endoderm secretes laminin and HyCol IV such that basal lamina is formed and hence leading to regaining the normal cuboidal morphology of the cells. Contact of the basal lamina with receptors of the ectodermal cells results in the secretion of components of the interstitial matrix and hence leading to complete formation of mesoglea within 20 hrs post-amputation[22].

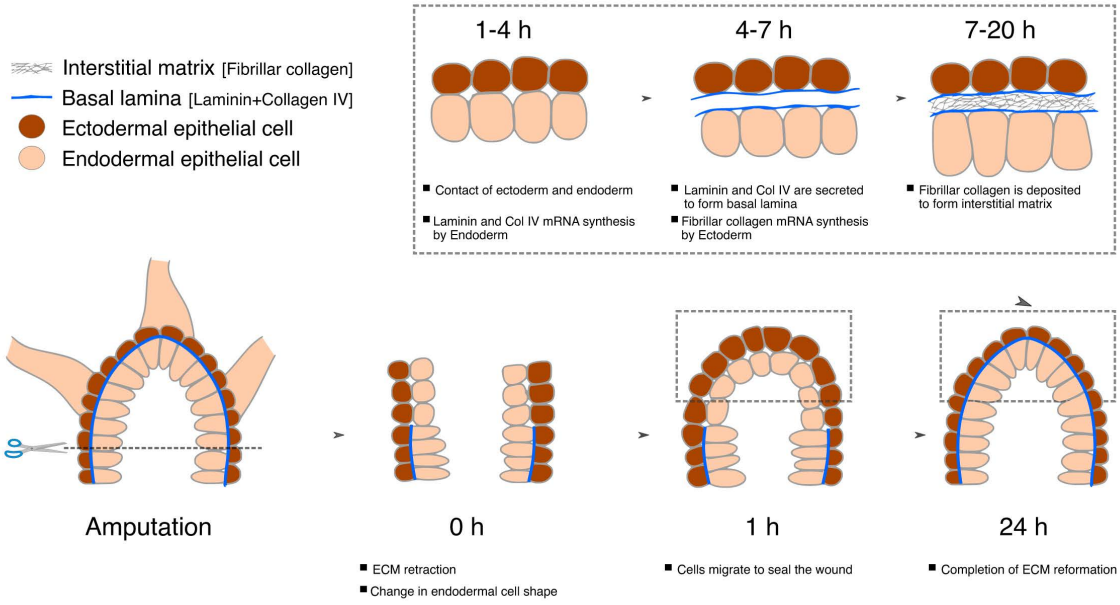

Figure 3.2: Cellular and structural changes in mesoglea during head regeneration in *Hydra*. ECM is retracted immediately upon decapitation followed by a change in cell shape. This is succeeded by wound closure and secretion of ECM components completing the early stages of head regeneration. (Reproduced from Reddy et al., 2019[23]).

During the regeneration of re-aggregated cells, it is reported that mesoglea formation takes place immediately after the reorganization of ectoderm and endoderm cells into a lumen[24]. The mesogleal components are first secreted by 12-17 hrs of aggregation, and the maturation of the mesogleal structure is reported to be completed by 48-72 hrs[25]. The morphogenetic processes required for regeneration of reaggregated cells succeed the mesoglea formation, and the formation of a mature mesoglea is an absolute necessity for the success of regeneration[25]. It has also been reported that disruption of any of this process either by knockdown of the ECM components or by inhibiting their biosynthesis chemically or by preventing ECM-receptor interaction, the process of regeneration is arrested[25]. Therefore, it seems very plausible that the important role of ECM in regulating regeneration and other

tissue function evolved very early during evolution. As can be noted from above, the precise mechanistic role of ECM during regeneration in more complex organisms is unclear despite strong pieces of evidence showing its importance. A highly regenerative model system such as *Hydra* with its less complicated tissue system and signalling networks could be crucial in shedding light to ECM mediated regulation. Studies focussing on biomechanical aspects of ECM in *Hydra* could unravel various aspects of their role in physiological regulation and how it evolved to perform the more complex function in a system such as a human. The previous chapter showed that the accelerated head regeneration from Vp treatment was also accompanied by faster actin dynamics and stiffer or less flexibility in polyps. These factors point towards an a possibility of active biomechanical regulation of ECM during *Hydra* head regeneration. Keeping in consideration that Hvul_YAP expressing cells are recruited early during regeneration and the fact that the Hippo pathway is a known mechano-sensitive signalling pathway, a detailed ultrastructural and biomechanical study was undertaken. This chapter discusses our findings from the ultrastructural and biomechanical study undertaken to elucidate how acceleration of head regeneration by disruption of YAP-TEAD interaction using Vp treatment is a function of increased tissue stiffness due to mesogleal ‘fibrosis’.

3.2. METHODS AND MATERIALS

3.2.1. Scanning Electron Microscopy (SEM) Imaging of *Hydra*

Anaesthetized polyps (using urethane (Sigma)) were fixed using EM fixing solution (2.5 % Paraformaldehyde (Electron Microscopy Sciences - EMS), 2.5 % Glutaraldehyde (EMS) and 0.1 M Cacodylate buffer (Sigma)) at 4 ℃ overnight. The polyps were then washed in 0.1 M Cacodylate buffer thrice. These polyps were then embedded in 5 % Agar. These were then cut into cubes of 1 cm^3 one polyp. These cubes were then mounted on a vibratome (Leica VT1200 S) and sectioned into 200 µm slices. These were then treated with 1 % Osmium tetroxide (Sigma) (5 mins) followed by 3 x washes with 0.1 M Cacodylate buffer and 3 x washes with Milli Q water. This was followed by treatment with 1% Tannic acid (EMS) (5 mins in dark) and 1 % Uranyl acetate (EMS) (30 mins in dark) sequentially with 3 x washes of Milli Q purified water after each treatment. These sections were then dehydrated by washing them with ice-cold ethanol with increasing concentration for 5 mins each: 30%, 50 %, 70%, 90 %, 96% and finally 100% ethanol at RT. The dehydration of these sections was then completed by drying them at CO_2 critical point using a critical point dryer (Leica CPD030). The dehydrated sections were then mounted on carbon-taped stubs. These were then coated with 5 nm platinum by sputtering. The coated samples were then imaged using Zeiss Ultra 55, Zeiss Sigma 500 or Zeiss Supra 55 FEG electron microscopes at 2-3 kV at 4-14 mm working distance.

3.2.2. Transmission Electron Microscopy (TEM) imaging of *Hydra*

The regenerating polyps were fixed and stained according to the protocol described for SEM. The stained were then dehydrated in an ethanol gradient similar to the one used for SEM. The polyps in 100 % ethanol were then replaced by 100 % Acetone and given 2 x washes for 10 mins each at RT. The polyps were then processed for resin infiltration (Epon/EMbed 812 EMS): 25% mix of Epon in acetone overnight, 50% mix of Epon in acetone for 8 hrs, 75% mix of Epon in acetone overnight, 100 % Epon for overnight & fresh 100 % Epon change incubation for 1 hr. The polyps were then transferred into the resin moulds with appropriately labelled paper prints. The polyps were oriented according to the sectioning requirements and then polymerized in a hot air oven at 70 ℃ for 12 hrs. These polymerized blocks were then sectioned into 70 nm slices from the regenerating tip using Leica EM UC7 ultramicrotome. The

slices were then mounted on carbon-coated grids (5 nm thick, 300 mesh type from EMS). They were then stained with Lead citrate (Thermo Scientific) for enhancing contrast. These sections were then imaged using FEI Tecnai T-12 Spirit Biotwin TEM (Thermo Scientific).

3.2.3. Measurement of *Hydra* tissue stiffness using an atomic force microscope (AFM)

Attaching bead to the AFM lever:

A tipless cantilever with a glass bead attached to its free end (stiffness ~ 0.2 N/m) was used for AFM measurements. The diameter of the glass bead is 20 µm (Figure 3.3 A). The attachment was accomplished using the micromanipulation available with the AFM. A small amount of UV curable glue (Dymax 431) was spread on the coverslip. Using the servo control of the AFM, the end of the tipless lever was lowered onto the glue. A drop of glue was picked up on the lever and lowered again on a bead. The lever was maintained under positive load and UV light was directed at the bead-lever assembly. After curing the lever was pulled back from the surface along with the bead (Figure 3.3 B). The elastic modulus of the glue is 570 MPa and it is not deformed while pushing on the tissue. Before performing force-distance measurements, the cantilever is calibrated using BSA coated glass surface by thermal tuning.

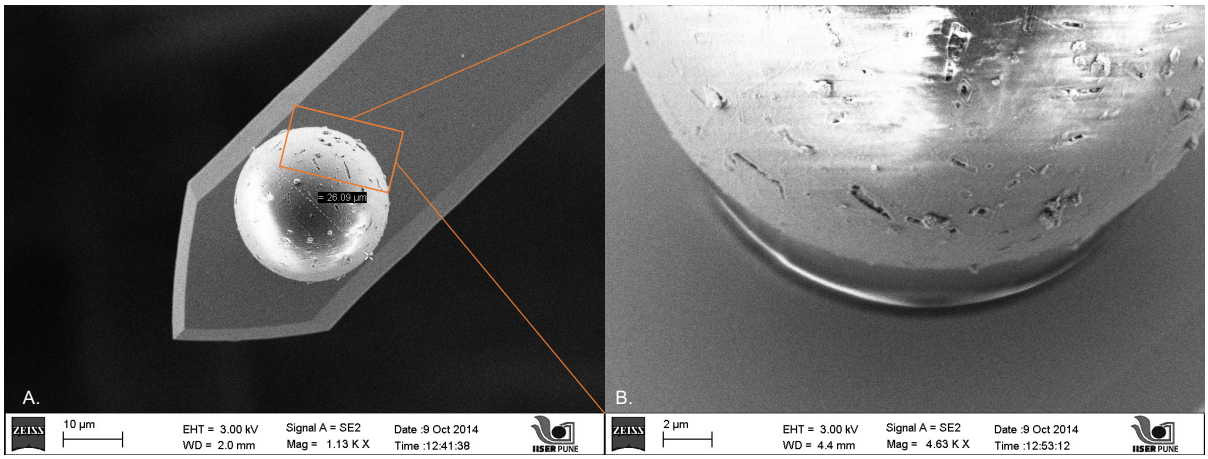

Figure 3.3: Attachment of glass beads to the cantilever. A. The figure shows the SEM image of the final placement of the 20 µm glass bead on the cantilever **B.** Magnified image showing the UV-cured glue at the bead-cantilever interface.

Measurement of tissue stiffness using AFM:

Since *Hydra* is an aquatic organism and posesses a protective slippery glycocalyx covering on its body, it is difficult to use adhesives to fasten them. *Hydra* body is unstable for mechanical measurements if it is not strongly adhered to the glass surface. A thin layer of BSA was coated on the glass for strong adherence of the tissue. Young's modulus of various tissues typically ranges from 100 Pa to 1 MPa. The Young's modulus of glass is of the order of 10-100 GPa. The coating of BSA alters it to some extent. Assuming the glass-glass contact to be infinitely stiff compared to the glass-tissue contact - a reasonable assumption since it is 10,000 times stiffer, the slope of the curve in the contact region for glass and BSA coated glass is nearly one implying no deformation. The slope of the curve on tissues is much less suggesting a certain amount of deformation. We use glass-glass contact for calibration of deflection sensitivity and the subtraction of cantilever deflection from the push given by the piezo extension yields deformation in the tissue. The force is calculated by multiplying the cantilever deflections by its stiffness. The force versus deformation curve is then fitted with the Hertz model.

$$F = \frac{E}{1-v^2}[\frac{a^2+R_s^2}{2} ln \frac{R_s+a}{R_s-a} - aR_s]$$

$$\delta = \frac{a}{2} ln \frac{R_s+a}{R_s-a}$$

Where F is the measured by the cantilever possessing the bead, which is pressed against the tissue. R is the bead radius, the delta is the deformation in the tissue, E is the Young's modulus and v is the Poisson ratio.

Hertz contact mechanics theory works for non-adhesive elastic contacts. It is important to establish that the pressing of bead over the tissue conforms to this requirement. For small loads (< 1 nN) the extend and retract curves do not show hysteresis indicating that the contact is non-adhesive and elastic.

Before AFM measurements, *Hydra* polyps were cultured and starved for a day to eliminate food material. They were relaxed with urethane (2% for 2 mins) and fixed immediately with glutaraldehyde (4%) for 30 mins. For regeneration assay, the polyps were amputated and then fixed after indicated time points. The coverslip (diameter: 22 µm) was coated with a layer of bovine serum albumin (BSA, 10

mg/ml), and this layer was allowed to dry. The coverslip was then placed in the AFM fluid-cell. A *Hydra* polyp was placed over the BSA layer, and a small amount of BSA was added to keep it from drying. As the BSA dried, the connections formed between the *Hydra* polyp and the surface by BSA were fixed using glutaraldehyde for 2 min and water was added in fluid cell for performing AFM measurements.

3.2.4. Dipyridyl treatment

2,2'-Dipyridyl (DP) is an inhibitor of lysyl oxidase[26]. Lysyl oxidase is an enzyme which cross-links two adjacent fibrillar collagens to make bundles. Inhibition of lysyl oxidase prevents the components of the ECM from polymerizing. DP has been shown to effectively inhibit Hydra ECM[27]. The concentration of 100 μM was shown to be useful in other strains of Hydra. To test the validity of this result and to study the behaviour of *Hydra* under this drug concentration from 50 μM to 200 μM DP in Hydra medium were tested and deleterious effects were detected under physiological conditions until 175 μM 24 hrs in treatment. We found the 100 μM concentration was sufficient to block the regeneration process in *Hydra* and hence used this concentration throughout this study.

3.3. Results and Discussion

3.3.1. Vp treatment alters the morphology of fibrillar collagens in Hydra mesoglea

Scanning electron microscopy (SEM) and transmission electron microscopy (TEM) protocol for *Hydra* tissue was standardized. A careful examination of the mesoglea ultrastructure in *Hydra* across the body revealed a differential organization of mesoglea between head and body region of the polyp (Figure 3.4). Using ImageJ, we found that the head region was wider (head mesoglea width - 2043nm ±744nm) and more densely packed mesoglea as compared to the body column (body mesoglea width - 750 ±205 nm). The thickness of the collagen fibrils was also found to be higher in the head region (41 nm ± 15 nm) as compared to the body (19.1 nm ±4.5nm). These findings indicate a higher cross-linking of fibrillar collagens in the interstitial matrix of the head region in *Hydra*.

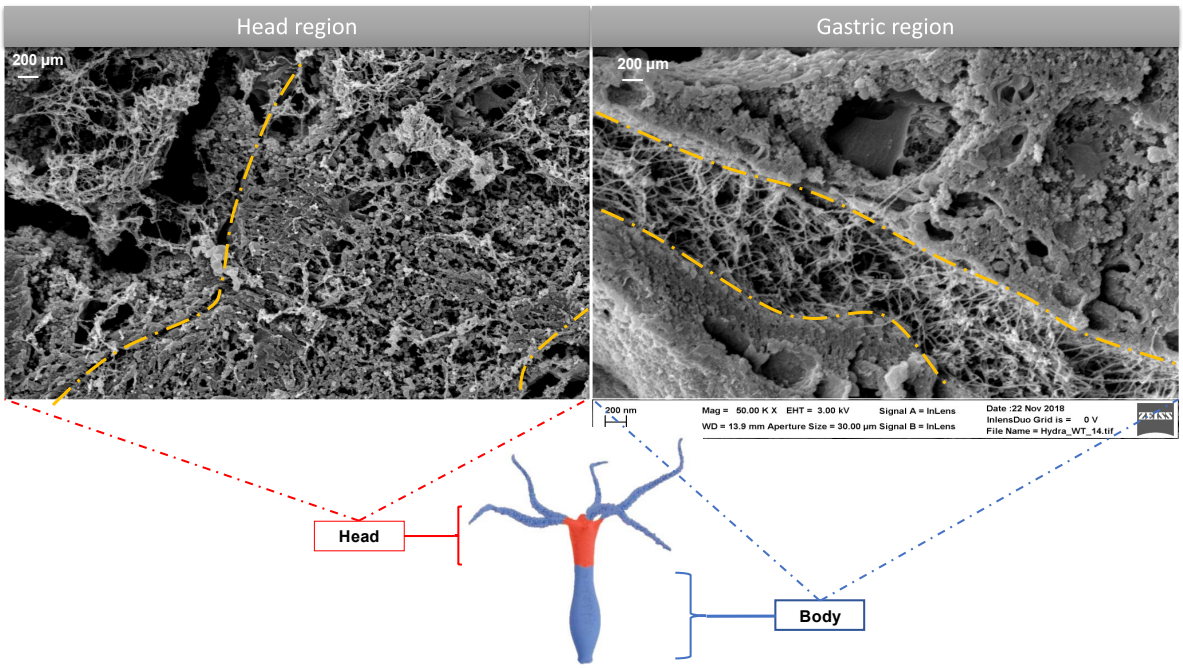

Figure 3.4: Differential organization of mesoglea in the head versus body regions. This image panel shows that the mesoglea in the head region is thicker than that of the gastric region. The collagen fibrils in the head are densely packed (panel on the left) as compared to the gastric region (panel on the right).

Considering the Hippo pathway has mechano-regulatory functions, we analysed the ultrastructural changes in mesoglea between Vp treated and DMSO treated *Hydra*. To this effect, we treated polyps for 12 hrs with Vp and performed SEM imaging. Mesoglea in Vp treated polyps were found to be more densely packed and narrower than the DMSO treated (Figure 3.5). This mesogleal packing seemed so compressed that the fibrillar component in the mesoglea is not visible at all.

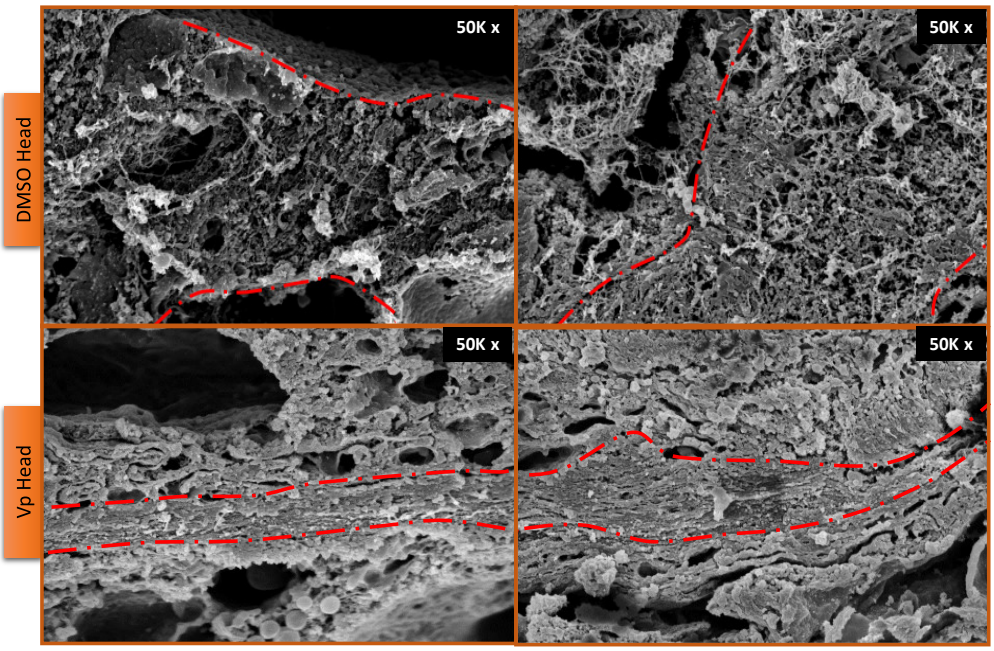

Figure 3.5: Vp treatment causes dense packing of ECM in the mesoglea. This transverse section (T.S.) of a polyp shows that the mesoglea in the head region is narrower and densely packed in Vp treated polyps.

To better understand what is happening in the mesoglea, TEM was performed to assess the ultrastructure of collagen fibrils in Vp treated polyps. TEM imaging allowed to see fibrils clearly at much higher magnification (Figure 3.6). A comparison of DMSO- treated polyps with Vp treated polyps clearly showed that the individual collagen fibrils in the mesoglea of Vp treated are short and highly branched while that control is long and less branched. This observation explains why the mesoglea is dense and narrow since this kind of structure can allow close packing of collagen fibrils leading to compression of the mesoglea. This also may complement the observation that the Vp treated polyps are stiffer than normal polyps. Taken together, the ultrastructural study of *Hydra* mesoglea reveals increased crosslinking, branching and shorter fibril length of fibrillar collagens upon Vp treatment.

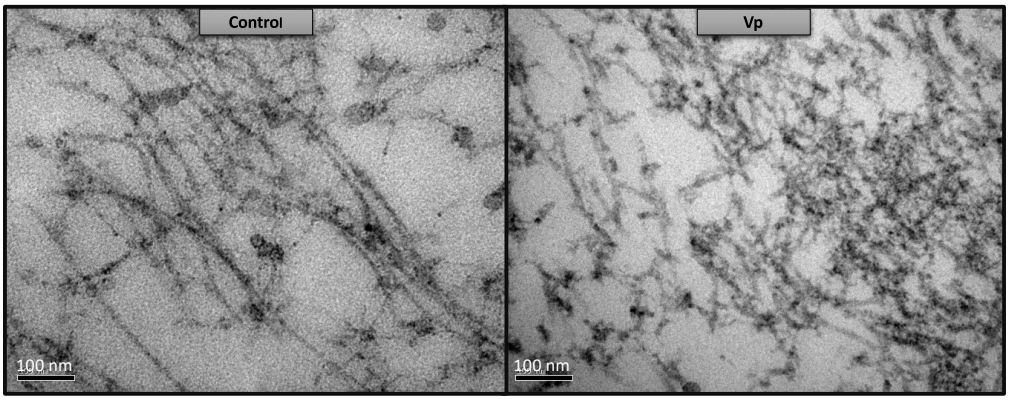

Figure 3.6: Vp treatment leads to shorter and more branched collagen fibrils in mesoglea. Longitudinal section (L.S.) of the polyp shows the differential organization of collagen fibrils in Vp and DMSO treated (control) *Hydra.* Scale bar = 100 nm.

3.3.2. Regenerating tip shows mesoglea in Vp treated polyps are less elastic

To further elucidate the effect of Vp treatment on mesoglea during regeneration of head amputated polyp, a SEM imaging of the retracted mesoglea immediately after decapitation was performed. A 2500X magnified image of the longitudinally sectioned 12 hr Vp pre-treated polyp at 2 hrs after amputation shows a reduced degree of retraction of mesoglea in Vp treated polyps as compared to the control (Figure 3.7). This data, combined with the observation noted in previous sections indicates that the mesoglea is more rigid than the control polyps after 12 hrs of Vp treatment. An amputation event after this causes less pronounced mesogleal retraction in these polyps and probably needing lesser time to repair the lost ECM from the wound.

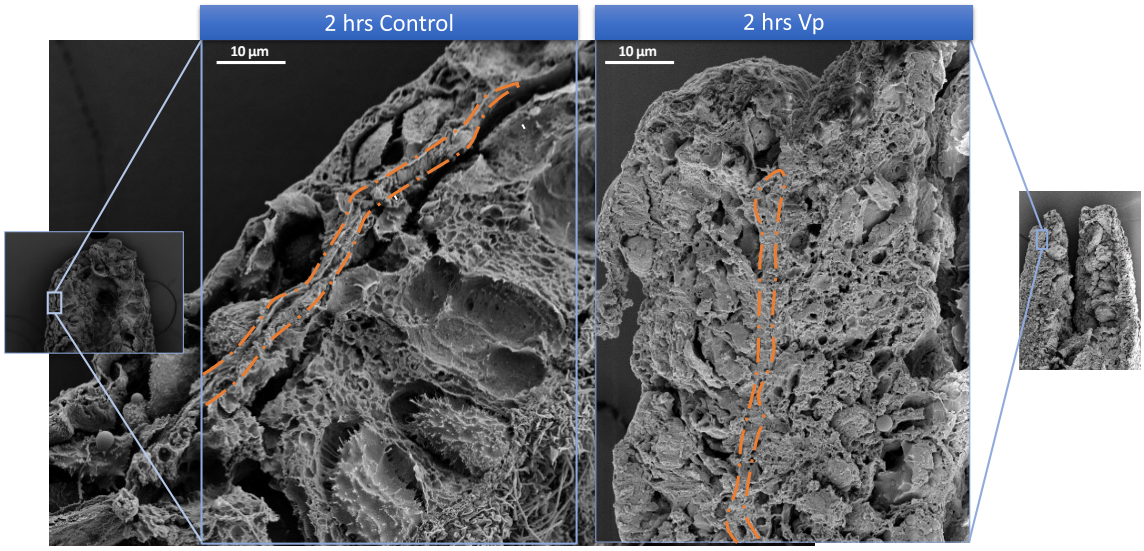

Figure 3.7: Vp pre-treatment causes reduced mesogleal retraction. Longitudinal section (L.S.) of the polyp placed with the regenerating tip oriented towards the top of the image shows the minimal

retraction in the Vp treated polyps as compared to the DMSO treated (control) *Hydra* polyps. Scale bar = 10 μm.

3.3.3. Newly formed mesoglea in amputated polyps exhibit a 'fibrosis' type of phenotype

Following the observation from 2 hpa, we monitored the organization of ECM after 24 hrs of amputation whereby a new ECM is generated and mesoglea is completely restored (Figure 3.8). We found that in 24 hrs, Vp treated polyps have a well organized and distinctive mesoglea with a very compact and aligned outlook. While in the control polyps, the mesoglea looked to be restored but the organization of ECM in the mesoglea looked still work-in-progress as compared to non-amputated polyps (See Figure 3.5 DMSO treated head). These suggest two interesting conclusions – 1) VP treatment accelerates ECM organization either due to faster kinetics or fewer repair requirements due to minimal retraction and 2) Vp treatment causes a very different ECM organization with collagen fibrils looking polarized and aligned as against the reticular phenotype we see in the normal mesoglea which can be compared to condition of 'Fibrosis' seen in mammalian organisms upon injury. This Vp related organization is distinct for a newly regenerated mesoglea since un-amputated tissue shows compact yet less polarized (Figure 3.4) and more reticulated (Figure 3.6) fibrils.

3.3.4. Atomic force microscopy (AFM) is a sensitive and robust tool to measure tissue stiffness differential in *Hydra*

Based on the results from previous experiments, it was evident that the mesoglea collagen fibrils were highly crosslinked and less flexible. This leads us to the next question of whether these changes in mesogleal flexibility or stiffness affect the tissue mechanics as a whole and as a corollary if these mechanical changes have any bearing on the accelerated regeneration dynamics as seen upon Vp treatment. To answer these questions, a method to measure tissue stiffness quantitatively in *Hydra* during regeneration was required. At the time the study was initiated, there were no methods developed or reported for measuring tissue stiffness of a living animal or even a heterogeneous tissue. Most of the methods involved measuring the stiffness of a single cell, group of cells from a cell culture in a controlled environment or tissues of relatively uniform cell-types. To address this question, we chose to

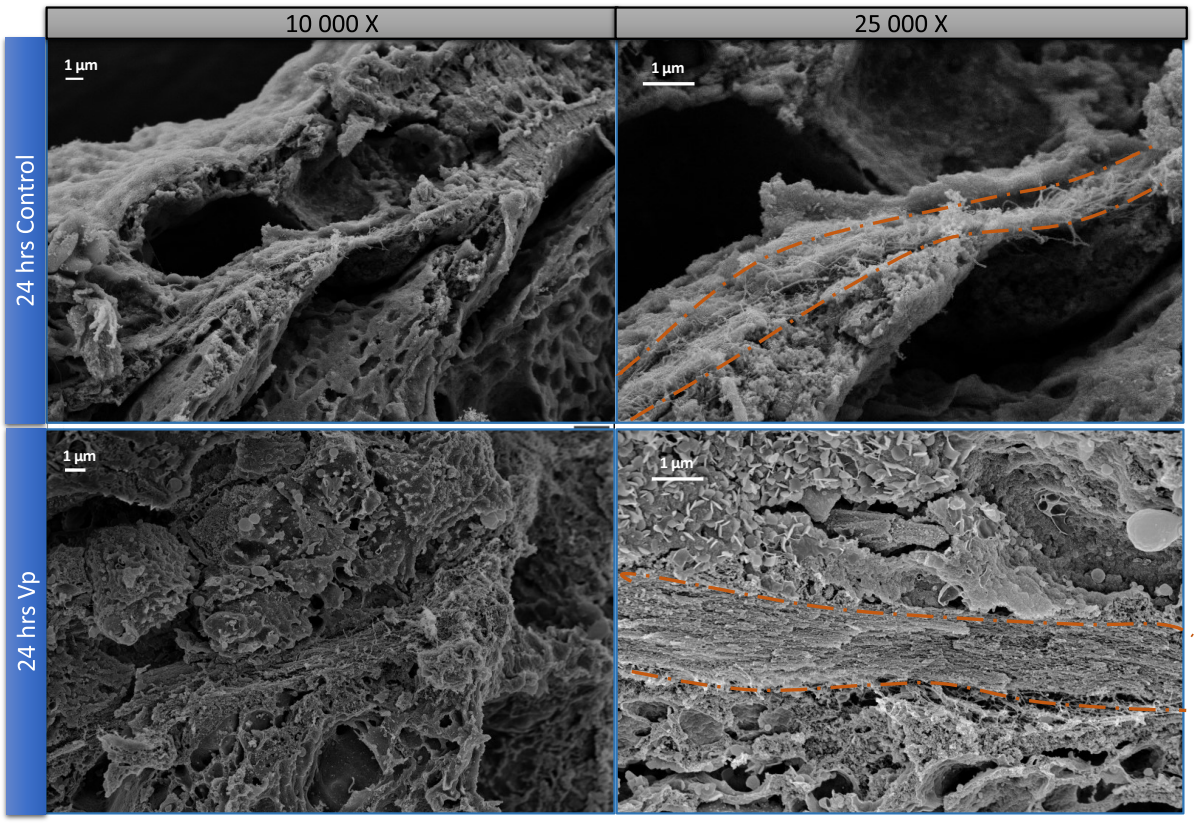

Figure 3.8: Vp pre-treatment causes less mesogleal retraction and a 'fibrotic' ECM organization. Longitudinal section (L.S.) of the polyp placed with the regenerating tip oriented towards the top of the image shows the minimal retraction in the Vp treated polyps as compared to the DMSO treated (control) *Hydra.* The organization of ECM appeared highly compact and polarized, mimicking 'Fibrosis'.

develop Atomic Force Microscopy (AFM) for probing *Hydra* tissue as a method to measure the Young's Modulus, indicative of tissue stiffness. Owing to its high sensitivity and amenability to customization, this method was selected[28, 29].

There were three major issues that needed to be addressed for performing AFM on *Hydra* tissue. The first one being the fact that *Hydra* is extremely dynamic in the sense that it consistently contracts and relaxes. This would pose a big problem for stiffness measurements as they would change the measurements drastically. To address this issue, we relaxed the polyps using Urethane treatment which renders the polyps to a state which is neither hyper-contracted nor hyper-extended. Since extended exposure to Urethane may lead to tissue disintegration, we fixed the polyps with Glutaraldehyde within 2 mins of Urethane treatment. Although Glutaraldehyde is known to affect the mechanical properties of collagen, it has been shown that the effect is expected to be uniform throughout[30]. We assume that the

A.

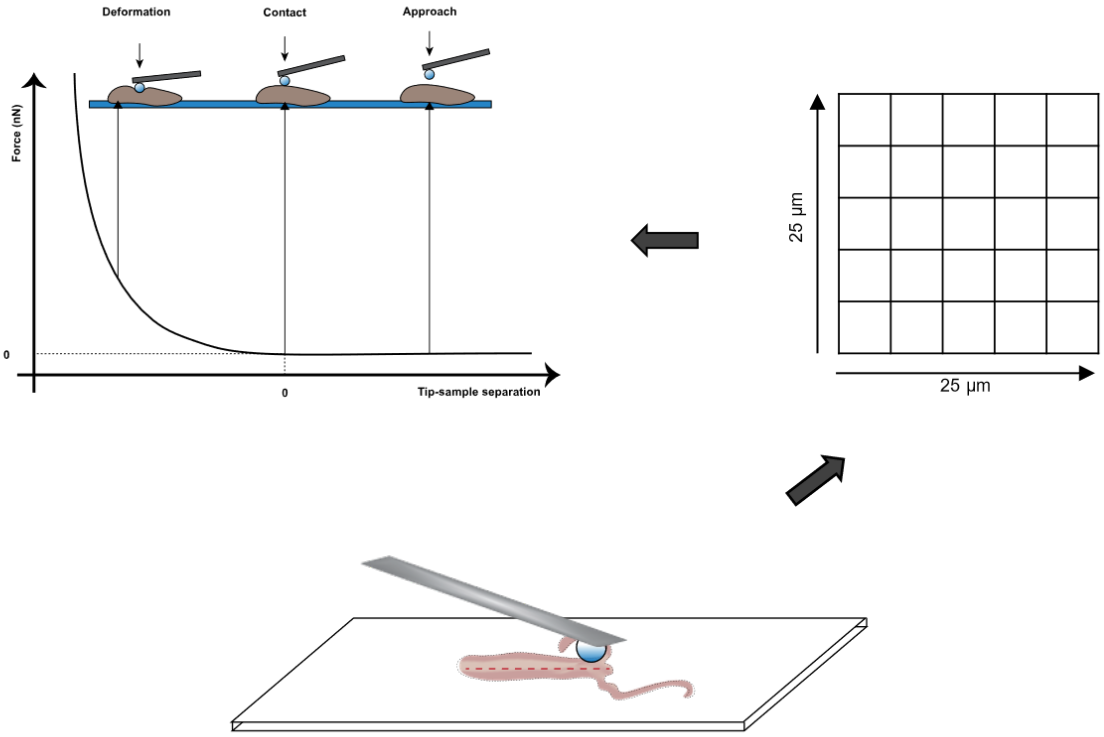

B.

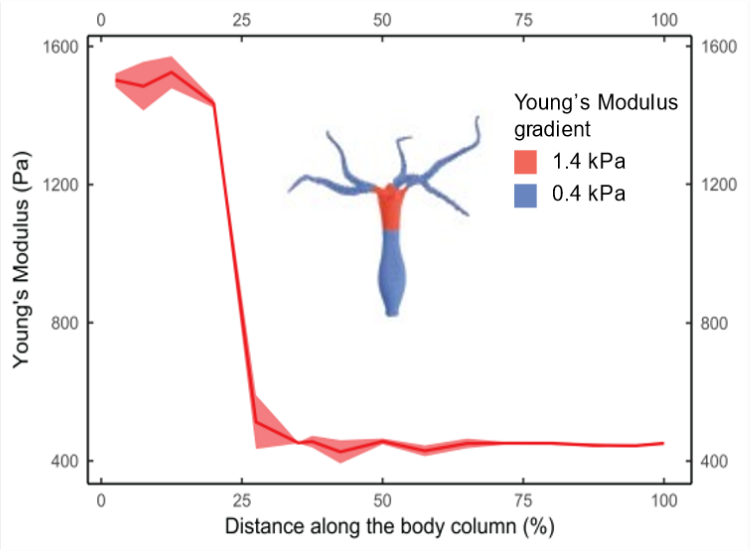

Figure 3.9: *Hydra* tissue stiffness measurement using AFM. A. The schematic represents the method of probing *Hydra* from head to basal disk 100 µm apart (red dotted line) using the AFM. Reading at each spot is measured in an area of 25 x 25 µm where 25 readings are taken at a distance of 5 µm apart. Force curve at each spot is represented in the graph showing a typical curve consisting of approach, contact and deformation. **B.** Young's modulus mapped across the polyp length at a spatial resolution of 100 µm apart indicating a stiffness differential between the head region and body.

stiffness increase in the ECM upon fixation will maintain the original stiffness differential. The second issue needed to be addressed was the high sensitivity of AFM cantilever. AFM is a very sensitive method which can have sensitivity at sub-nanometer resolution. For tissue stiffness, use of a conical or pyramidal type of cantilever will be counter-productive since it will measure stiffness at the molecular level. For tissue level stiffness, a less sensitive probe needed to be designed and hence we attached a spherical glass bead of about 20 µm diameter to a tip-less cantilever. This way, we could probe a larger surface area and hence we could measure the stiffness of the tissue in that area. The third issue that needed to be addressed, was a method to adhere the polyp to the glass coverslip on which the sample needed to be probed using AFM. Sample to be probed needs to be firmly tethered to coverslips. Any movement in the sample can lead to false readings in the force curve. Typically, tissues are adhered to coverslip using poly-l-lysine or gelatin. Gelatin cannot be used here since it is much softer than the tissue and hence AFM reading will give stiffness readings of gelatin instead of tissue. Poly-l-lysine did not work for *Hydra* owing to a multi-layered covering of epithelial cells by the glycocalyx. We fixed this issue by using Bovine serum albumin (BSA) as adhesive to be used by coating the glass coverslip and then dried. The coated proteins from albumin were then crosslinked to *Hydra* glycocalyx using glutaraldehyde flash fixation.

After addressing the issues mentioned above, we wished to validate the utility of Young's modulus measured using AFM and verify whether the ECM organization differential can be correctly captured using measurements of the Young's modulus in the same region. Based on understanding that ECM organization is different between the head region and the body, we measured Young's modulus across the polyps using the method shown in the schematic (Figure 3.9 A). The AFM readings from this experiment supported the observation from SEM and showed conclusively that the top 25 % of the polyp is about 3 times stiffer than the rest of the body column (Figure 3.9 B). This experiment also shows a steep gradient or drop in the stiffness at about 25 % of the body length. A value of approximately 1480 ± 20 Pa was measured for the head region compared to 450 ± 6 Pa for the rest of the body. For tentacles, Young's modulus (Y) was 378 ± 11 Pa. For ease of recalling, we will term the value of 1480 Pa as the "Physiological tissue stiffness" of the head region from

here on. Such sensitivity for measuring Young's modulus and ability to capture stiffness changes is in congruence with the ECM organization observed with SEM supports that we could successfully develop AFM as an effective tool to understand tissue stiffness with respect to various aspects of *Hydra* biology as long as there is no requirement of absolute Young's modulus reading. This also meant that we could develop *Hydra* as a model system to study biomechanics.

3.3.5. Regenerating tip undergoes dynamic changes in tissue stiffness reflecting changes in mesoglea

After developing the AFM technique to quantify the mechanical change in *Hydra* tissue, next we wished to understand and quantify the dynamically changing tissue mechanics during regeneration as a function of ECM dynamics. To this effect, we chose regeneration time points reflecting changes in the mesoglea. We used the un-amputated head with tentacles clipped as a control (Y = 1275 ± 23 Pa). We used 2 hrs post-amputation as the earliest time-point which will reflect the stiffness of polyps after wound-healing is achieved (Figure 3.10). We then used 4 hrs post-amputation (hpa) for a time point before basement membrane secretion begins at 7 hpa. The 8 hpa time-point was used to reflect completion of basal lamina formation. Sixteen hpa was used for a time-point between completion of the interstitial matrix and mesoglea as a whole. Twenty four hpa was used to probe the stiffness when the mesoglea is understood to be completely reformed. Young's modulus measurements using AFM for regenerating polyps at the wound showed a drastic drop in stiffness at 2 hpa (Y = 242 ± 16 Pa) which would be expected upon retraction of mesoglea upon amputation. No significant change was observed in the stiffness at 4 hpa reflecting no change in mesoglea during the period. A doubling of stiffness was observed from the previous time-point at 8 hpa (Y = 757 ± 124 Pa) which could reflect the deposition of non-fibrillar collagens in the basal lamina. No significant change in stiffness was observed at 16 hpa. By 24 hpa, the Young's modulus jumped to the "Physiological tissue stiffness" range attaining the similar stiffness as compared to the control (Y = 1509 ± 308 Pa). These results point towards a dynamic modulation of tissue mechanics as a function of ECM during the course of regeneration. Further, these findings clearly establish that AFM can be used as a tool to robustly measure and reflect changes in mesogleal dynamics and tissue stiffness during regeneration.

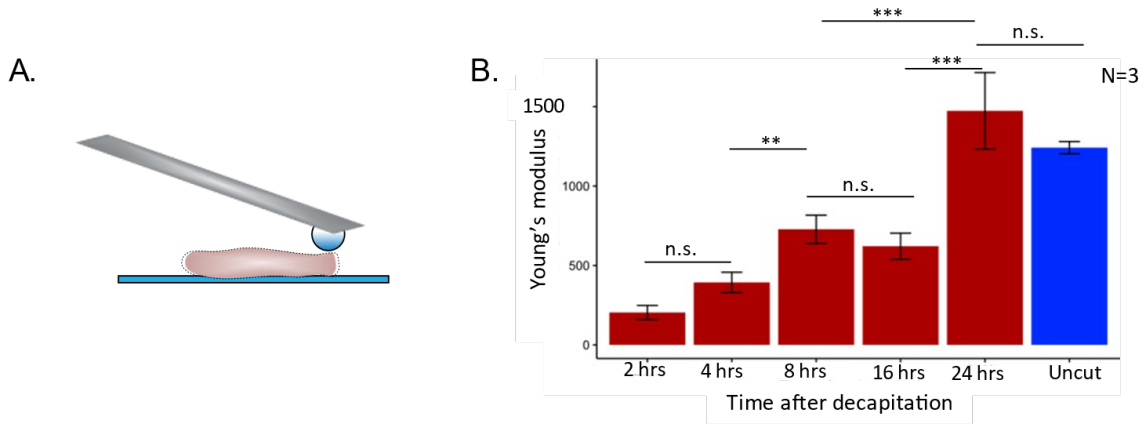

Figure 3.10: Tissue stiffness changes during *Hydra* regeneration reflects mesogleal dynamics. A. Schematic representation of AFM on regenerating tip of *Hydra*. **B.** Changes in Young's modulus in early regenerative time points after decapitation. Red bar indicates regenerating samples and blue bar denote uncut polyps (N=3) (Astrix signify p values with *=0.05-0.01,**=10^{-3},***>10^{-4}. n.s. not significant).

3.3.6. Vp treated polyps attain "Physiological tissue stiffness" early during regeneration

Since the ECM organization could affect the tissue stiffness, we next asked whether structural changes in ECM due to Vp treatment as discussed before (See section 3.3.1-3.3.3) could also reflect in the stiffness measurements. More specifically, we wished to check the effect of pre-treatment of Vp at earliest regeneration time points to try to shed light on the cause of accelerated regeneration. To this effect, the experiment was designed to assay the tissue stiffness in regenerating tip of *Hydra* at 0.5, 1 and 2 hpa in Vp vs DMSO treated (Control) polyps (Figure 3.11 A). AFM measurements revealed that at these time points, the stiffness of control tissue dropped from the "physiological tissue stiffness" to the values reported in the previous section (Y = 429 ± 11 Pa), without changing through 0.5 to 2 hpa (Figure 3.11 B). In contrast, in the Vp treated polyps, the tissue stiffness in the regenerating tips were much stiffer than the control even at 0.5 hpa (Y = 1393 ± 68 Pa). This indicates that Vp pre-treatment results in an increase in stiffness, which post-amputation does not drop to the level of the control amputated polyp. This result aligns with our observation using SEM and TEM that the fibrillar collagens become more densely packed and branched upon 12 hrs of Vp treatment (Figure 3.4) and undergoes minimal mesogleal retraction upon amputation (Figure 3.7). It is interesting to note that the stiffness of Vp treated tissue at 0.5 hpa is well within the "physiological tissue stiffness" range of uncut polyp head region. This value remains more or less unchanged in the next half an hour (Y= 1420 ± 52 Pa). The stiffness

can then be seen jumping to a much higher level at 2 hpa (Y= 2253 ± 74 Pa) indicating a much-accelerated consolidation of ECM organization during the course. The AFM measurements for the rest of the time points until the 24 hpa time point and for the whole body-length will be required for a better understanding of the biomechanical modulation of tissue and mesoglea upon disruption of YAP-TEAD interaction. In summary, these findings demonstrate that Vp treatment linked changes in ECM organization result in an increase in the tissue stiffness, which leads to attaining the "physiological tissue stiffness" level as early as 30 mins post-amputation.

3.3.7. Dipyridyl can be used to inhibit crosslinking of fibrillar collagen in *Hydra*

Based on the results obtained and discussed above, we understand that there is a dynamic change in tissue stiffness during *Hydra* head regeneration and this stiffness is a function of the structural organization of the ECM. We also note that tissue

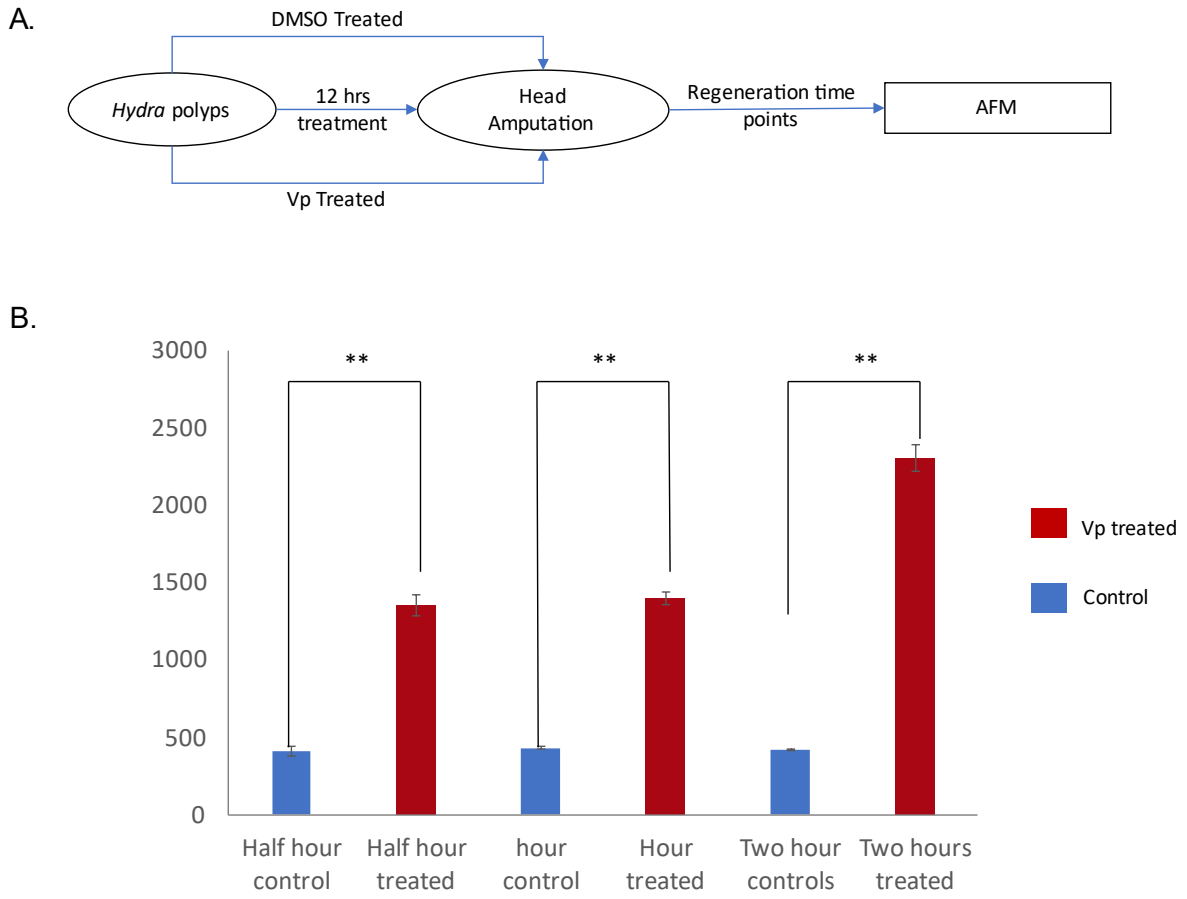

Figure 3.11: Vp treatment leads to an increase in tissue stiffness . A. Schematic representation of the protocol for performing tissue stiffness assay on head regenerating *Hydra*. **B.** Changes in Young's modulus in early regenerative time points (0.5-2 hpa) after decapitation in Vp vs DMSO treated

polyps. Blue bars indicate DMSO treated samples & Red bars indicates Vp treated sample (N=3) (Astrix signify p values with **≈10^{-3})

stiffness re-attains the "physiological tissue stiffness" value upon the reformation of mesoglea at about 20-24 hpa. We see that Vp treatment causes collagen fibrils to be densely packed and branched. This, in turn, causes an increase in the tissue stiffness eventually leading to minimal mesogleal retraction and negligible loss or early attainment of the "physiological tissue stiffness". Interestingly, we noted that it takes about 24-30 hrs for the appearance of most of the tentacle-buds (at about 48 hpa) after the mesoglea formation is complete. We also observed that in Vp treated polyps, early attainment of "physiological tissue stiffness" (at about 0.5 hpa) is accompanied by the appearance of tentacle-buds within 28-30 hpa. We, therefore, hypothesize that this "physiological tissue stiffness" serves as a stiffness threshold for downstream signalling events (possibly head organizer activation), presumably communicating with the cells that the physical cellular niche has been re-established and hence to proceed for morphogenesis as a part of the regenerative programme.

A.

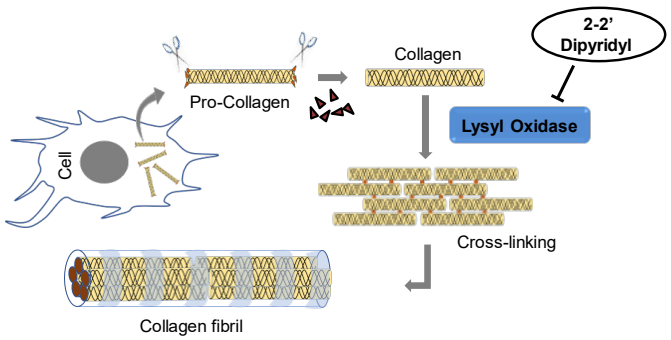

B.

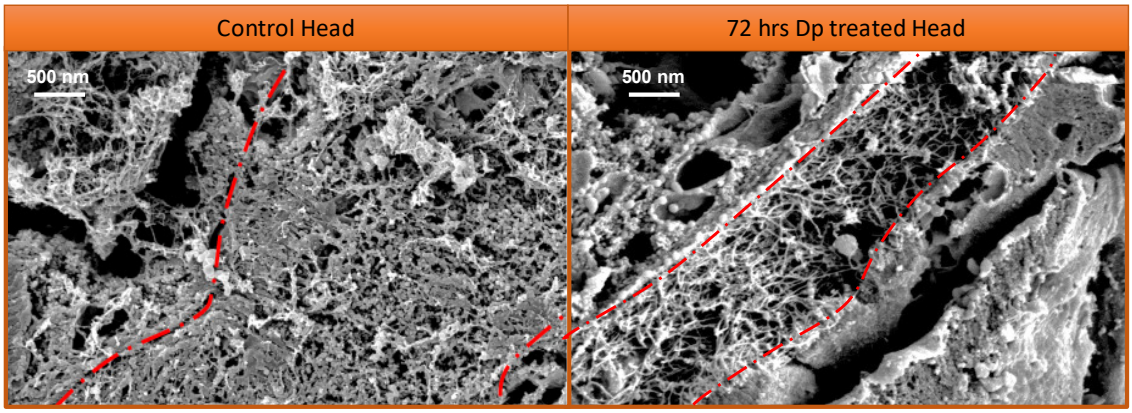

Figure 3.12: Dp treatment can result in loss of collagen crosslinking in newly secreted collagens. A. Schematic representation activity of Dp. **B.** The transverse section (T.S.) of a polyp shows that the mesoglea in the head region is less densely packed in Dp treated polyps due to reduced cross-linking of fibrillar collagens.

To test this hypothesis, we needed to disrupt this threshold such that tissue never attains the “physiological tissue stiffness” value. Considering the tissue stiffness measured by us using AFM is a function of ECM organization, we needed to develop a strategy to disrupt collagen organization without affecting cell-ECM attachment. In the mesoglea, the fibrillar type of collagens, present exclusively in the interstitial matrix, can be assumed to contribute more towards tissue stiffness owing to its structural properties. Taking advantage of the unique organization of *Hydra* mesoglea where cells interact exclusively with basal lamina and not with the interstitial matrix, presented us the possibility of disrupting the fibrillar collagen in an isolated manner. We used the inhibition of Lysyl oxidase activity as a means to disrupt collagen fibril formation. Such a strategy would effectively cause disruption of physical bundling of fibrillar collagen in newly formed or secreted collagen without chemically modifying any pre-existing collagens or newly secreted ECM components of the basal lamina. 2,2’-Dipyridyl (DP) is one such inhibitor which can specifically disrupt the lysyl oxidase activity (Figure 3.12 A). Hence, in a normal polyp where ECM is recycled every 3 days, treatment with DP for 72 hrs will lead to a drastic change in ECM organization and assume a less densely packed and cross-linked interstitial matrix. As can be seen from the results, DP treatment indeed leads to loosely packed mesoglea with individual collagen fibrils easily visible (Figure 3.12 B). These results indicate that we could successfully target the structural organization of fibrillar collagen and implement a biochemical strategy to disrupt tissue stiffness.

3.3.8. Dp treatment leads to failure in attaining the ‘stiffness threshold’ and inhibition of regeneration

We performed AFM measurements on DP treated polyps at early regenerative time points to assay the efficacy of the treatment to disrupt tissue stiffness in regenerating polyps. We found that as per our strategy, we could successfully prevent the tissue from attaining the “physiological tissue stiffness” value or the stiffness ‘threshold’ (Figure 3.13 A). We observed a slight increase in tissue stiffness at 8 hpa which might reflect basal lamina formation. No significant increase in tissue stiffness was observed at 24 and 48 hpa (Y= 544 ± 124 Pa and 554 ± 82 Pa respectively). The regeneration assay, in turn, revealed that these polyps were unable to regenerate as long as they were incubated in DP (Figure 3.13 B). The effect of DP is reversible and the polyps start to regenerate three days after removing DP. These observations hence bolster the ‘Stiffness setpoint’ hypothesis where polyps unable to attain the

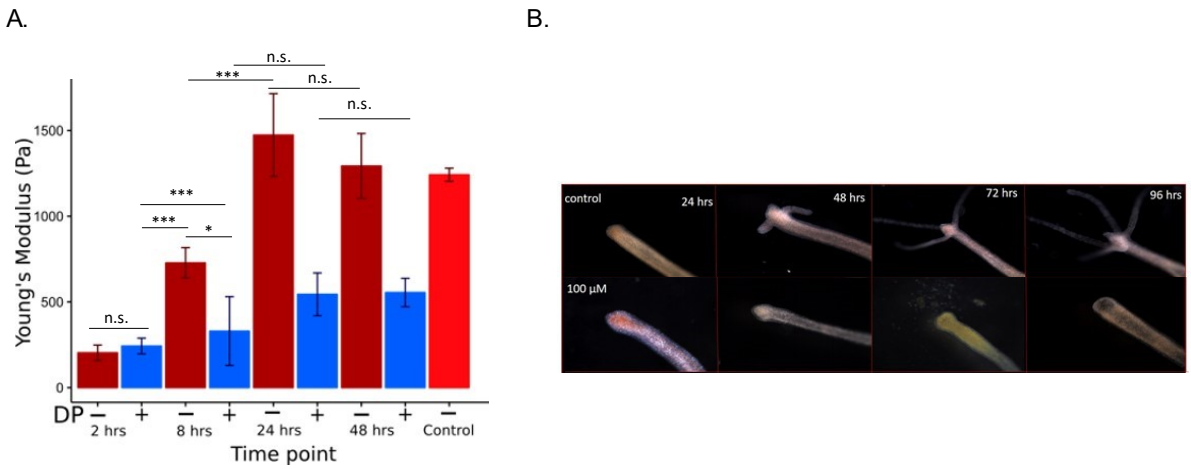

Figure 3.13: DP treatment causes loss of tissue stiffness and a regenerative arrest. To study the effect of Dp on *Hydra* regeneration, regeneration assay was performed following 100 µM Dp treatment. The regenerating polyps were then used for measuring the tissue stiffness using AFM or were imaged to assay the morphological changes during the time course.**A.** Regeneration assay for comparing the tissue stiffness between control vs DP treated reveals an inability to attain the "physiological tissue stiffness" in DP treated polyps. Dark Red bars indicate control samples, Bright red bar indicate uncut 12 hrs DP treated head & Blue bars indicate DP treated sample (N=3) (Astrix signify p values with *=0.05-0.01,**=10^{-3},***>10^{-4}. n.s. is not significant) **B.** DP treatment causes a complete regeneration arrest at 100 µm concentration.

'threshold', do not proceed with the regeneration process whereas the polyps attaining the 'threshold' earlier can regenerate faster.

3.3.9. Vp treatment can rescue the inhibitory effects of Dp in regenerating polyp

To further confirm the 'stiffness threshold' hypothesis, we designed combinatorial treatment of DP and Vp to assess the ability of Vp to rescue the inhibitory effects of DP. The strategy was to increase the tissue stiffness using Vp in DP treated polyps and assay the regenerative kinetics in terms of the number of newly formed tentacles. Mechanistically, there are two ways in which Vp treatment or YAP-TEAD disruption may lead to increase tissue stiffness: a) by increasing synthesis and secretion of fibrillar collagens & b) by increasing the production or secretion of enzymes (such as Lysyl oxidase) catalysing the cross-linking of fibrillar collagen. It could be one of the above or a combination of both. Keeping in mind that presence of DP would effectively inhibit the effect of Vp under all circumstances, we instead assayed the ability of Vp treatment to accelerate the reversal of the inhibitory effect of 3-day DP pre-treatment with a combination of pre- and post-Vp treatment (Figure 3.14). As can be seen from the graph, Dp pre-treatment causes a significant slowdown of regenerative kinetics in terms of the average number of tentacles per *Hydra* (TPH). We see about 1.25 TPH at 60 hrs and 2.5 THP at 72 hrs in DP pre-

treated (PreDP+washout (wo)) polyps as compared to 2.75 and 3.4 respectively in DMSO control. A Vp pre-treatment (PreVP+wo) shows accelerated regenerative kinetics with respect to the DMSO control polyps with 3.1 TPH at 60 hrs and 4 THP at 72 hrs. A combined pre-treatment of DP and Vp (PreDP and VP+wo) shows a faster recovery as compared to PreDP+wo with a 2.7 THP at 60 hrs and 72 hrs.

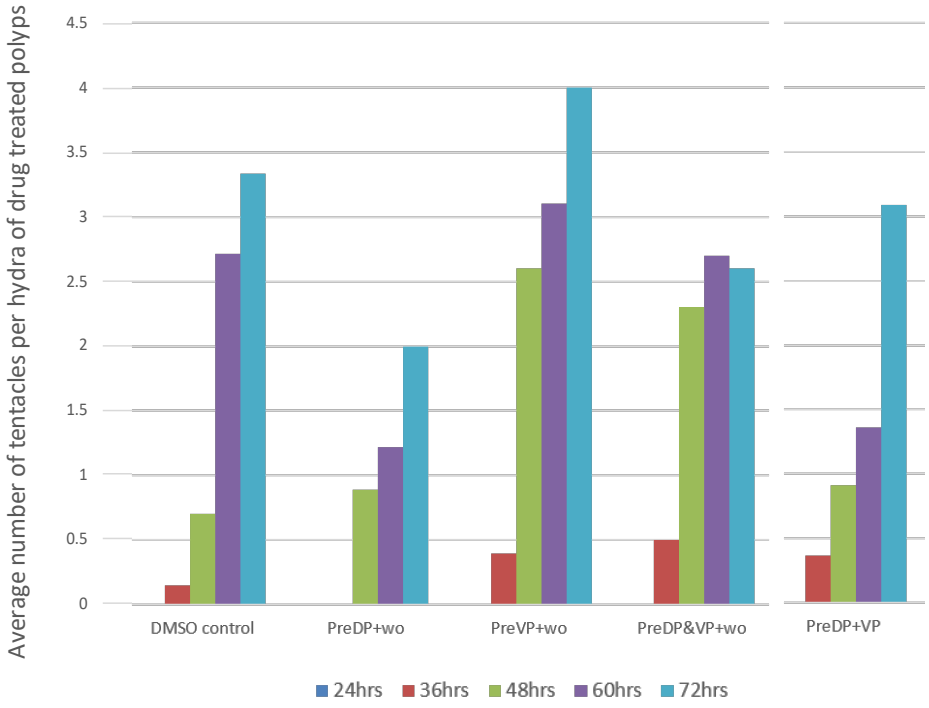

Figure 3.14: Vp treatment can rescue the inhibitory effects of DP treatment to help in faster recovery during regeneration. This graph represents the average number of tentacles per *Hydra* upon various drug treatments at different regeneration time points. Colour legends are indicated below the graph. The drug treatment labels mean the follows from left to right of the label in x-axis: DMSO control- No drug treatment, PreDP+wo- 3-day DP pre-treatment followed by washout (wo) with HM and amputation without any post-treatment, PreVP+wo- 12hrs Vp pre-treatment followed by washout with HM and amputation without any post-treatment, PreDP & VP+wo- Combined 3-day DP and 12hrs Vp pre-treatment followed by washout with HM and amputation without any post-treatment, PreDP+VP- 3-day DP pre-treatment followed by washout with HM and amputation with continuous Vp post-treatment. (n=48, N=1).

polyps subjected to Vp post-treatment on DP pre-treated (PreDP+VP) exhibit an accelerated recovery as compared to PreDP+wo but slower recovery as compared to PreDP and VP+wo with THP values of 1.75 and 3.1 for 60 and 72 hrs respectively. These experiments effectively present the following two points: 1) the disruption of YAP-TEAD interaction presumably induces molecular changes in the regenerating cells which can reverse the effects of DP to effect accelerated regenerative kinetics

upon combinatorial treatment. This effect is irrespective of pre- or post-amputation treatment regime; 2) The difference in regeneration kinetics between PreDP and VP+wo and PreDP+VP suggests that Vp helps DP treated polyps attain ‘Stiffness threshold’ faster and also indicates that the earlier the ‘threshold’ is achieved, the faster the regeneration. A detailed AFM study indicative of these inferences showing dynamics of ‘stiffness threshold’ attainment in these combinatorial drug treatments will conclusively prove the ‘stiffness threshold’hypothesis.

3.4. CONCLUSIONS

This chapter reveals multiple key biophysical aspects of tissue regeneration. More specifically, we report the presence of dynamic regulation of tissue stiffness during regeneration. Using a combination of ultrastructural and AFM studies, we show that tissue stiffness is regulated by fibrillar collagen organization within the interstitial matrix of the mesoglea. We find that intrinsically such a stiffness differential is also seen between the head region and other regions of the *Hydra.* We have found that this stiffness differential along the body column is presumably co-opted as a pseudo-skeletal system in *Hydra* (Naik et. al., manuscript submitted). *Hydra* has evolved to use such a stiffness differential for aiding locomotion process like somersaulting/looping. We believe that this stiffness differential may be the modest beginning of specification of cell lineage or identity by matrix identity which is reported in mammalian cells[2]. By investigating the mechanism of accelerated regeneration upon disruption of YAP-TEAD interaction by Vp, we uncover for the first time that *Hydra* head regeneration is tightly controlled by tissue stiffness. We uncover that Vp treatment-induced ECM fibrosis contributes to the observed acceleration in regeneration by attaining the pro-regenerative 'stiffness threshold' faster. By preventing the tissue from attaining the 'stiffness threshold' during regeneration, we show that the regeneration programme is reversibly arrested after wound healing. This shows that the process of wound-healing is independent of the 'stiffness threshold' and hints that the morphological processes downstream to wound-healing exhibit a stiffness requirement. We postulate that in *Hydra*, the morphological processes controlling the development of lost tissue require the tissue to attain a 'Stiffness threshold' which enables the cells to activate the pro-regenerative signalling network. We find that DP treatment can negate the effect of Vp (data not shown) and block the regeneration. We also show that the recovery of regenerative capability after DP treatment is enhanced by Vp treatment. Combined, these observations argue strongly for the 'Stiffness threshold' hypothesis. Another unique finding from this work is the fact that 'Fibrosis' is pro-regenerative in *Hydra*. It is well known that in mammalian model systems, fibrosis is considered as anti-regenerative and causes scar tissues.

Many recent studies have found that the regulation of ECM is critical in regulating regeneration for multiple model systems. One such study reported that the loss of

ability to regenerate heart in the neonatal mouse after day 2 is due to a 50 % increase in elastic modulus of cardiac ECM causing scar tissue instead[10]. Using β-aminopropionitrile (BAPN), a drug similar to DP in action, the authors were able to restore the ability of the 3-day old mouse to regenerate injured heart. While this study showed for the first time that by reducing the cross-linking of fibrillar collagen and hence lowering the tissue stiffness rescues the tissue from scarring, the mechanistic regulation for the same is unresolved. While fibrosis is considered pro-scarring in mammalians, a recent study in zebrafish heart regeneration shows that fibrosis is required for proper regeneration[31]. This study showed that there is transient fibrosis which occurs in response in injury which is later resolved during the course of regeneration. The study is also unable to elucidate the mechanistic importance of fibrosis but it leaves a clue that there are specific fibroblasts which are involved in collagen type I secretion required for fibrosis. In *Hydra,* it is not known which specific ectodermal and endodermal cell types are responsible for regulating collagen secretion during regeneration, therefore it is tempting to speculate that YAP positive cells recruited to the site of injury early might have a role in the same.

A study to identify the exact cell type expressing ECM during regeneration and it's relation with the YAP positive cell will help us understand how the 'stiffness threshold' are linked with regulation of regenerative programme. There are many interesting aspects of this study that need further experimentation like what is the organization of ECM in the later Vp time points (post-24 hpa) and the how the tissue stiffness of Vp treated regeneration tips changes beyond the 2 hpa time points. The fact that the organization of Vp treated polyps in an intact head versus a regenerating head is very different- The regenerating head assumes a fibrotic organization whereas an unamputated head assumes a more compact and reticulated form. It will be interesting to investigate the nature of this difference. It will also be interesting to observe the dynamics of tissue stiffness in polyps which are undergoing a combination of DP and Vp treatment to confirm the ability of Vp to rescue effects of DP treatment.

3.5. REFERENCES

1. Grau-Bove, X. et al. Dynamics of genomic innovation in the unicellular ancestry of animals. Elife **6** (2017).
2. Engler, A.J., Sen, S., Sweeney, H.L. & Discher, D.E. Matrix elasticity directs stem cell lineage specification. Cell **126**, 677-689 (2006).
3. Mao, Y. & Baum, B. Tug of war—the influence of opposing physical forces on epithelial cell morphology. Developmental biology **401**, 92-102 (2015).
4. Nistala, H. et al. Fibrillin-1 and-2 differentially modulate endogenous TGF-β and BMP bioavailability during bone formation. The Journal of cell biology **190**, 1107-1121 (2010).
5. Crest, J., Diz-Muñoz, A., Chen, D.-Y., Fletcher, D.A. & Bilder, D. Organ sculpting by patterned extracellular matrix stiffness. Elife **6**, e24958 (2017).
6. Lane, M.C., Koehl, M., Wilt, F. & Keller, R. A role for regulated secretion of apical extracellular matrix during epithelial invagination in the sea urchin. Development **117**, 1049-1060 (1993).
7. Sakai, T., Larsen, M. & Yamada, K.M. Fibronectin requirement in branching morphogenesis. Nature **423**, 876 (2003).
8. Vracko, R. & Benditt, E.P. Basal lamina: The scaffold for orderly cell replacement: Observations on regeneration of injured skeletal muscle fibers and capillaries. The Journal of cell biology **55**, 406-419 (1972).
9. Gulati, A.K., Reddi, A. & Zalewski, A. Changes in the basement membrane zone components during skeletal muscle fiber degeneration and regeneration. The Journal of cell biology **97**, 957-962 (1983).
10. Notari, M. et al. The local microenvironment limits the regenerative potential of the mouse neonatal heart. Science advances **4**, eaao5553 (2018).
11. Seifert, A.W. et al. Skin shedding and tissue regeneration in African spiny mice (Acomys). Nature **489**, 561 (2012).
12. Maden, M. et al. Perfect chronic skeletal muscle regeneration in adult spiny mice, Acomys cahirinus. Scientific reports **8**, 8920 (2018).
13. Lukjanenko, L. et al. Loss of fibronectin from the aged stem cell niche affects the regenerative capacity of skeletal muscle in mice. Nature medicine **22**, 897 (2016).
14. Mailman, M.L. & Dresden, M.H. Collagen metabolism in the regenerating forelimb of Notophthalmus viridescens: synthesis, accumulation, and maturation. Developmental biology **50**, 378-394 (1976).
15. Tassava, R.A., Nace, J.D. & Wei, Y. Extracellular matrix protein turnover during salamander limb regeneration. Wound Repair and Regeneration **4**, 75-81 (1996).
16. Contreras, E.G., Gaete, M., Sánchez, N., Carrasco, H. & Larraín, J. Early requirement of Hyaluronan for tail regeneration in Xenopus tadpoles. Development **136**, 2987-2996 (2009).
17. Wang, J., Karra, R., Dickson, A.L. & Poss, K.D. Fibronectin is deposited by injury-activated epicardial cells and is necessary for zebrafish heart regeneration. Developmental biology **382**, 427-435 (2013).
18. Bai, S. et al. Matrix metalloproteinase expression and function during fin regeneration in zebrafish: analysis of MT1-MMP, MMP2 and TIMP2. Matrix biology **24**, 247-260 (2005).
19. Davis, L.E. & Haynes, J.F. An ultrastructural examination of the mesoglea of Hydra. Zeitschrift für Zellforschung und Mikroskopische Anatomie **92**, 149-158 (1968).
20. Shimizu, H. et al. The extracellular matrix of hydra is a porous sheet and contains type IV collagen. Zoology **111**, 410-418 (2008).
21. Shimizu, H. et al. Epithelial morphogenesis in hydra requires de novo expression of extracellular matrix components and matrix metalloproteinases. Development (Cambridge, England) **129**, 1521-1532 (2002).

22. Sarras Jr, M.P. Components, structure, biogenesis and function of the Hydra extracellular matrix in regeneration, pattern formation and cell differentiation. International Journal of Developmental Biology **56**, 567-576 (2012).
23. Reddy, P.C., Gungi, A. & Unni, M. Cellular and Molecular Mechanisms of Hydra Regeneration, in Evo-Devo: Non-model Species in Cell and Developmental Biology 259-290 (Springer, 2019).
24. Technau, U. & Holstein, T.W. Cell sorting during the regeneration of Hydra from reaggregated cells. Developmental biology **151**, 117-127 (1992).
25. Sarras Jr, M.P. et al. Extracellular matrix (mesoglea) of Hydra vulgaris: III. Formation and function during morphogenesis of hydra cell aggregates. Developmental biology **157**, 383-398 (1993).
26. Siegel, R.C., Pinnell, S.R. & Martin, G.R. Cross-linking of collagen and elastin. Properties of lysyl oxidase. Biochemistry **9**, 4486-4492 (1970).
27. MICHAEL JR, P.S., MEADOR, D. & ZHANG, X. Extracellular Matrix (Mesoglea) of Hydra Vulgaris. DEvELOPMENTAL BIOLOGY **48**, 495-500 (1991).
28. Engler, A.J., Rehfeldt, F., Sen, S. & Discher, D.E. Microtissue elasticity: measurements by atomic force microscopy and its influence on cell differentiation. Methods in cell biology **83**, 521-545 (2007).
29. Stolz, M. et al. Dynamic elastic modulus of porcine articular cartilage determined at two different levels of tissue organization by indentation-type atomic force microscopy. Biophysical journal **86**, 3269-3283 (2004).
30. Lu, M., Song, X., Yang, M., Kong, W. & Zhu, J. Combined effects of glutaraldehyde and riboflavin/uv365 on the self-assembly of type I collagen molecules observed with atomic force microscopy. International journal of food properties **21**, 2181-2192 (2018).
31. Sánchez-Iranzo, H. et al. Transient fibrosis resolves via fibroblast inactivation in the regenerating zebrafish heart. Proceedings of the National Academy of Sciences **115**, 4188-4193 (2018).

4. EFFECT OF DISRUPTION OF YAP-TEAD INTERACTION ON DEVELOPMENTALLY REGULATED GENES DURING REGENERATION IN *HYDRA*

4.1. INTRODUCTION

Regulation of fibrosis during wound healing

Fibrosis is defined as the excessive accumulation of specific extracellular matrix components in response to injury. Fibrosis is commonly observed upon chronic tissue injury causing a disturbance in the normal wound healing process resulting in aberrant tissue regeneration and organ failure[1]. In adult humans, injury is almost always followed by fibrosis and if the wound healing time is prolonged due to deep injuries, scarring ensues[2]. Such scarring is seen commonly in mammals and in other vertebrates. Scarring seems to have evolved as a way to gain an evolutionary advantage by adapting the ability to close and heal the wound faster. The fibrosis inherent to the process of wound healing seems to feed into the process of scarring in scar-prone organisms. In response to injury, specific fibroblasts (myofibroblasts) are recruited to the site of injury in response to inflammatory cues. These cells then secrete profibrotic extracellular matrix (ECM) components such as collagens, glycoproteins, proteoglycans and cytokines[1]. The ECM components are deposited rapidly at the site to provide a quick template for tissue structure. However, due to such parallelly arranged collagen fibrils, the ECM ends up being stiff and anisotropically weak. This ECM milieu further causes the transition of nearby endothelial cells, epithelial cells and macrophages to myofibroblasts causing progression in fibrosis[1, 3]. These myofibroblasts respond to higher matrix stiffness in an integrin-dependent manner and trigger cellular contractility in the region which leads to local deformation in the tissue and finally causing defects in tissue and organ function in the long term[1].

Myofibroblast differentiation is driven by cytokines or extracellular growth factors and mechanotransduction. It is a carefully orchestrated process which is under intense

study. TGF-β signalling has been long identified as an important cytokine required for fibrotic myofibroblasts with Smads having an effector role[4]. Wnt signalling has also been reported to be involved in the pro-fibrotic response to injury[5, 6]. Hyperactivation of agonists or inhibition of antagonists of Wnt signalling such as DKK and sFRP have been reported to exacerbate fibrosis[7, 8]. YAP signalling regulates myofibroblasts through mechanotransduction via integrin signalling (Integrin α11β1) upregulation of pro-fibrotic myofibroblast marker genes including *α-sma* and *pia1*[9]*.* Because all these three regulators of fibrosis are known to cross-talk and function as co-regulators, several studies have implicated their inter-regulation in the processes of myoblast differentiation and fibrosis pathogenesis[10-12]. Such examples raise the possibility that in an environment where these three pathways seemingly function simultaneously such as that seen during *Hydra* head regeneration, mechanical changes as observed in upon Vp treatment may cause drastic changes in regeneratory signalling network.

Regulation of developmentally essential genes by YAP signalling

Other than the important role of fibrotic regulation of profibrotic factors such as TGF-β and WNT by YAP signalling through cross-interaction, such regulation has also been reported in other developmentally important contexts. YAP signalling and WNT signalling have been reported to regulate each other closely. YAP is in fact an important component of the β-catenin destruction complex wherein the association of YAP with the destruction complex is required for the recruitment of β-TrCP for degradation of both YAP and β-catenin[13]. This is also the manner in which the sequestration and destruction of YAP is regulated in a Wnt-dependent manner. Further, YAP activity has been reported to induce WNT16 production leading to canonical activation of Wnt signalling in nearby genes through paracrine signalling[14]. Many such examples of the developmental co-regulation of YAP and β-catenin have been reported[15-17]. A recent study has reported that YAP, Wnt and BMP together regulate neural crest emigration in a concerted manner by inducing EMT[18]. Multiple reports have documented similar co-regulation of YAP and TGF-β[19-21]. Most of these studies report their cross-communication in regulating epithelial to mesenchymal transition (EMT) during embryonic and oncogenic development.

During *Hydra* head regeneration many of these developmental proteins are reported to be absolutely essential for reforming the oral-aboral polarity by re-establishing the head organizer activity. Some of them are important in stem-cell differentiation and trans-differentiation during the regenerative process whereas the others are required for cellular movement and morphogenesis. In this study, we observe that YAP-TEAD disruption not only causes matrix stiffening and fibrosis but also accelerates morphogenesis involved in regeneration as reflected by the accelerated appearance of tentacles upon amputation. It seems that these two observations are inter-connected as disruption of matrix stiffness can negate the effect of Vp treatment completely and block regeneration. To better understand this observation, we will need to understand the perturbation in the molecular process upon Vp treatment. To this effect, this chapter is focused on delineating the molecular signatures associated with Vp treatment or disruption of YAP-TEAD interaction during the paradigm of *Hydra* head regeneration. We have attempted to understand how the signalling network during regeneration is changed upon Vp treatment during the early time points and how they correlate to observations including fibrosis and faster regeneration by analysing the differential expression of genes in the regenerating tip between control and Vp treated *Hydra* in a time-dependent manner. Collectively, this analysis reveals that Vp treatment leads to upregulation of pro-fibrotic genes causing the observed matrix stiffening. This further leads to early activation of β-Catenin transcriptional targets required for oral fate determination during head regeneration through a YAP- β-Catenin-Bra-dependent manner.

4.2. METHODS AND MATERIALS

4.2.1. RNA sequencing

The regenerating tips isolated from the regeneration assay were used for extracting total RNA using TRIzol (Thermo Fisher). Three biological replicates were prepared and shipped to an NGS provider (Macrogen, Korea) for quality control (QC) and transcriptome sequencing. Two randomly selected replicates at each time point were tested for QC. The QC report of the two each of the replicates indicated an RNA integrity number (RIN) value varying between 7.7 to 10 with a concentration varying between 141-485 ng/µl. All the samples selected passed the QC requirements for transcriptome sequencing (Illumina). The sequencing library is prepared by random fragmentation of the cDNA sample, followed by 5' and 3' adapter ligation. For cluster generation, the library is loaded into a flow cell where fragments are captured on a lawn of surface-bound oligos complementary to the library adapters. Each fragment is then amplified into distinct, clonal clusters through bridge amplification. When cluster generation is complete, the templates are ready for sequencing. Adapter-ligated fragments are then PCR amplified and gel purified. Sequencing data is then converted into raw data for the analysis. Following are the details of the sample preparation for the sequencing performed by Macrogen:

Type of Read	Paired-end
Read Length	151
Number of Samples	16
Library Kit	TruSeq Stranded mRNA LT Sample Prep Kit
Library Protocol	TruSeq Stranded mRNA Sample Preparation Guide, Part #15031047 Rev. E
Type of Sequencer	Illumina platform (Hiseq2500)

The Illumina sequencer generated raw images utilizing sequencing control software for system control and base calling through an integrated primary analysis software called RTA (Real Time Analysis). The BCL (base calls) binary were converted into FASTQ utilizing the Illumina package bcl2fastq. Adapters were not trimmed from the reads. The details of the raw data produced can be found in Appendix 5.4.

4.2.2. Differential expression analysis

Differential gene expression analysis was performed using the EdgeR method [22] integrated in the Trinity pipeline[23]. Here, raw reads from experimental conditions were aligned to the *in-house* hybrid transcriptome[24] by the bowtie2 and RSEM method using 'align_and_estimate_abudance.pl' script. Read count matrix was generated using 'abundance_estimate_to_matrix.pl' script. This read count matrix was used in EdgeR by running 'run_DE_analysis.pl'. Differentially expressed genes were selected using a log2 fold change cut-off of ±0.58 (~1.5 absolute fold change) and an adjusted p-value of 0.05). Normalized count tables were generated in R and used to plot heatmaps of differentially expressed genes[25]. Venn diagrams were built using Venny 2.1 (https://bioinfogp.cnb.csic.es/tools/venny/). Gene Ontology (GO) term analysis was conducted using REVIGO[26].

4.2.3. siRNA mediated knockdown of Hvul_YAP

The siRNA oligo sequences Hvul_YAP was predicted using the siDESIGN Center tool (https://dharmacon.horzondiscovery.com/design-center/). The sequence used for siRNA targeting of Hvul_YAP was: Sense: 5'-CAG CUG AAG GUG AGG UUU AUU-3' and Antisense: 5'-UAA ACC UCA CCU UCA GCU GUU-3'. siβ-catenin sequences were used from the previous report[27]. The siLuciferase (5'-CUUACGCUGAGUACUUCGA-3) was used as a negative control (Eurogentec SR-CL010-005). Forty non-budding polyps were taken for each condition and incubated in water for 30 min. The polyps were then placed into an electroporation cuvette with a 4 mm gap (Bio-Rad), and water was aspirated. Two hundred microliters of sterilized 10 mM HEPES (pH 7.0) containing 2 μM siRNA was then added. After the animals relaxed in the cuvettes, two consequent pulses of 100 V, 750 Ω, and 75 μF were given using the Gene Pulser II electroporation system (Bio-Rad). The animals were then immediately transferred to 10 ml of restoration medium (20% dissociation medium (6 mM $CaCl_2$, 1.2 mM $MgSO_4$, 3.6 mM KCl, 12.5 mM N-Tris-[hydroxymethyl]methyl-2 aminoethanesulphonic acid (TES), 6 mM sodium pyruvate, 6 mM sodium citrate, 6 mM glucose) + 80% Hydra medium) and allowed to recover for 1 day. On the following day, the animals were transferred to Hydra medium. This process was repeated thrice on alternate days following feeding and cleaning of the animals. After the third pulse, the polyps were allowed to recover for 24 hrs before

being harvested for RNA isolation by disrupting them in Trizol (Thermo Fisher Scientific).

4.2.4. Uniaxial regenerating tip compression

To apply external mechanical pressure or strain to the regeneration tip of *Hydra*, we applied uniaxial tissue compression at the tip. To achieve the same, we placed 5 decapitated *Hydra* parallelly on a glass slide and trapped the regenerating tip under a 22 x 22 mm coverslip supported by another glass slide (Figure 4.1 A). A total pressure of 56 Pa was exerted on regenerating tip in this experiment to assay the effect of tip compression on regeneration. The compression was limited to just one hour immediately after amputation to induce brachyury expression early during regeneration mechanically. The coverslip covered about 2 mm of the regenerating tip. The glass slide contacted the coverslip at about 70 % mark at point C (Figure 4.1 B), while the centre of mass was at point B. Point A indicates contact with *Hydra*. With the weight of the coverslip as mg, Force exerted by coverslip on *Hydra* as N and total length the coverslip as x, and a torque of 0 at point C, we calculate the force using the following formula:

Torque= Force perpendicular to length X length.
Hence, at point C:
$0.7x \times N.\cos\theta - 0.2x \times mg.\cos\theta = 0$
Coverslip used in the experiment has a mass of 0.1 g and hence solving for N gave:
$N = 2.8 \times 10^{-4}$ N

Now,
Pressure = Force per unit area.

Area (A) = 5 *Hydra* X 2mm length X 0.5 mm width.

Hence, Pressure = N ÷ A
Which gives a pressure of 56 Pa by the glass coverslip on the regenerating tip.

Therefore, we used an external mechanical pressure of 56 Pa to perturb regeneration.

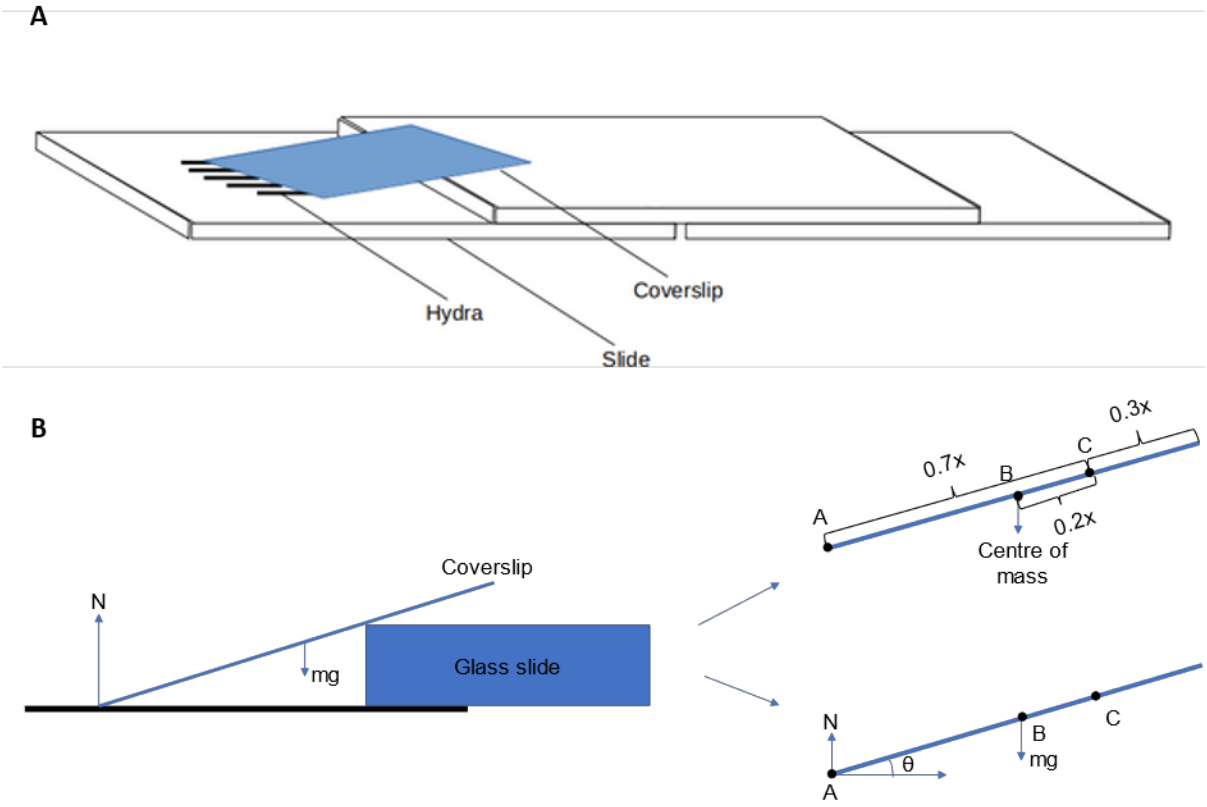

Figure 4.1: Schematic representation and force body diagram of the experimental setup of the application of uniaxial compression on regenerating tip of *Hydra*. (A) The schematic representation of the experiment shows the placement of the glass slides and coverslip in manner that the regenerating tip of the parallelly aligned amputated polyps are compressed uniformly**. (B)** The force body diagram depicts the angles, direction and distances of force, weight and distances from the centre of mass used for calculating the pressure applied by the coverslip on *Hydra*.

4.3. Results and Discussion

4.3.1. Transcriptome analysis to delineate changes in the molecular signalling network during head regeneration

To gain insights into the molecular changes at the level of gene expression upon Vp treatment, we performed differential transcriptome analysis. Towards this, RNAseq of regenerating tip of the decapitated polyps was performed at early time points chosen from the clues obtained from previously discussed experiments (Chapter 2 and 3). The time points chosen were 0, 2, 8 and 24 hrs post-amputation. Hundred polyps starved for 24 hrs were pre-treated with DMSO or Vp for 12 hrs before amputation (Figure 4.2). After amputation, the polyps were allowed to regenerate according to the time points chosen and then the regenerating tips were harvested for RNA isolation. A total of 3 biological replicates were performed. These samples were then sent for sequencing.

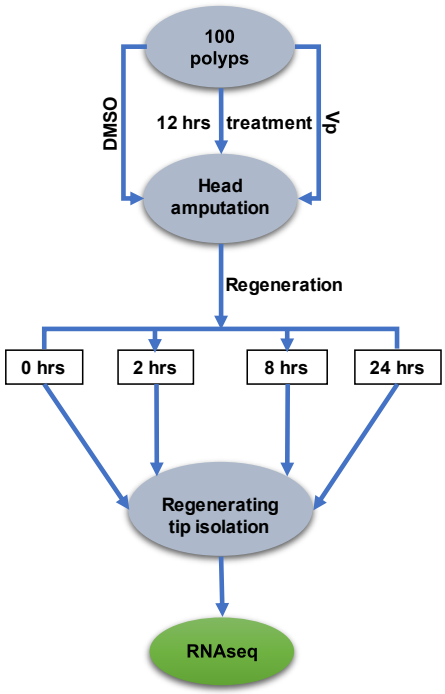

Figure 4.2: Schematic representation of the experimental setup used for preparing samples for differential transcriptome analysis of DMSO vs Vp treated *Hydra* using RNAseq.

Differential expression analysis of regenerating tip of Vp treated polyps revealed that about 860 genes were dysregulated at 0 hpa as compared to control indicating that 12 hrs of Vp pre-treatment itself caused these changes. 423 genes were

dysregulated at 2 hpa, about 395 genes were dysregulated at 8 hpa and 200 genes were dysregulated at 24 hpa. To find out how many unique genes were up-regulated (Figure 4.3 A-C) or down-regulated (Figure 4.3 D-E) at each time points, Venn diagrams of up-regulated or down-regulated genes upon Vp treatment at each time points were plotted against the genes which are differentially expressed between each time point in DMSO treated polyps. Such analysis revealed that 239

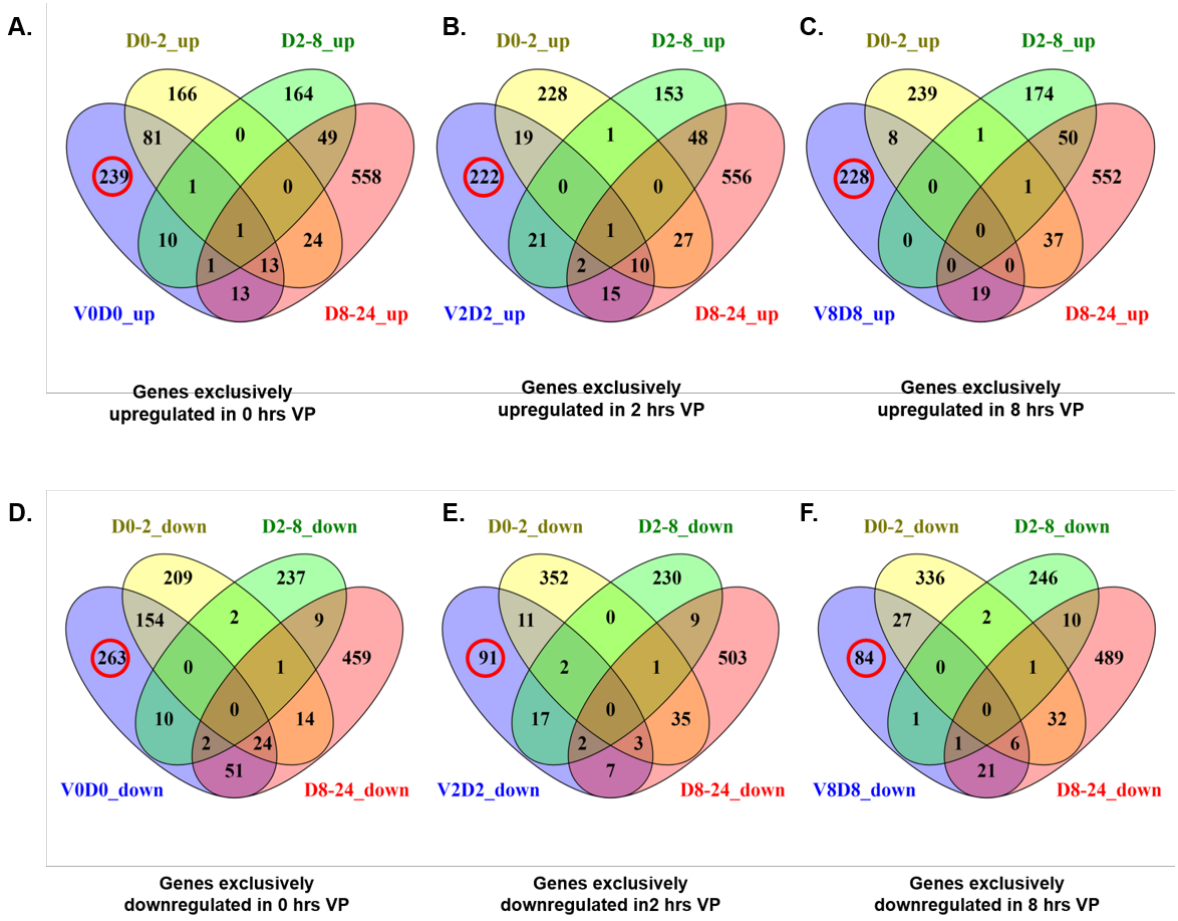

Figure 4.3: Venn diagram of genes exclusively dysregulated upon Vp treatment. A. Shows genes exclusively upregulated upon Vp treatment at 0 hpa. **B.** Shows genes exclusively upregulated upon Vp treatment at 2 hpa. **C.** Shows genes exclusively upregulated upon Vp treatment at 8 hpa. **D.** Shows genes exclusively downregulated upon Vp treatment at 0 hpa. **E.** Shows genes exclusively downregulated upon Vp treatment at 2 hpa. **F.** Shows genes exclusively downregulated upon Vp treatment at 8 hpa.

unique genes were up-regulated exclusively at 0 hpa in Vp treated polyps out of which only 11 were up-regulated in DMSO treatment during the first 24 hrs of regeneration (Figure 4.3 A). Hence, these genes indicate the unique targets of Vp in the first 12 hrs of pre-treatments. About 222 unique genes are up-regulated exclusively at 2 hpa in Vp treated polyps out of which 45 are up-regulated in DMSO

treatment during the first 24 hrs of regeneration (Figure 4.3 B). About 228 unique genes were up-regulated exclusively at 8 hpa in Vp treated polyps out of which 95 were up-regulated in DMSO treatment during the first 24 hrs of regeneration (Figure 4.3 C). Among the downregulated genes, about 263 unique genes were down-regulated exclusively at 0 hpa in Vp treated polyps out of which 48 were up-regulated in DMSO treatment during the first 24 hrs of regeneration (Figure 4.3 D). Only 91 unique genes were down-regulated exclusively at 2 hpa in Vp treated polyps out of which 14 were up-regulated in DMSO treatment during the first 24 hrs of regeneration (Figure 4.3 E). Eightyfour unique genes were down-regulated exclusively at 8 hpa in Vp treated polyps out of which 13 were up-regulated in DMSO treatment during the first 24 hrs of regeneration (Figure 4.3 E).

4.3.2. A large number of genes involved in important biological processes is dysregulated exclusively in Vp treated polyps

Gene Ontology (GO) terms were assigned to the genes which were exclusively dysregulated upon Vp treatment during early regenerative time points – 0-2 and 2-8 hpa. The GO analysis revealed that during the 0-2 hpa transition, genes known to be associated with biological processes of metabolic process, cell adhesion, cytoskeleton organization and growth were represented highly (Figure 4.4). These genes are indicative of cells responding to mechanical changes and movement of cells required for morphogenesis. While for the 2-8 hpa transition, genes known to be associated with biological processes of metabolic process, cytoskeleton organization, cell adhesion, microtubule-based movement, multicellular organismal development and RNA processing were represented highly. Such representations are indicative of a shift from the initial mechano-responsive and preparative phase to morphogenetic developmental phase. These changes hint at earlier activation of developmental pathways that may be required for regeneration.

4.3.3. Vp treatment leads to upregulation of pro-fibrotic genes and specific cell-cell adhesion genes

SEM and AFM studies of Vp treated tissues were indicative of fibrosis-like ECM deposition (Figures 3.7 & 3.10). To confirm the molecular signatures of the same, the

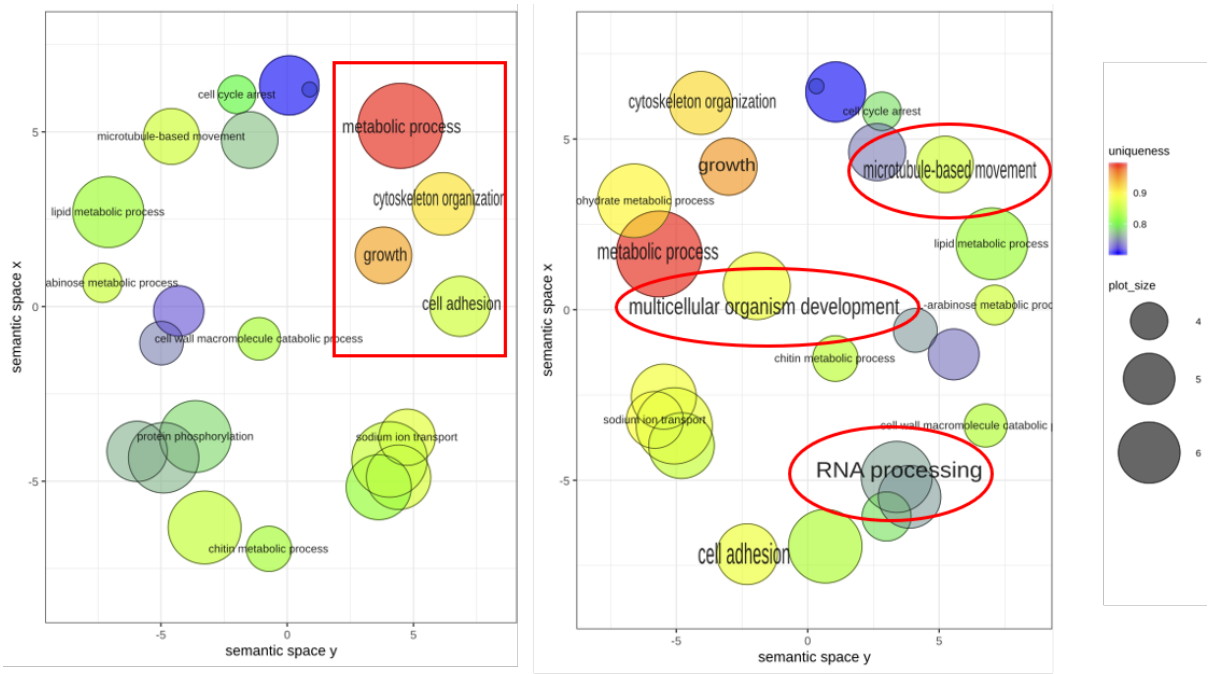

Exclusive DE genes in Vp 0-2 hrs

Exclusive DE genes in Vp 2-8 hrs

Figure 4.4: Scatterplot of gene ontology (GO) terms representing the involvement of the dysregulated genes in various biological processes exclusively at 0-2 hpa transition and 2-8 hpa upon Vp treatment. The scatterplot was generated using REVIGO which shows the cluster representatives in two-dimensional space by application of multidimensional scaling to Biological Process GO terms' semantic similarities. The circle color represents the uniqueness of the GO term and the size of the circle is indicative of the frequency of the GO term.

differential expression of pro-fibrotic genes[28-32] were studied from the RNAseq data (Figure 4.5 A).Profibrotic genes which are significantly differentially expressed were fibrillar collagens (*Collagen Type I, Type III, Type V and Type IX*), *LOXL2-like* (lysyl oxidase) and *PLOD2-like* (Procollagen-lysine,2-oxoglutarate 5-dioxygenase). A close look at the dynamics of expression reveals that all these genes are up-regulated during early regenerative time points (2-8 hpa) and almost all of these are upregulated earlier upon Vp treatment. During fibrosis, up-regulation of *Collagen type III* and *V* indicates active regulation of the fibril diameters and have been reported that ECM containing *Collagen Type I, Type III* and *Type V* constitute very thick collagen fibrils[33]. While the inclusion of *Collagen type IX* is indicative of the additional flexibility to the matrix[34]. Upregulation of *LOXL2* and *PLOD2*-like indicates higher collagen fibril cross-linking activity upon Vp treatment. Together, the upregulation of these genes represents the molecular signature required for ECM mediated fibrosis during regeneration. The higher levels of these pro-fibrotic genes

upon Vp treatment, together with the observations from SEM, TEM & AFM studies on Vp treated polyps supports the hypothesis that disruption of YAP-TEAD interaction causes fibrosis-like condition at the wounded site during early regeneration.

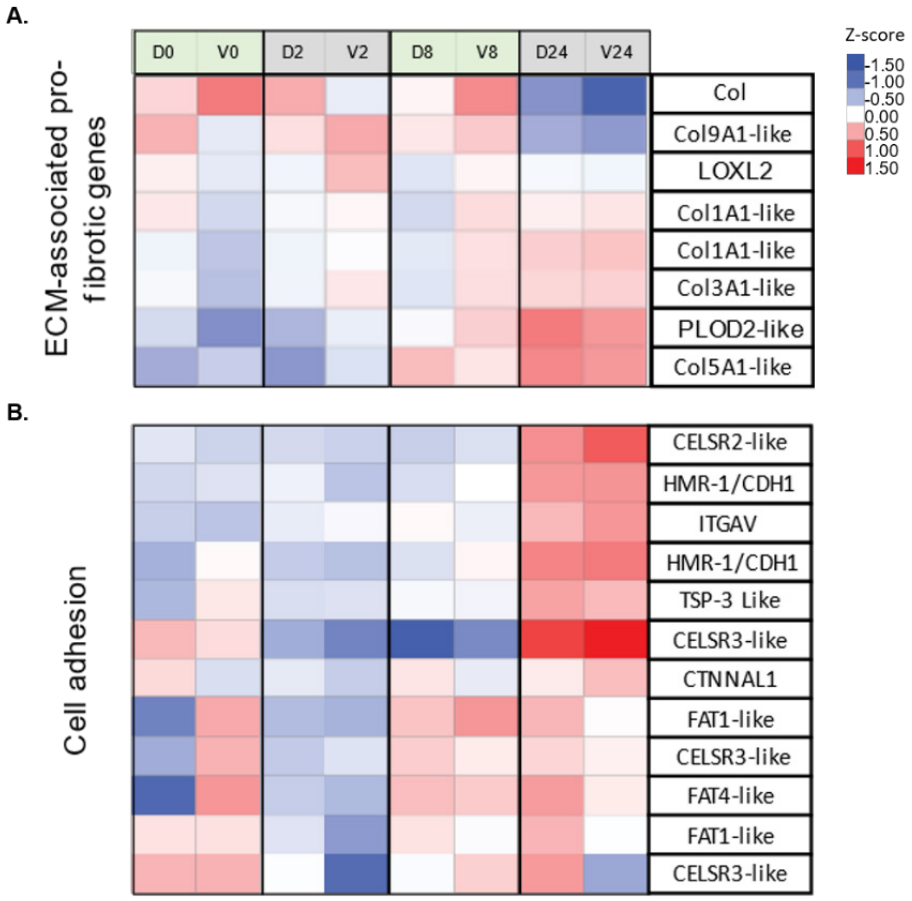

Figure 4.5: Genes involved in cell-ECM interaction are dysregulated upon Vp treatment. A. The heatmap depicts differentially expressed profibrotic genes upon disruption of YAP-TEAD interaction. **B.** The heatmap represents differentially expressed cell-adhesion genes upon disruption of YAP-TEAD interaction. D0, D2, D8 and D24 are the respective regenerative time points of DMSO treated (control) samples while V0, V2, V8 and V24 are the respective regenerative time points of Vp treated samples. The intensity of red and blue colours is indicative of the higher and lower expression levels of genes respectively compared to the controls; red and blue colours denote significantly up- and downregulated genes with log2 fold change cut-off of ±0.58 with a p-value of 0.05, respectively. Each block represents an average value of two biological replicates.

This study reports the first instance of fibrosis among basal metazoans possessing a high regenerative capability. The general consensus in the field of regenerative biology is that fibrosis is anti-regenerative and pro-scar forming. However, a few recent studies report that zebrafish heart regeneration undergoes transient fibrosis only to be resolved later[35-37].This fibrosis was found to be crucial for regenerative capacity. A similar process might be in place in other organisms too and hence might

be indicative of a tissue stiffness regulatory role of fibrosis which may be crucial for initiating a pro-regenerative response. In zebrafish and mice models, macrophages are known to be involved in contributing to collagen secretion for fibrosis along with specific fibroblasts in response to injury[38]. These macrophages are also known to secrete MMPs and cytokines involved in resolving fibrosis[39]. Presently, our understanding of which specific cell-types secrete and regulate ECM in *Hydra* is weak. Understanding how such cell-mediated regulation is orchestrated in diploblastic organisms like *Hydra* will shed light on how basal animals having less complex cell-types evolved to regulate the regenerative process.

To understand how the cells respond or integrate these changes, we then looked into cell adhesion molecules which are capable of sensing and transducing extracellular cues. Among the dysregulated cell adhesion genes, members of Cadherin superfamily were the most perturbed ones (Figure 4.5 B). E-cadherin (*HMR-1*) involved in cell-cell adhesion, cell maturation and movement can be seen upregulated as early as 8 hpa upon Vp treatment. Among the atypical cadherins, members of Flamingo (*CELSR 2 &3-like*) known to be involved in planar cell polarity (PCP) under the control of Wnt signalling in *Drosophila*[40] can be seen dysregulated upon Vp treatment. Another class of atypical cadherins belonging to protocadherin family – *FAT1* and *FAT4* were also seen dysregulated upon Vp treatment. FAT1 has been reported to modulate cell-cell contact and migration in a Wnt-dependent manner[41]. While FAT4 is known to be important in regulating (PCP)[42] and more importantly is reported to inhibit YAP nuclear translocation[43]. From the heatmap, it can be seen clearly that FAT4 expression is tightly regulated during regeneration in control animals where it is slowly upregulated over the regeneration time course indicative of inhibition of Hvul_YAP during regeneration. Interestingly, upon Vp treatment, *FAT4* was seen upregulated in response to Vp pre-treatment (0 hpa) and could be seen down-regulated over the regenerative course.

Among other dysregulated genes involved in cell adhesion, Thrombospondin-3 (*TSP3*), a protein known to regulated integrin-ECM interaction and responsible for promoting fibrosis[44] can be seen upregulated upon Vp treatment. Integrin α V (*ITGAV*) can also be seen upregulated upon Vp treatment. ITGAV has been reported to act as receptor for vitronectin, cytotactin, fibronectin, fibrinogen, laminin, matrix metalloproteinase-2, osteopontin, osteomodulin, prothrombin, thrombospondin and

vWF. ITGAV can interact with different integrin β chains to act as a receptor or co-receptor for a wide variety of secretory proteins like- FGFs, CX3CL1, NRG1, IGFs, IL1B, fibrillin-1[45-52]. ITGAV is also known to activate TGF-β1 by mediating the force-dependent release of LAP from TGF-β1[53]. With so many important activities of ITGAV in cellular response and regulation of ECM and extracellular niche, any change in expression in *ITGAV* gene will, therefore, mean important changes in Cell-ECM regulations upon Vp treatment.

4.3.4. Vp treatment leads to upregulation of developmentally important genes in *Hydra*

Since the regeneration process requires tight regulation of developmental genes, we focused at their dynamic regulation upon Vp treatment. Since YAP and β-catenin are known to be co-regulated in a context-dependent manner in mammals, we first examined if genes involved in Wnt signalling were perturbed upon disruption of YAP-TEAD interaction (Figure 4.6). Many of these dysregulated genes were picked up as multiple variants indicative of possible use of specific variant for a faster regenerative response. Among *Wnt* genes, a close look at the heatmap reveals that most of these *Wnt* genes were strongly down-regulated at 8 hpa upon Vp treatment. Also, all the *Wnt*s were observed to be highly upregulated at 24 hpa. We also noted a higher expression of *wnt3* and *wnt9b* upon Vp treatment. While *wnt3* (WNT3a) is considered as an important component of the head organizer, *wnt9b* is considered to be expressed at extremely low levels in adult *Hydra* and hypothesized as a requirement only during the embryonic development. In alignment with the Wnt gene expression pattern, inhibitors of WNT signalling – Dickkopf (*dkk3)* and soluble Frizzled (*sFrzb*) were upregulated between 0-8 hpa and then downregulated at 24 hpa to enable WNT signalling to elicit its effect. Both DKK and sFRP have been reported to be important in the regulation of fibrosis in humans[7, 8]. These genes were further upregulated at these time points upon Vp treatment. Dishevelled (*DVL2)* is known to be important in transducing Wnt ligand-Frizzled interaction and was found to be upregulated during regeneration. One of the variants was seen to be expressed higher upon Vp treatment as compared to the control set. As reported in the previous studies, Brachyury (*bra*), one of the genes required for head formation[54, 55], was observed to be up-regulated during regeneration. Interestingly, all the 3 variants were dysregulated upon Vp treatment out of which one variant seems to be highly upregulated very early during regeneration (from 0 hpa). Since

Brachyury expression is regulated by *wnt3a* signalling[56], it is interesting to find a Brachyury variant being highly expressed immediately upon amputation when *wnt3a* expression is very low. This observation is indicative of *wnt3a*-independent regulation of *bra* expression. Another possibility is wnt-independent activation of β-catenin. Such a possibility has been reported in Xenopus during mesoderm induction [57]. The Wnt signalling component Frizzled 8 (*Fzd8*) has been reported to be important in inducing TGF-β-Wnt5 mediated pro-fibrotic responses in lungs[58]. Upon Vp treatment, FZD8 is up-regulated during 2 and 8 hpa as compared to the control and hence further supporting its pro-fibrotic properties.

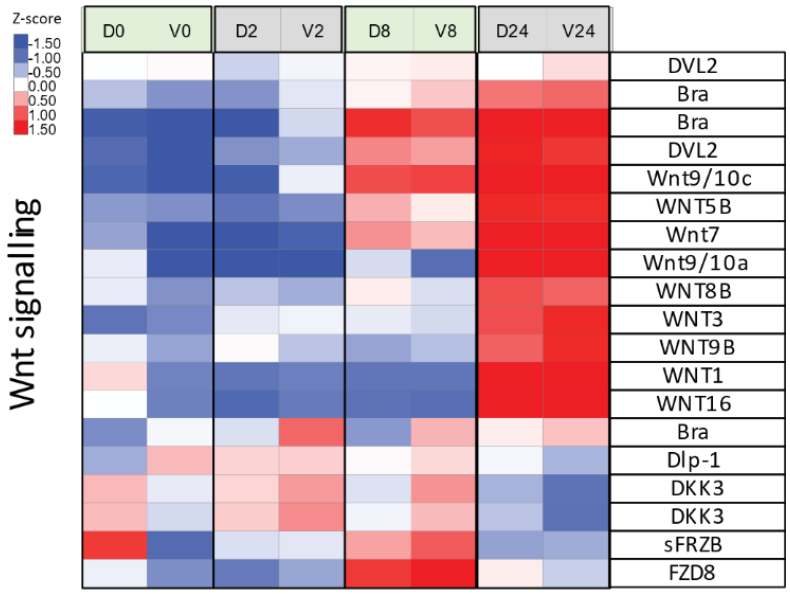

Figure 4.6: Genes involved in Wnt signalling are up-regulated upon Vp treatment. The heatmap shows differentially expressed Wnt responsive and regulatory genes upon disruption of YAP-TEAD interaction. D0, D2, D8 and D24 are the respective regenerative time points of DMSO treated (control) samples while V0, V2, V8 and V24 are the respective regenerative time points of Vp treated samples. The intensity of red and blue colours is indicative of the higher and lower expression levels of genes respectively compared to the controls; red and blue colours denote significantly up- and downregulated genes with log2 fold change cut-off of ±0.58 with a p-value of 0.05, respectively. Each block represents an average value of two biological replicates.

Looking at the other developmentally important genes known to be involved in regeneration (Figure 4.7), we find that most of them were upregulated early during regeneration upon Vp treatment. Genes known to regulate the TGF-β/ BMP signalling such as *bmp4, kcp* and *grem2* were upregulated upon Vp treatment. Genes involved in head formation in *Hydra* during regeneration such as *vegf* and *fgfr2* were upregulated early during regeneration. Genes encoding important developmentally regulated transcription factors such as *bra, arx, otx and foxa2* that

are known to be required for head formation were also upregulated early upon Vp treatment. Notch and Ephrin signalling are juxtacrine signalling pathways known to be involved in the boundary formation. Their early upregulation upon Vp treatment is indicative of early establishment of boundaries required for developmental signalling and compartmentalization which may aid in faster regeneration.

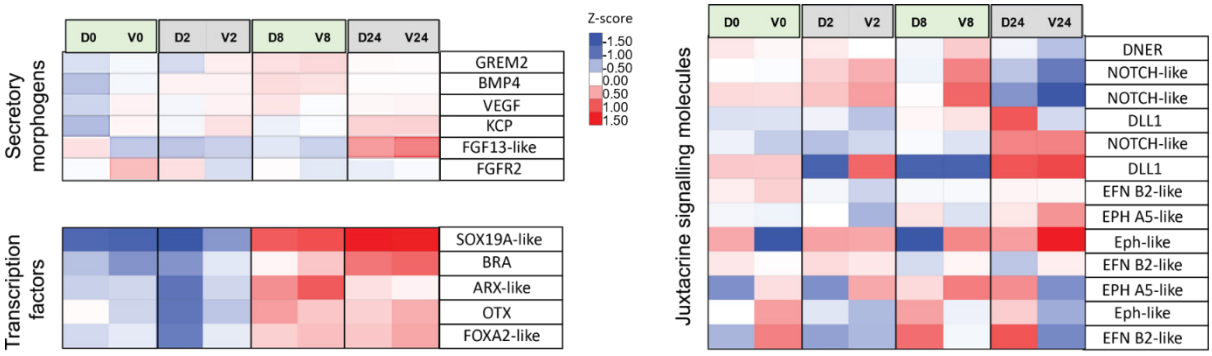

Figure 4.7: Genes involved in developmental pathways are up-regulated early upon Vp treatment. The heatmap shows differentially expressed secretory morphogens, developmentally important transcription factors and boundary forming juxtacrine signalling genes upon disruption of YAP-TEAD interaction. D0, D2, D8 and D24 are the respective regenerative time points of DMSO treated (control) samples while V0, V2, V8 and V24 are the respective regenerative time points of Vp treated samples. The intensity of red and blue colours is indicative of the higher and lower expression levels of genes respectively compared to the controls; red and blue colours denote significantly up- and downregulated genes with log2 fold change cut-off of ±0.58 with a p-value of 0.05, respectively. Each block represents an average value of two biological replicates.

Based on these observations, we find that even though *Wnt* genes are up-regulated strongly by 24 hpa, some regulators and targets of WNT signalling were up-regulated much early. Many of the other developmentally important genes known to be required for establishing head organizers can also be seen up-regulated earlier than the control polyps. In summary, we find that there is a general acceleration of activation of many crucial head organizer related genes upon Vp treatment.

4.3.5. YAP and β-catenin expression are co-regulatory in *Hydra*

In the previous section, we reported that WNT signalling components are dysregulated upon drug-induced disruption of YAP-TEAD interaction. Based on the previous reports of YAP-β-catenin co-regulation, we validated whether the same holds true in Cnidarians as well. To this effect, we performed siRNA-mediated knockdown of YAP and β-catenin separately and monitored the effects on the

expression of the other (Figure 4.8 A and B). Upon Hvul_YAP knockdown (96%), we observed 48 % reduction in Hvul_β-catenin levels whereas as low as 30% knockdown of Hvul_β-catenin lead to 98% reduction in Hvul_YAP expression. Such an effect indicates regulation of YAP and β-catenin are dependent on each other's level of expression in *Hydra* as well. Further studies will be required to monitor whether this is a direct promoter level regulation or an indirect regulation.

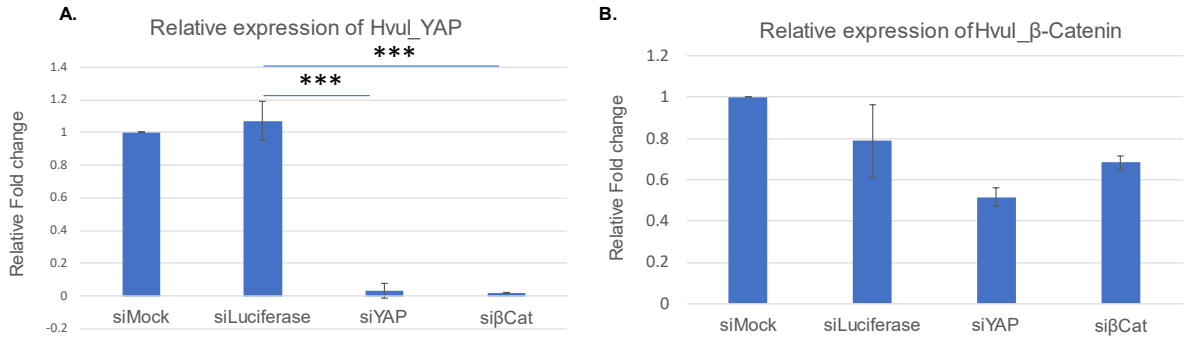

Figure 4.8: siRNA-mediated knockdown of Hvul_YAP and Hvul_ β-catenin suggests their expression is co-regulatory. A. Hvul_YAP mRNA expression measured by qPCR from RNA collected from polyps after YAP and β-catenin RNAi as indicated. (N=3, n=40) (Asterisk indicates p values with ***>10^{-4}) **B.** Hvul_ β-catenin mRNA expression measured by qPCR from RNA collected from polyps after YAP and β-catenin RNAi as indicated. (N=1, n= 40)

4.3.6. YAP and β-catenin mediated mechano-sensing may regulate head organizer function by modulation of Brachyury

A recently study has reported β-catenin-dependent mechanism of mechanotransduction in an anthozoan Cnidarian *Nematostella*[59]. In this study, the authors demonstrated that external mechanical compression of the *Nematostella* embryo lead to disruption of *brachyury* expression pattern and hampered the embryonic development[59]. In *Hydra*, *brachyury* is important for head development and regeneration[55]. From the transcriptomic analysis, we found that *brachyury* is upregulated upon Vp treatment early during regeneration. To monitor the precise spatio-temporal tissue expression pattern of *bra*, we performed RNA whole-mount *in situ* hybridization (WISH) of *bra* upon Vp treatment and compared it with that of the DMSO treated polyps. WISH clearly revealed the expression of *bra* within 2 hpa and strong establishment of localized high expression at the tip characteristic of head organizer activity[55].

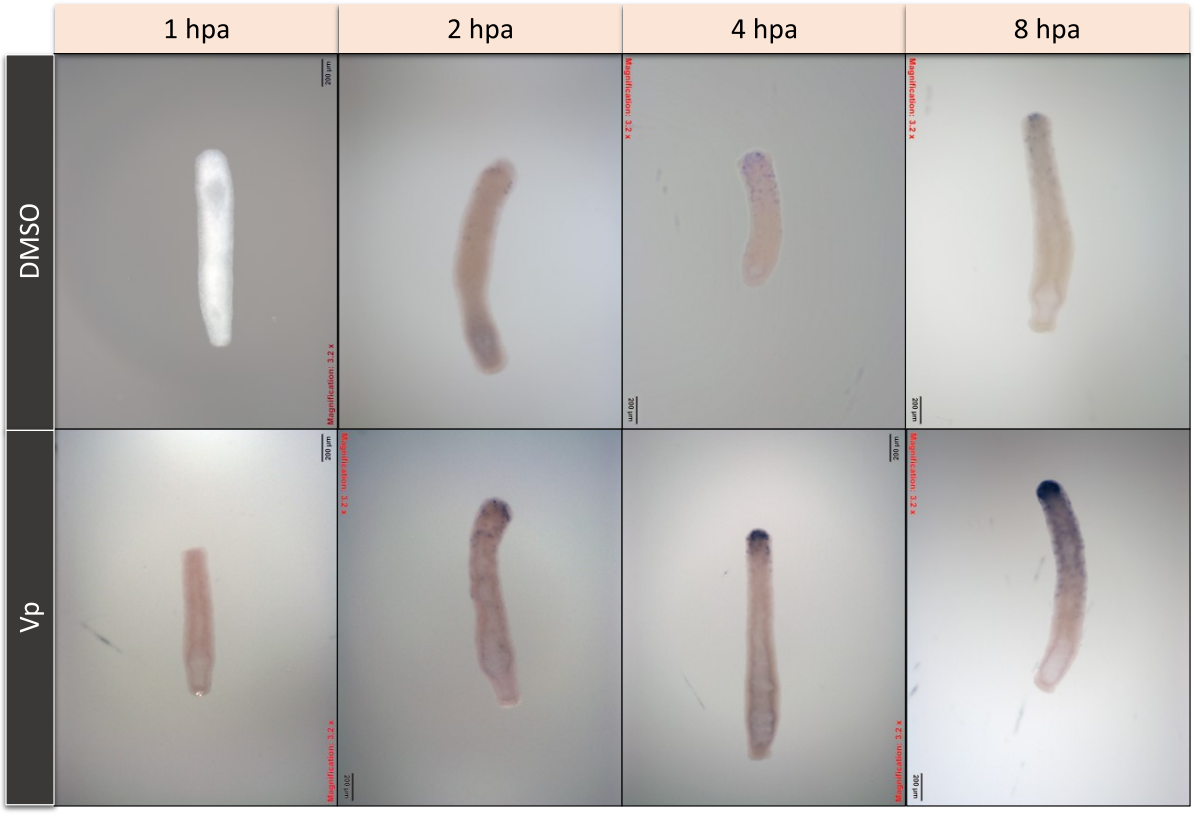

Figure 4.9*: Hvul_Bra* expression during head regeneration in DMSO and Vp treated *Hydra* shows early establishment and stabilization of *Brachyury* required for head organizer activity. Whole-mount *in situ* hybridization of *Hvul_Bra* expression for the whole polyp performed at early regenerative time points (1, 2, 4 & 8 hpa) upon DMSO and Vp treatment (5 µM). Scale Bar= 200 µm.

To test whether external strain can hamper the head an experiment to apply uniaxial compression to decapitated polyp at the regenerating tip (Figure 4.1 A). When we applied a uniaxial compression using a single 22 x 22 mm glass coverslip, we could create an external 56 Pa pressure on the regenerating polyp tip. Using this setup, we found that a transient external pressure early during regeneration (during the first 1 hpa) was sufficient to disrupt the normal kinetics of tentacle morphogenesis during regeneration (Figure 4.10). A significant delay in the appearance of tentacles (at 48 hpa) was observed in the polyps which underwent compression. No other visible defect was seen in the regenerative process and all tentacles were formed by 60-72 hpa like the normal polyps. This observation indicates that similar to Vp treated increase in tissue stiffness, an external pressure on the tissue could also induce dysregulation of regenerative kinetics albeit in a completely opposite outcome presumably due to difference in the duration and extent of pressure applied.

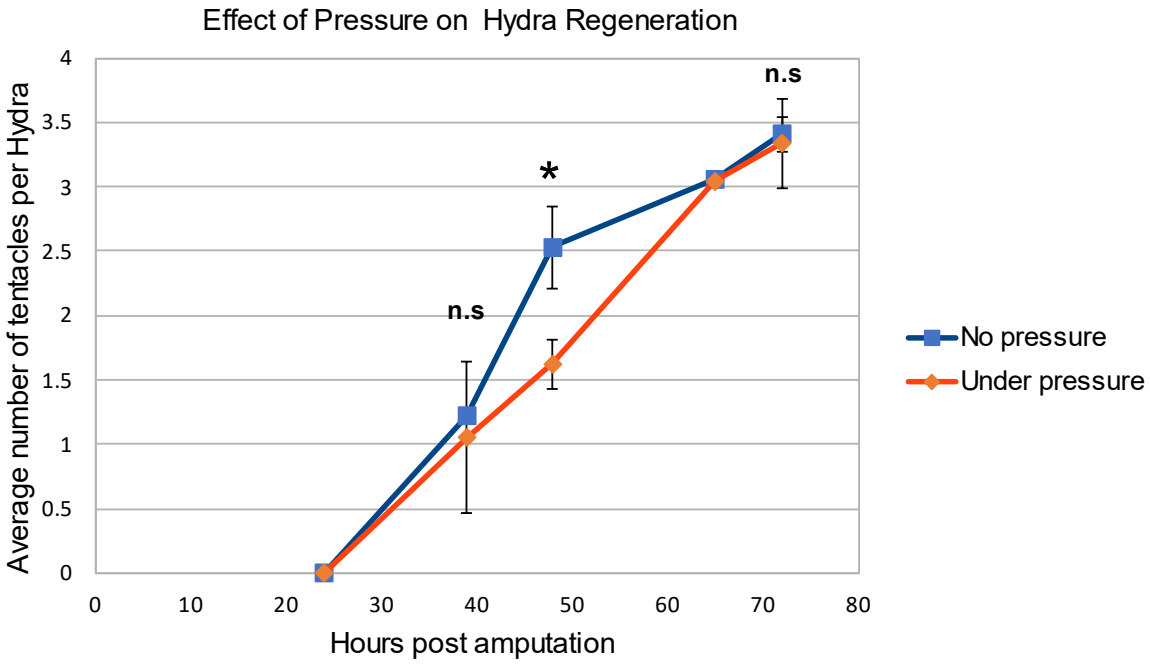

Figure 4.10: External compression (pressure) on regenerating tip causes altered regeneration kinetics in *Hydra*. Transient uniaxial compression of regenerating tip of decapitated polyps for 1 hr at 1 hpa was performed to measure its effect on tentacle formation. After the compression, the regenerating polyps were scored for new tentacles at 24 to 72 hpa. The graph indicates the average number of tentacles per *Hydra* at the given regenerating time point ranging from 24 to 72 hpa) (N=3, n=20) (Asterisk signify p values with *=0.05-0.01 & n.s. is not significant)

4.4. CONCLUSIONS AND FUTURE PERSPECTIVES

In this chapter, the differential transcriptomic analysis of Vp treated *Hydra* revealed an earlier expression of many of the developmentally important genes required for head regeneration. The data also suggested co-regulation of Hvul_YAP and Hvul_β-catenin. Further, we show that the application of transient external pressure during early regenerative time point causes disruption in the regeneration kinetics. These results corroborate the observation reported for *Nematostella* wherein the application of external pressure lead to the disruption of the embryonic development through *bra* dysregulation[59]. This study reported that during embryonic development, myosin-dependent contractility of blastopore lip cells might create a local region of high stiffness, which is then transduced in a β-catenin-dependent manner to enforce *brachyury* expression at the oral pole. Such mechanisms are known to exist in bilaterians as well wherein the β-catenin-dependent mechanosensitive pathways in *Drosophila* and zebrafish have been shown to regulate the expression of *brachyury* to direct the mesodermal fate specification despite having a divergent mode of gastrulation[60]. However, the precise molecular mechanism of how the mechanical strain leads to β-catenin-dependent activation of *brachyury* is not clearly understood. Such a conserved mechanosensitive mechanism for *bra* expression across the phyla despite differing modes of morphogenesis indicates such mechanism(s) could exist for regulating other processes such as regeneration. Our study indicates that *brachyury* is activated earlier upon Vp treatment. We also speculate that this activation may be Wnt-independent. Such Wnt-independent mechanisms have been reported for nuclear translocation of β-catenin by phosphorylation of specific tyrosine residues which causes disengagement of β-catenin from cadherins associated with the cell-membrane and finally nuclear translocation[60, 61]. β-catenin stabilization and nuclear localization is also known to be regulated by YAP in a Wnt-independent-E-Cadherin dependent manner[62]. We hypothesize that Vp treatment leads to the upregulation of pro-fibrotic genes. This, in turn, causes an increase in matrix stiffness. During regeneration, higher tissue stiffness may lead to Wnt-independent and YAP-dependent stabilization and nuclear localization of β-catenin. Finally, this may lead to early activation of β-catenin transcriptional targets, which are required

for *Hydra* head regeneration. The RNA *in situ* hybridization analysis of *bra* expression during regeneration revealed early consolidation of *bra* expression at the distal regenerating tip upon Vp treatment (Figure 4.9). Interestingly, multiple *bra* expressing foci were also evident near the regenerating tip before the expression is consolidated to the distal regenerating tip (2 hpa). Such foci can also be seen getting stronger and more spread out (may be indicative of a gradient of expression away from the hypostome) as the regeneration progresses (4 and 8 hpa). It should also be noted that such foci can also be observed in the DMSO treated polyps but with very low signal intensity and could have been considered as non-specific or background signal in previous studies. This observation might be linked to one of the popular theories by the illustrious theoretical biologist Hans Meinhardt that predicted how cells at the regenerating tip are chosen to act as head organizers[63]. The theory suggests stochastic activation of head organizer genes in the cells present at the regenerating tip that may get consolidated with pre-existing cues. The *bra* expression pattern we find here does conform to such suggestions where consolidation of *bra* expression could be a function of stabilization of β-catenin by higher stiffness associated with the curvature inherent to the regenerating tip. WNT family of proteins have long been considered as the component of the head organizer.

Our observations from this study indicate a tantalizing prospect of β-catenin being the main head organizer which can be regulated either biochemically (through WNT ligands and other WNT regulators) or mechanically (through various external forces) to regulate its potential head organizer activity. Such a theory could also explain how the WNT gradient can also act as head activator and inhibitor in presence or absence of the appropriate mechanical tissue strain. The fact that induction of Wnt signalling by Alsterpaullone treatment only causes ectopic tentacle formation throughout the body rather than the expected multiple new heads indicate that WNT signalling itself is not enough for the head formation.

Such a theory can also be used to explain how excess of cell proliferation in a well fed *Hydra* causes emergence of a secondary head organizer for bud formation. Budding is known to be a function of cell movement and cell proliferation in *Hydra*[64]. When there is increase in rate of cell proliferation due to excessive feeding as compared the rate of cells sloughed being off, the budding occurs to compensate

this as mechanism to sustain the steady state of body size to cell number ratio. The explanation of specific location of budding region is theorized as a result of region of minimum head inhibitor density originating from the head and foot regions[65, 66]. This theory could easily explain how a local excessive cell proliferation at the budding region lead to a localized stress in the budding region and lead to spontaneous activation of β-catenin and hence giving rise to a new head organizer required for budding. As a corollary, in Vp treated polyps, a uniform increase in tissue stiffness throughout the body combined with a local minima of head inhibitor concentration at the budding region can lead to spontaneous activation of β-catenin and hence increase in rate of budding without the need of increase in cell proliferation. To conclusively prove the hypothesis of β-catenin head organizer function, the localization of β-catenin should be monitored during early regeneration time points upon Vp treatment. Blocking the canonical Wnt signalling in this context and monitoring whether Vp treatment can still cause the observed phenotype will complement the hypothesis. It remains to be confirmed whether tissue compression during regeneration defines the *bra* expression pattern during regeneration. A high resolution proteomic study also needs to be undertaken during regeneration to precisely delineate the transcriptional factor YAP uses upon disruption of the its interaction with TEAD, to orchestrate its synergistic effect with β-catenin as is observed upon Vp treatment. This model can then be exploited to delineate the fine-tuned molecular mechanism of regulation of *bra* expression pattern during regeneration.

A recently published study also reports a similar finding in terms of upregulation of WNT-signalling related genes in human embryonic stem cells (hESCs) upon YAP repression[67]. The study not only shows that YAP represses Activin induced expression of WNT3 but also shows that WNT-Activin-dependent β-catenin and SMAD transcriptional co-regulation of genes by co-binding to the promoter region required for meso-endodermal lineage differentiation is controlled by YAP. YAP restricts the meso-endodermal lineage differentiation by binding to the promoter region of these genes and preventing recruitment of SMAD to the site. Such an observation becomes extremely interesting in the context of this study and explains many of the observations. Such a mechanism might be in place to establish tissue stiffness-dependent checkpoints during regeneration by YAP to control the WNT3a-

dependent activation of head-organizer genes. The perceived delay in regeneration dynamics under normal head regeneration paradigm might be a mechanical coupling of regaining lost ECM (hence the tissue stiffness) and setting up head organizer function. YAP might have a role in regulating this such that the system is only allowed to start the regenerative program when the ECM is re-synthesized completely. Such a regulation also predicts a restriction of WNT3a expression in rest of the body in *Hydra* to prevent a head-specific fate which may only be relieved by a mechanical inhibition of YAP. No studies have yet implicated Activin in *Hydra* regeneration. However, it has been shown that the Activin-like 1 gene is expressed at about the same time when the WNT-signalling is activated at stage 3 of the *Hydra* bud development[27]. A detailed study of WNT3a signalling and Activin signalling in the context of YAP-TEAD disruption during regeneration using a combinatorial treatment of GSK inhibitor ALP, Vp and Activin-receptor-like kinase 4 like A-83-01 might shed more light on this hypothesis.

4.5. REFERENCES

1. Rockey, D.C., Bell, P.D. & Hill, J.A. Fibrosis—a common pathway to organ injury and failure. *New England Journal of Medicine* **372**, 1138-1149 (2015).
2. Tam, J. *et al.* Reconstitution of full-thickness skin by microcolumn grafting. *Journal of tissue engineering and regenerative medicine* **11**, 2796-2805 (2017).
3. Wang, Y.-Y. *et al.* Macrophage-to-myofibroblast transition contributes to interstitial fibrosis in chronic renal allograft injury. *Journal of the American Society of Nephrology* **28**, 2053-2067 (2017).
4. Leask, A. & Abraham, D.J. TGF-β signaling and the fibrotic response. *The FASEB Journal* **18**, 816-827 (2004).
5. Surendran, K., McCaul, S.P. & Simon, T.C. A role for Wnt-4 in renal fibrosis. *American Journal of Physiology-Renal Physiology* **282**, F431-F441 (2002).
6. Ye, B. *et al.* Canonical Wnt/β-catenin signaling in epicardial fibrosis of failed pediatric heart allografts with diastolic dysfunction. *Cardiovascular Pathology* **22**, 54-57 (2013).
7. Kobayashi, K. *et al.* Secreted Frizzled-related protein 2 is a procollagen C proteinase enhancer with a role in fibrosis associated with myocardial infarction. *Nature cell biology* **11**, 46-55 (2009).
8. Ren, S. *et al.* LRP-6 is a coreceptor for multiple fibrogenic signaling pathways in pericytes and myofibroblasts that are inhibited by DKK-1. *Proceedings of the National Academy of Sciences* **110**, 1440-1445 (2013).
9. Martin, K. *et al.* PAK proteins and YAP-1 signalling downstream of integrin beta-1 in myofibroblasts promote liver fibrosis. *Nature communications* **7**, 12502 (2016).
10. Toyama, T. *et al.* Therapeutic targeting of TAZ and YAP by dimethyl fumarate in systemic sclerosis fibrosis. *Journal of Investigative Dermatology* **138**, 78-88 (2018).
11. Lee, M.-J., Byun, M.R., Furutani-Seiki, M., Hong, J.-H. & Jung, H.-S. YAP and TAZ regulate skin wound healing. *Journal of Investigative Dermatology* **134**, 518-525 (2014).
12. Carthy, J.M., Garmaroudi, F.S., Luo, Z. & McManus, B.M. Wnt3a induces myofibroblast differentiation by upregulating TGF-β signaling through SMAD2 in a β-catenin-dependent manner. *PloS one* **6** (2011).
13. Azzolin, L. *et al.* YAP/TAZ incorporation in the β-catenin destruction complex orchestrates the Wnt response. *Cell* **158**, 157-170 (2014).
14. Mendoza-Reinoso, V. & Beverdam, A. Epidermal YAP activity drives canonical WNT16/β-catenin signaling to promote keratinocyte proliferation in vitro and in the murine skin. *Stem cell research* **29**, 15-23 (2018).
15. Pan, J.-X. *et al.* YAP promotes osteogenesis and suppresses adipogenic differentiation by regulating β-catenin signaling. *Bone research* **6**, 1-12 (2018).
16. Park, H.W. *et al.* Alternative Wnt signaling activates YAP/TAZ. *Cell* **162**, 780-794 (2015).
17. Deng, F. *et al.* YAP triggers the Wnt/β-catenin signalling pathway and promotes enterocyte self-renewal, regeneration and tumorigenesis after DSS-induced injury. *Cell death & disease* **9**, 1-16 (2018).
18. Kumar, D., Nitzan, E. & Kalcheim, C. YAP promotes neural crest emigration through interactions with BMP and Wnt activities. *Cell Communication and Signaling* **17**, 1-17 (2019).
19. Pefani, D.-E. *et al.* TGF-β targets the Hippo pathway scaffold RASSF1A to facilitate YAP/SMAD2 nuclear translocation. *Molecular cell* **63**, 156-166 (2016).
20. Varelas, X. *et al.* The Crumbs complex couples cell density sensing to Hippo-dependent control of the TGF-β-SMAD pathway. *Developmental cell* **19**, 831-844 (2010).
21. Liu, Y. *et al.* YAP modulates TGF-β1-induced simultaneous apoptosis and EMT through upregulation of the EGF receptor. *Scientific reports* **7**, 45523 (2017).

22. Robinson, M.D., McCarthy, D.J. & Smyth, G.K. edgeR: a Bioconductor package for differential expression analysis of digital gene expression data. *Bioinformatics* **26**, 139-140 (2010).
23. Haas, B.J. *et al.* De novo transcript sequence reconstruction from RNA-seq using the Trinity platform for reference generation and analysis. *Nature protocols* **8**, 1494 (2013).
24. Reddy, P.C. *et al.* Molecular signature of an ancient organizer regulated by Wnt/β-catenin signalling during primary body axis patterning in Hydra. *Communications Biology* **2**, 1-11 (2019).
25. De Hoon, M.J., Imoto, S., Nolan, J. & Miyano, S. Open source clustering software. *Bioinformatics* **20**, 1453-1454 (2004).
26. Supek, F., Bošnjak, M., Škunca, N. & Šmuc, T. REVIGO summarizes and visualizes long lists of gene ontology terms. *PloS one* **6** (2011).
27. Watanabe, H. *et al.* Nodal signalling determines biradial asymmetry in Hydra. *Nature* **515**, 112 (2014).
28. Ding, N. *et al.* BRD4 is a novel therapeutic target for liver fibrosis. *Proceedings of the National Academy of Sciences* **112**, 15713-15718 (2015).
29. Mederacke, I. *et al.* Fate tracing reveals hepatic stellate cells as dominant contributors to liver fibrosis independent of its aetiology. *Nature communications* **4**, 1-11 (2013).
30. Bataller, R. & Brenner, D.A. Liver fibrosis. *The Journal of clinical investigation* **115**, 209-218 (2005).
31. Wynn, T.A. Cellular and molecular mechanisms of fibrosis. *The Journal of Pathology: A Journal of the Pathological Society of Great Britain and Ireland* **214**, 199-210 (2008).
32. Vittal, R. *et al.* Type V collagen induced tolerance suppresses collagen deposition, TGF-β and associated transcripts in pulmonary fibrosis. *PloS one* **8** (2013).
33. Spiess, K. & Zorn, T.M.T. Collagen types I, III, and V constitute the thick collagen fibrils of the mouse decidua. *Microscopy research and technique* **70**, 18-25 (2007).
34. Parsons, P. *et al.* Type IX collagen interacts with fibronectin providing an important molecular bridge in articular cartilage. *Journal of Biological Chemistry* **286**, 34986-34997 (2011).
35. Sánchez-Iranzo, H. *et al.* Transient fibrosis resolves via fibroblast inactivation in the regenerating zebrafish heart. *Proceedings of the National Academy of Sciences* **115**, 4188-4193 (2018).
36. Chablais, F., Veit, J., Rainer, G. & Jaźwińska, A. The zebrafish heart regenerates after cryoinjury-induced myocardial infarction. *BMC developmental biology* **11**, 21 (2011).
37. González-Rosa, J.M., Martín, V., Peralta, M., Torres, M. & Mercader, N. Extensive scar formation and regression during heart regeneration after cryoinjury in zebrafish. *Development* **138**, 1663-1674 (2011).
38. Simões, F.C. *et al.* Macrophages directly contribute collagen to scar formation during zebrafish heart regeneration and mouse heart repair. *Nature Communications* **11**, 1-17 (2020).
39. Wynn, T.A. & Vannella, K.M. Macrophages in tissue repair, regeneration, and fibrosis. *Immunity* **44**, 450-462 (2016).
40. Usui, T. *et al.* Flamingo, a seven-pass transmembrane cadherin, regulates planar cell polarity under the control of Frizzled. *Cell* **98**, 585-595 (1999).
41. Nishikawa, Y. *et al.* Human FAT1 cadherin controls cell migration and invasion of oral squamous cell carcinoma through the localization of β-catenin. *Oncology reports* **26**, 587-592 (2011).
42. Saburi, S. *et al.* Loss of Fat4 disrupts PCP signaling and oriented cell division and leads to cystic kidney disease. *Nature genetics* **40**, 1010 (2008).
43. Ma, L. *et al.* Fat4 suppression induces Yap translocation accounting for the promoted proliferation and migration of gastric cancer cells. *Cancer biology & therapy* **17**, 36-47 (2016).

44. Schips, T.G. *et al.* Thrombospondin-3 augments injury-induced cardiomyopathy by intracellular integrin inhibition and sarcolemmal instability. *Nature communications* **10**, 1-15 (2019).
45. Fujita, M., Takada, Y.K. & Takada, Y. Integrins αvβ3 and α4β1 act as coreceptors for fractalkine, and the integrin-binding defective mutant of fractalkine is an antagonist of CX3CR1. *The Journal of Immunology* **189**, 5809-5819 (2012).
46. Ieguchi, K. *et al.* Direct binding of the EGF-like domain of neuregulin-1 to integrins (αvβ3 and α6β4) is involved in neuregulin-1/ErbB signaling. *Journal of Biological Chemistry* **285**, 31388-31398 (2010).
47. Mori, S. *et al.* Direct binding of integrin αvβ3 to FGF1 plays a role in FGF1 signaling. *Journal of Biological Chemistry* **283**, 18066-18075 (2008).
48. Mori, S. *et al.* The integrin-binding defective FGF2 mutants potently suppress FGF2 signalling and angiogenesis. *Bioscience reports* **37** (2017).
49. Saegusa, J. *et al.* The direct binding of insulin-like growth factor-1 (IGF-1) to integrin αvβ3 is involved in IGF-1 signaling. *Journal of Biological Chemistry* **284**, 24106-24114 (2009).
50. Prieto, D.M.C. *et al.* Direct integrin binding to insulin-like growth factor-2 through the C-domain is required for insulin-like growth factor receptor type 1 (IGF1R) signaling. *PloS one* **12** (2017).
51. Takada, Y.K. *et al.* Direct binding to integrins and loss of disulfide linkage in interleukin-1β (IL-1β) are involved in the agonistic action of IL-1β. *Journal of Biological Chemistry* **292**, 20067-20075 (2017).
52. Bax, D.V. *et al.* Cell adhesion to fibrillin-1 molecules and microfibrils is mediated by α5β1 and αvβ3 integrins. *Journal of Biological Chemistry* **278**, 34605-34616 (2003).
53. Dong, X. *et al.* Force interacts with macromolecular structure in activation of TGF-β. *Nature* **542**, 55-59 (2017).
54. Bielen, H. *et al.* Divergent functions of two ancient Hydra Brachyury paralogues suggest specific roles for their C-terminal domains in tissue fate induction. *Development* **134**, 4187-4197 (2007).
55. Technau, U. & Bode, H.R. HyBra1, a Brachyury homologue, acts during head formation in Hydra. *Development* **126**, 999-1010 (1999).
56. Yamaguchi, T.P., Takada, S., Yoshikawa, Y., Wu, N. & McMahon, A.P. T (Brachyury) is a direct target of Wnt3a during paraxial mesoderm specification. *Genes & development* **13**, 3185-3190 (1999).
57. Schohl, A. & Fagotto, F. A role for maternal β-catenin in early mesoderm induction in Xenopus. *The EMBO journal* **22**, 3303-3313 (2003).
58. Spanjer, A.I. *et al.* TGF-β-induced profibrotic signaling is regulated in part by the WNT receptor Frizzled-8. *The FASEB Journal* **30**, 1823-1835 (2016).
59. Pukhlyakova, E., Aman, A.J., Elsayad, K. & Technau, U. β-Catenin–dependent mechanotransduction dates back to the common ancestor of Cnidaria and Bilateria. *Proceedings of the National Academy of Sciences* **115**, 6231-6236 (2018).
60. Brunet, T. *et al.* Evolutionary conservation of early mesoderm specification by mechanotransduction in Bilateria. *Nature communications* **4**, 1-15 (2013).
61. Monga, S.P. *et al.* Hepatocyte growth factor induces Wnt-independent nuclear translocation of beta-catenin after Met-beta-catenin dissociation in hepatocytes. *Cancer Res* **62**, 2064-2071 (2002).
62. Benham-Pyle, B.W., Pruitt, B.L. & Nelson, W.J. Mechanical strain induces E-cadherin–dependent Yap1 and β-catenin activation to drive cell cycle entry. *Science* **348**, 1024-1027 (2015).
63. Meinhardt, H. Modeling pattern formation in hydra: a route to understanding essential steps in development. *International Journal of Developmental Biology* **56**, 447-462 (2012).

64. Webster, G. & Hamilton, S. Budding in Hydra: the role of cell multiplication and cell movement in bud initiation. *Development* **27**, 301-316 (1972).
65. Alvarado, A.S. Planarian regeneration: its end is its beginning. *Cell* **124**, 241-245 (2006).
66. Berking, S. A model for budding in hydra: pattern formation in concentric rings. *Journal of theoretical biology* **222**, 37-52 (2003).
67. Estarás, C., Hsu, H.-T., Huang, L. & Jones, K.A. YAP repression of the WNT3 gene controls hESC differentiation along the cardiac mesoderm lineage. *Genes & development* **31**, 2250-2263 (2017).

5 APPENDIX

5.1 PRIMER SEQUENCES

Table 5.1: Primer sequences and their details

Primer No.	Description	Sequence	Expected size (bp)	Purpose
SG8324	Hydra YAP (HyYAP) forward full length	ATGGATATGAATTCTACGCAACGGC	1170	cloning
SG8325	Hydra YAP (HyYAP) reverse full length	CTACAACCAAGTCATATATGCATTAGGC	1170	cloning
SG8326	HyYAP qPCR forward	CCTCGAAAAGCACAATCCATG	105	qPCR
SG8327	HyYAP qPCR reverse	CCTCACCTTCAGCTGTAACAG	105	qPCR
SG8329	Hydra TEF1 (HyTEF1) forward2 full length	ATGGCGGAAAACTGTCGAGATCC	1356	cloning
SG8374	Hydra TEF (HyTEF) Reverse primer_2 Full length	TCAGTCTCTGACTAATTTAAATATGTGGT	1356	Cloning
SG8331	HyTEF1 qPCR forward	TGGCGGAAAACTGTCGAG	100	qPCR
SG8332	HyTEF1 qPCR reverse	TTGCTCAATGTCTGGACTCC	100	qPCR
SG8339	Hydra RASSF (HyRASSF) forward full length	ATGGCAACTCCAAATTCCAA	1260	cloning
SG8340	Hydra RASSF (HyRASSF) reverse full length	TCACACTATTCGATCTTTTA	1260	cloning
SG8341	HyRASSF qPCR forward	AGCTTTTATATGCCAAGAGGAAC	147	qPCR
SG8342	HyRASSF qPCR reverse	TGCTGGAACATGCTTTTCG	147	qPCR
SG8343	Hydra Hippo (HyHpo) forward partial	AGTTTGAAGAAGTTGAGCGAAGAA	1494	cloning
SG8344	Hydra Hippo (HyHpo) reverse partial	TTAAAAATTTGCTTGCCTGCGTT	1494	cloning
SG8431	Hydra Hippo(HyHpo)Fwd qPCR primer	CACAGAGGGTCATTCAAAATTAGC	95	qPCR
SG8432	Hydra Hippo(HyHpo)Rev qPCR primer	TGTGTTCCGTTTTGCCATTG	95	qPCR
SG8839	Hydra YAP (HyYAP) pGEX 4T-1 forward full length	CGCGTGGATCCATGGATATGAATTCTACGCA	1192	Sub-cloning
SG8840	Hydra YAP (HyYAP) pGEX 4T-1 reverse full length	GGCCGCTCGAGCTACAACCAAGTCATATATGC	1192	Sub-cloning
SG8880	Hydra TEF (HyTEF) pGEX 4T-1 forward full length	CCCGGGTCGACGCATGGCGGAAAACTGTCGAGAT	1378	Sub-cloning
SG8881	Hydra TEF (HyTEF) pGEX 4T-1 reverse full length	ACGATGCGGCCGCTCAGTCTCTGACTAATTTAAA	1378	Sub-cloning
SG9382	HyYAP Partial ISH Fwd	GACTCAGACACTGACTTGGAAC	625	in situ hybridization probe
SG9383	HyYAP Partial ISH Rev	GACGCTTCTCTTGCTGGTAATA	625	in situ hybridization probe
SG9384	HvHpo Full length Fwd	ATGTCTCGCAGTTTGAAGAAGTTGAG	1503	Cloning
SG9385	HvLATS Full length Fwd	ATGGCAGCTAATAATCTTTTTAGTAG	1360	Cloning
SG9386	HvLATS Full length Rev	TTATATGGGGAGATTTCGCAATC	1360	Cloning
SG9387	HvMob1 Full length Fwd	ATGAGTTTCCTGTTTGGCTCCA	645	Cloning

SG9388	HvMob1 Full length Rev	TTATTTATTAATTAACTTATCCATAAGTTC	645	Cloning
SG9389	HvRunx Full length Fwd	ATGTCAACAATGACATTAACTCAACTG	1266	Cloning
SG9390	HvRunx Full length Rev	TTAATATGGTCGCCAAACTTTCGGA	1266	Cloning
SG9391	HvSav Full Length Fwd	ATGTTTAAGAAAAAAGATATTATCAAAACA	1434	Cloning
SG9392	HvSav Full Length Rev	TTAAACATGAGTTTTTTTAAAAGAAATACT	1434	Cloning
SG9924	HyYAP qPCR forward	CCTCGAAAAGCACAATCCATG	105	qPCR
SG9925	HyYAP qPCR reverse	CCTCACCTTCAGCTGTAACAG	105	qPCR
SG9926	Hvul_MobKinase qPCR Forward	AGCTACTCTTGGTTCTGGAAAC	92	qPCR
SG9927	Hvul_MobKinase qPCR Reverse	AATCTACTGTGTTCACTGCGAT	92	qPCR
SG9928	Hvul_Runx qPCR Forward	GAAGATCGGGTAGAGGAAAGAC	110	qPCR
SG9929	Hvul_Runx qPCR Reverse	TCTTGGTCCGTCAACAGTAAC	110	qPCR
SG9930	Hvul_Salvador qPCR Forward	GAAAGAGAATATAAGGCAAGAATGGAG	98	qPCR
SG9931	Hvul_Salvador qPCR Reverse	TGCTGGAATTTTGGGTTTATCTTG	98	qPCR
SG9932	Hvul_LATS-like qPCR Forward	AGGATTGGACGAGAGGATTTTG	105	qPCR
SG9933	Hvul_LATS-like qPCR Reverse	CATAGCATAAACATGACCAGTGTC	105	qPCR
SG9934	Hvul_LATS qPCR Forward	CCATTACAACGTAGAAACATGCG	96	qPCR
SG9935	Hvul_LATS qPCR Reverse	GCGCATCAAAACTTCAGGAG	96	qPCR
SG10571	Hvul_YAP Fwd (exon1-intron1)	ACAACTGCTTCTGGTCTAAAGT	66	qPCR
SG10572	Hvul_YAP Rev (exon1-intron1)	TGAGGGTTTGCTGGTAACAC	66	qPCR
SG10573	Hvul_LATS1 Fwd Full length	ATGACTGAACCTAGTAAGAAAAGTTCAATC	3171	PCR/Sequencing
SG10574	Hvul_LATS1 Rev Full length	TCATACAAAAACAGGCAACTTGCTTTTATT	3171	PCR/Sequencing
SG10575	Hvul_LATS1 Rev1	GTAAATCAACTCCAGTTCGAACATTTTCTA	1111	Sequencing
SG10576	Hvul_LATS1 Fwd2	CTGGAGTTGATTTACCTACATATAATGGAT	1118	Sequencing
SG10577	Hvul_LATS1 Rev2	AGGTTTGATGTCTCTATGAATAAAACCTAA	1118	Sequencing
SG10578	Hvul_LATS1 Fwd3	CATAGAGACATCAAACCTGATAATGTTTTA	995	Sequencing
SGC921	TEAD_pET28a_subcloneFwd	GCTAGCATGGCGGAAAACTGTCGA	1367	Expression
SGC922	TEAD_pET28a_subcloneRev	GCGGCCGCGTCTCTGACTAATTTA	1367	Expression
SGD566	Hpo_partial ISH sense with SP6 promoter	ATTTAGGTGACACTATAGATT TAT TAA AAA CTC AA	619	ISH
SGD567	Hpo_partial ISH anti-sense with T7 promoter	TAA TAC GAC TCA CTA TAG GG ACG TAA ATC TTC TAT TT	619	ISH
SGD568	LATS_partial ISH sense with SP6 promoter	ATT TAG GTG ACA CTA TAG CAA GAT ACT AAT AAC TT	604	ISH
SGD569	LATS_partial ISH anti-sense with T7 promoter	TAA TAC GAC TCA CTA TAG GG AAT AAT CTT TAA TTG AAT	604	ISH
SGD570	Sav_partial ISH sense with SP6 promoter	ATT TAG GTG ACA CTA TAG AAC ATT AGA CAA TGA TA	714	ISH
SGD571	Sav_partial ISH anti-sense with T7 promoter	TAATACGACTCACTATAGGG AAT TCT ATA TTC TTC ATA	714	ISH
SGD572	TEAD_partial ISH sense with SP6 promoter	ATT TAG GTG ACA CTA TAG TAC ACA TGT CTC GAA TA	554	ISH
SGD573	TEAD_partial ISH anti-sense with T7 promoter	TAA TAC GAC TCA CTA TAG GGG TAA TAT AAT TCG AT	554	ISH

5.2 NUCLEOTIDE SEQUENCE OF HIPPO PATHWAY CORE COMPONENTS

>m.197192 | Hvul_Hpo mRNA

ATGTCTCGCAGTTTGAAGAAGTTGAGCGAAGAAAGCTTGAATCGGCCAGCAGAAGAAGTGTTTGATCTTTTG
GCAAAACTTGGTGAAGGAGCTTATGGATCTGTGTACAAAGCTATGCATAAAGAAAGTGGAGAGGTTCTGGCT
ATAAAGCAAGTTCCTGTTGATACAGACCTTCAAGAAATCATAAAAGAAATAAGCATCATGCAGCAGTGTGACA
GCCCATATGTTGTGAAGTATTTTGGAAGTTATTTCAAAAACACAGATTTATGGATTGTAATGGAATATTGTGGA
GCTGGTTCTGTATCAGACTGCATGCGTCTTCGAAATAAAACATTAACTGAAGATGAAATTGCTTGCATCTGTCG
AGACACATTAAAAGGATTAGAGTATTTACATCTGAGAAGAAAAATCCACAGAGATATTAAGGCTGGAAATATT
CTTCTAAACACAGAGGGTCATTCAAAATTAGCTGATTTTGGTGTTGCTGGTCAGTTGACTGATACAATGGCAA
AACGGAACACAGTCATTGGAACTCCATTCTGGATGGCTCCTGAAGTTATACAAGAGATAGGATATGATTGTAA
AGCTGATATTTGGTCATTGGGAATTACATTGTTGGAAATGGCAGAAGGCAAGCCACCACATGCGGATATTCAT
CCTATGAGAGCAATATTTATGATTCCTACAAAACCTCCTCCAACTTTTAAACATCCTGAAAAGTGGTCTAAAGA
TATGATTGATTTTGTTTCAAAATGTCTTGTAAAAAACCCCGATGATAGATTGTCTGCTACAGCTCTTCTCCAGCA
CCCATTTATTAAAAACTCAAAACCAGTAGAAGTGTTAGCACAAATGTTAAGTGATGCAATGCGCATTCGTGAA
GAAGAAGTTGAAAAAAATAATGGAAATGACGATGAAGATGGAATTGATGACAATGATCAGGATATCTTTGTG
ACAGCTCACACAGACACTATTATGGCAAATCAAGATATGGGGACTATGATATTGAACAATGATATTGATTCCA
ATAATGGTACAATGATTATAAATAGTGGTACAATGATTGGTCACGAAATGGATACAATGATTACAATTAACTC
TGGTACTATGATTGAAAACATGGGAACTATGGTCATTAATGATGGGGATGATTGTACAATGAAAAGTTTGGA
ATCGAGTACAGGAAAATCAACACAATATAGACCGGCATATCTTGAACATTTTGAGAAATTAGAACTTCAAAAT
CAAAGAAATATAGTAGGAAATAAAAGAGTCAATGAAAATATGCTTAAAGGGTCAGATCCAAATGTACCAGGG
AAACTTTTAGGACCAATTGATTTTGAATTTTTAAAGAATCTTTCATTTGAAGAACTTCAACAGAGAATGAGTTC
GCTTGATACGGATATGGAAAGAGAAATAGAAGATTTACGTAGACGTTACCAAGTCAAACGTCACCCTATTATT
GAAGCCATGGAAGTAAAGAAACGCAGGCAAGCAAATTTTTAA

>m.186168| Hvul_MOB mRNA

ATGAGTTTCCTGTTTGGCTCCAAAAATACTAAAACATTTAAGCCAAAAAAAAGCATACCAGAAGGTACTCATCA
GTATGATTTGTTAAAGCATGCTGAAGCTACTCTTGGTTCTGGAAACTTGCGCAATGCAGTCATGTTACCAGAG
GGTGAAGATCTTAATGAGTGGATCGCAGTGAACACAGTAGATTTTTTTAATCAAATAAACATGTTGTTTGGTA
CAATAACAGACCATTGTACTTCTGAATCATGTCCCGTTATGTCTGCAGGACCGAAGTTTGAGTATTTATGGGCA
GATGGCACATCTGTGAAAAAGCCAATAAAATGTTCTGCTCCTAAGTATATAGATTATTTAATGACATGGGTGC
AAGATCAATTGGACAATGAAGCGCTCTTTCCATCAAAAATCGGCGTCCCATTTCCTAAAAATTTTGTATCTATT
GCCAAGACTATTTTGAAAAGGTTGTTTCGTGTTTATGCACACATTTATCACCAGCATTTCCCTCAAGTTGTCAGT
TTAGGTGAAGAAGCACATCTTAATACTTCATTCAAACATTTTATATATTTTGTCCAAGAGTTTGGATTGATTGAC
AAAAGAGAGCTAGCTCCTTTGCAAGAACTTATGGATAAGTTAATTAATAAATAA

>m.3961 | Hvul_LATS1 mRNA

ATGACTGAACCTAGTAAGAAAAGTTCAATCATTTCAAGTAATCAACTGCTAAGAAATGTACCCTATAATGTTCTCAGTCATC
ATCTTCATCATGAACATCAACAGCCAAGGCACCTTGATAGTGCTCATATTCAAAGTCAATCTAAGGAATTTGAAGATTTTTT
ATCGCAAAGTTATAATATCCATGCTCTTTCTCAAAGTGCAGCTGGAGATCGCAGATCTTATCCTCGAGCATCAAAAGCTTTT
ACTCTTGAAGAAATTAGGAAAGATCTTCAACCCTTTGCATGGAAAAATGGATTTGTGGCTTCAAATTTAAGCAGCAGCAAA
AACAATATCAAAAGTAGTTCAATAAATGACTTACATCAAGCTGCTATAGAAGTTAATAATTCTGTTCAATCAGAACAACAA
AAGTTGTCACAGCTTGTTTCATATGGCTATGATGAGGCTATTGCGGCTGATGTTTTACGAAATAACAGTAACAAAAGTATT
GAAGTTCTTGTGGATATTTTAAATTCGATTATTGGATGTCACAAAATGAAAGTTCCAAGTAGGGTTTTGACTAATCATAGA
GTCCTTGGTAATAATAATCACTTTCAGCCTTCTTTTTTACAAACTTTACAAAACAAGTATGCCTCAAACAGTCGATACTATCC
TTCAAATGATTTAACTAGGAAAGGAATGCAGTATAAAGATTTATCTCCCACCAATTTTACCAATAATTTGCCATTTGAACAT
TTTTCCAATGTTCAAAGCCAATGCAAATACCCTCGAGAAACAGACCATGCTCAGCGATATCAGTCTAGTGTTTTTGTGAGT
GCTCACAATCTTTACCACCAAGATATGCCAGATGATTCTTATTTACAAAACTTGGGAGCAGAAAATTTTGGTCGGCCAAGT
GTTGTTACCATGAGGCAAAAGAAAACAGATAAGCAATTCAATCCTCAAAATCGCTGGTCAGCTGATGTTTTACAAACGTAT

GAAATTGAAAATGTTCCCAACAAACCACCGCCTCCTTATCCAGGATTGTTAAAACGACCATCTCTTCCAGACAATTTTTCAG
TAACTAATATCTCAGATGCATTAGAAAATGTTCGAACTGGAGTTGATTTACCTACATATAATGGATATACAAAAAACTCAA
ATCATTTATCTACCACACAGGGAAGAAATATTATCAATTCTCCTCATAACATACAGGCAGTGCATGTTTTTGGAACTCCAAC
AAAAATGGATTCTAACTTTTCTCCTATAGTTGAATCTGTCATTCCTCGTCGTTCGCCTCCTCCTTATTCAGCAGGTGGATCGC
AAAGATCAAGTAAATGTAATTCTCTTAATATAGAAGAATTAGAAAATAGTTTGTTGTACACATTTTCAAATTTAGATGACA
GAAATTTTAATAAGGAAGATGTAGAGTCAAACCTAGGTGACTCTTCACCAACCTTTTTATCCAATTCTGATAATACTGAGC
GTTTTGATGGTGTCAAGCGTTCTTACTCCCCTCTGCCAGAATGCTCAAACTCACCATATGTTACAATGATTGTAAGGAAAG
ATCATGAAAAAGAAAGTGCAATTGAAGAAAATGAAAATCAGCATGAAAATGCAAGTTTGCGCTTAAAGAATTACACACCA
CAAGCTTGTAAATTCTATCTAGAACAGCATTTTGAAAATTTACTTAAAAGACAAGAGCAGCGTGAGGTTAGACGCAAACA
ACTTGAAGATGAGATGTCTAGAGTTGGTCTACCATTACAAGACCAAGAGCAAATGAGAAAGTTACTTAGACAAAAAGAAT
CAAATTATATACGCTTACGAAGAGCTAAAATGGATAAAACTATGTTTACAAAGATAAAAATTATTGGAATTGGTGCATTTG
GTGAAGTTAGTCTTGTACGTAAAAATGGAACTGAGGCCTATTATGCTATGAAAACTTTAAGAAAAAGTGAAGTTGTTCGC
AGAAATCAAGTTGCTCATGTCAAGGCAGAAAGAGATATATTGGCTGAGGCTGATAATGAATGGGTAGTAAAACTTTATTA
CTCTTTTCAAGATACTAATAACTTATATTTTGTGATGGATTATGTACCTGGGGGTGATTTAATGGCTCTTTTAATTAAACGA
GGTATTTTTGAAGACAATTTAGCTCGTTTTTATATTGGAGAGTTAGTACTTGCAATTGAATCAGTTCACAAATTAGGTTTTA
TTCATAGAGACATCAAACCTGATAATGTTTTAATTGACAGATATGGTCATATTAAGTTAACTGACTTTGGCCTGTGTACTGG
TTTCCATTGGACTCATGATTCAAAATATTATCAGCCTGAGCAAGCTCTTGAAAATCATTCACGACAGTTTTCAATGGAACCT
GAGGGAGGTTGGGATTCTTTAGTTGAAGAGGGTGACTGTGGTTGTAAAAGTAGTGAACGTCTTGATAATGATTTATATGA
GCCATTACAACGTAGAAACATGCGACGGCATATGAGATGTCAGGCACATTCTTTAGTAGGCACACCAAATTATATAGCTCC
TGAAGTTTTGATGCGCATTCCATACTCACAACAATGTGATTGGTGGTCTGTTGGTGTTATTCTTTATGAAATGCTTATTGGC
CATCCTCCATTTATGGCTCGCACTCCAGCTGAGATTCAATTAAAGATTATTAATTGGAAAGAGACTTTAACTATCCGCAAAA
AACTACCTCGTCATTCAGAGAACCTTATTTTACAGTTATGCAGCGCTCCTGAAAATCGAATCGGAAGGAATGGTGCTCATG
AAATAAAAAACCATCCTTATTTTGATAATTTTAATTTTTTGTCCATACATGAGGAAAAGGCACCTTTTGTTCCTATAATCAAT
CATCCAACCGACACTTCTAACTTTGATCCAGTTCCTGAAAGTAAATCTAATGAGTTTGATATTGGGGATGTGTCCAGCCAA
GATGTAGATGACAAATTAGGTCCTGGAGCCTATGCGTTTTATGAATTCACTTTTCGTCATTTTTTTGATGATGGAGGCTTTG
CAAATCCAGTTGCAAAGAAAATTGAGCAAAATATTAAGCCAAACACAGTATCACCTGCAAAGCGTTCTGCAACAACAACA
AGCAATTCAATTAGTATACCTAATAAAGTTTCAGTACCTAATTCAGATGCTAATAAAAGCAAGTTGCCTGTTTTTGTATGA

>m.44944 |Hvul_SAV mRNA

ATGTTTAAGAAAAAAGATATTATCAAAACAATCAATTCTGACATACCCGCACGGTTTGTAAAAAAAGATGGAG
TTGCTGAAGATAATATGGTTGGAGCGATTCAAACACCAACCAGAAAGCAAAAAACTCCTATTCCCTTTCGAAA
ACTAAATTTTCCTCCAAATGATATCCCCATTTTGCGCTACCCAAAAGATAACAAAATTCCTTCGGATGAAATTTC
TGAATCATATATTTCAAGTAATTGTCATAATGTTGTTCACCAAAAAAATATTCGACATCGATTTTCTCCTTCATTT
TTGCTGTTGCGCAAGAAAAAGCACCCTTCGGTTAACAATTGTGATTTAAATGGAATTATTAAAGAAGAAGATA
TGACTGATATTGTTTGTTATAAGGATGTTGCAGAGCATGAATCATCTAAATCAATAACAATGAGTCAACTTGAT
GATACACAACTTCATGTGATGGATTTAGAAGCATGTGAAAGAGAATATAAGGCAAGAATGGAGTATATAATG
AAAAACTATCGACACCCACCACCCTATCAAAGCAAAAAGCAAGATAAACCCAAAATTCCAGCAGCTGATGCCC
CTTTAATCAGTAAATTGCTAAAGGAAACACAACTAAAAGATAATACTAGTATGAATAATTACTGGCAATCCAAT
TTAACATTAGACAATGATATTCCGCAAGTTAAAAAGAAGTTATCTGTTAGTGATAAACTTGTAAAAAGAACCA
GAGAGCAAATTAATTTAGCTCATAACAATAACAATAATAATAATTATTCTAACAATAATATCAACCAAGTTTCTT
ATTTTAATGTTGTAGACAATATGCAGAGGTTCTCTAAAGACAGAGATACAATGAGTGCAGTATATGGGGATCA
ATATAACCACAATGAGGCAACAATTAGGGGTTGCTCTTCTGTACCTAATTTATCTATACAATATGAAAACTCTC
TTGAAAGTATAATAAATGCACAAAGAGTTCAACAACCCAGAGCACACTTAGAACCTGGGGAACTTGAACTTTT
GATTTCACACTATAGAAAATCAAGTTTAGACATTTTAGCTCCTGATAGCGCAAACAACTATTTTACTACTGATA
GCGCGAACAACCATTTTACTCGTGATAGTACAAACAACTATTTTACTCCGTATCTTAAAGAATCTCCTTCTTATG
TTCCACCAAGTGCATATCTTAATGCTGAAATCCCGGATTGGTTACAAGTATATGCAAAAGCATCTCCTGATCTT
GACAAATATTTAAAGTGGGAAATGTTTCGCTATCCAGAATTAGATTGTTGGCAAACTATGCTTAAACGACTCTA
CAGAAAAGAAGTTGAACAAGTCGTACTTTGGTATGAAGAATATAGAATTGCGCTTCAGCAAGAAGTAGAGAG
ACGAAGTATTTCTTTTAAAAAAACTCATGTTTAA

>m.4630 |Hvul_YAP mRNA

ATGGATATGAATTCTACGCAACGGCAGGGTAACTTTGTTCTTCATGTGCGGCAAGACTCAGACACTGACTTGG
AACAGTTGTTTAAAAATTCAGTTTCAACCAATAAGGATATACCAAGATCTAAGCCTTTTCGTGACAGAAAGTTA
CCTGCTTCATTTTTTAGACCTCCTCCATCTCTAGAGACAGATCAAACCGCTCCAATACACACCAGAGCTCGTTCA
CTTCCTTCTAATATTGGTCAGATTGCTCAGGATCAAGTTATTTTACAGCAGCAACAACTTCAACAACAACATCCA
CAAAATAATTTTTTACTTACCCCAAGTCATCAAAGAACACAATCTTATGGTACTCTTGAATCAAATTATTTACCA
TCAGGATGTGAAATGAGAACAACTGCTTCTGGTCTAAAGTATTACATAAATCACCAAAATCAATCAACATCTTG
GCAAGATCCTCGAAAAGCACAATCCATGACAGTGTTACCAGCAAACCCTCAAAACCTTTTAATGGATGATTTG
CCAGAAGGTTGGGAACGTGCTGTTACAGCTGAAGGTGAGGTTTATTTTATTAATCATCAAACAAAAACTACAA
GTTGGTTTGATCCACGTCTGAATCGGCCTAATAATAATTTGTTGTTGGGAGGCACAAACATACAATATTACCAG
CAAGAGAAGCGTCATCGTCAACAGCAAATTCAAAACCAACTACTCGAAAGAGAGTTTTTTATTCATCAAAGAA
TGAATGGCCAGCACACTGACTCTGTACTAAACAACAATTCTTTGATAAATAACCTTGTTAGAGAGAAATATACT
GCTTATATGAATTCTAGTGTTCTTGGTAGAGGAAGCTCTGTTGATTCTGGTTTAGATGGAATGGAGTCTTATTT
AACATCTACTTCAACAGATGGGTTGAATGATATGGACACAGCTGATGTTGATCGTAATAATCAATTTGATAAA
AATACCTCAATGGAACAAGGTATTTGTTTCAATAATCGACTTCCTGAATTTTTTGATAGTTTACAAGCATCAAAT
GTTGATTTAGATATTCTTGAAGATGGTTCTGAGTTAAGTAGTGATTTAGAGGCTATCAACACTGAGGCTCTGA
ACGATGTTGACATGATTTTATCTCCAAACAATAAGCCTAATGCATATATGACTTGGTTGTAG

>m.21664| Hvul_TEAD mRNA

ATGGCGGAAAACTGTCGAGATCCGTCTACACATGTCTCGAATACTGATCCAGAACAAATGGCTTCTGATGCTG
AGGGAGTTTGGAGTCCAGACATTGAGCAAAGTTTTCAAGAGGCTTTAGCAATATATCCCCCATGTGGAAGAA
GAAAAATAATTCTTTCTGATGAAGGAAAAATGTATGGAAGGAATGAGCTTATAGCAAGATATATAAAATTACG
TACAGGAAAGACACGTTCTAGAAAACAGGTATCTAGTCATATTCAAGTTTTGGCCAGAAGAAAGGATCCTCAT
GTTAAAGACAAAGCTGGTATTCATCCTATGAATTCAATGACATCACCACAGATTGTTTCAGTTAGTGCTATACA
CTCAAAACTTGGTCTTCAAGGTGTTGATTCAGTTGCAGTTAAAAGAGAAATGAATTTAAGTCCACCTCTTGGGT
ATTGGGCACCTGGATTGCCACAACCTGGACTTCCGATTCCTCCACCACCTATTGGTTTTCCATACACTTCTGCAG
GAGCTTATTACGCAAATGCTATTACACATGCAACATCTATTTCACAATCTGGTAATATAATTCGATCTTCAAATG
CCCCACCTGGCAGCTCTTCTTCACCTACTGCTCATCACATGACAAGTTCTTTACCACATGGCTCTTCTAACCCTCA
TGTTAATCACAGTTCTTCATGGCAATCTCGAGTATCAACGACACAAATGCCTCTGCGCTTAATTGATTTTTCTGC
TTATATTGACCAACAACGACTTGAACAACCAGAAACGTACCACAAACATTTGTTTGTTCATATTGGTTCACAAA
GAAGTTTTGAAGATCCAAACTTAGAAGCCATTGATATTCGACAAATATATGATAAGTTTCCAGAAAAAAAAGG
GGGGCTTAAAGAATTTTATGATAAAGGTCCACAGCATCTATTTTTTCTTGTAAAATTTTGGGCGGATTTGAATA
CTAGCATTCCTGATGACGCTGGCTCGTTTTATGGTGTATCAACAACATATGAATCTTCTGAAAATATGACCGTC
ACTTGCTCAACAAAAGTTTGCTCATTTGGTAAACAAGTTGTGGAAAAAGTTGAAACTGAATATCCTCGCTACG
AAAATGGACGCTTTGTGTATCGCATTCAAAGGTCGCCTATGTGTGAATACATGATAAACTTTATAAGAAAACT
GAAGCATCTTCCTGAAAAGTTTATGATGAATTCAGTACTCGAAAATTTTACTATTCTTCAAGTTGTAAGTAATC
GAGACACTCAAGAAACACTTCTTTGTCTTGCTTTTGTATTTGAAATATCATCTAGCGAGCACGGAGCGCAGCAC
CACATATTTAAATTAGTCAGAGACTGA

5.3 AMINO ACID SEQUENCE OF HIPPO PATHWAY COMPONENTS

>Hvul_Hpo

MSRSLKKLSEESLNRPAEEVFDLLAKLGEGAYGSVYKAMHKESGEVLAIKQVPVDTDLQEIIKEISIMQQCDSPYVVK
YFGSYFKNTDLWIVMEYCGAGSVSDCMRLRNKTLTEDEIACICRDTLKGLEYLHLRRKIHRDIKAGNILLNTEGHSKL

ADFGVAGQLTDTMAKRNTVIGTPFWMAPEVIQEIGYDCKADIWSLGITLLEMAEGKPPHADIHPMRAIFMIPTKP
PPTFKHPEKWSKDMIDFVSKCLVKNPDDRLSATALLQHPFIKNSKPVEVLAQMLSDAMRIREEEVEKNNGNDDED
GIDDNDQDIFVTAHTDTIMANQDMGTMILNNDIDSNDGTMIINSGTMIGHEMDTMITINSGTMIENMGTMVIN
DGDDCTMKSLESSTGKSTQYRPAYLEHFEKLELQNQRNIVGNKRVNENMLKGSDPNVPGKLLGPIDFEFLKNLSFE
ELQQRMSSLDTDMEREIEDLRRRYQVKRHPIIEAMEVKKRRQANF

> Hvul_MOB

MSFLFGSKNTKTFKPKKSIPEGTHQYDLLKHAEATLGSGNLRNAVMLPEGEDLNEWIAVNTVDFFNQINMLFGTIT
DHCTSESCPVMSAGPKFEYLWADGTSVKKPIKCSAPKYIDYLMTWVQDQLDNEALFPSKIGVPFPKNFVSIAKTILK
RLFRVYAHIYHQHFPQVVSLGEEAHLNTSFKHFIYFVQEFGLIDKRELAPLQELMDKLINK

>Hvul_LATS

MTEPSKKSSIISSNQLLRNVPYNVLSHHLHHEHQQPRHLDSAHIQSQSKEFEDFLSQSYNIHALSQSAAGDRRSYPR
ASKAFTLEEIRKDLQPFAWKNGFVASNLSSSKNNIKSSSINDLHQAAIEVNNSVQSEQQKLSQLVSYGYDEAIAADVL
RNNSNKSIEVLVDILNSIIGCHKMKVPSRVLTNHRVLGNNNHFQPSFLQTLQNKYASNSRYYPSNDLTRKGMQYKD
LSPTNFTNNLPFEHFSNVQSQCKYPRETDHAQRYQSSVFVSAHNLYHQDMPDDSYLQNLGAENFGRPSVVTMRQ
KKTDKQFNPQNRWSADVLQTYEIENVPNKPPPPYPGLLKRPSLPDNFSVTNISDALENVRTGVDLPTYNGYTKNSN
HLSTTQGRNIINSPHNIQAVHVFGTPTKMDSNFSPIVESVIPRRSPPPYSAGGSQRSSKCNSLNIEELENSLLYTFSNL
DDRNFNKEDVESNLGDSSPTFLSNSDNTERFDGVKRSYSPLPECSNSPYVTMIVRKDHEKESAIEENENQHENASLR
LKNYTPQACKFYLEQHFENLLKRQEQREVRRKQLEDEMSRVGLPLQDQEQMRKLLRQKESNYIRLRRAKMDKTM
FTKIKIIGIGAFGEVSLVRKNGTEAYYAMKTLRKSEVVRRNQVAHVKAERDILAEADNEWVVKLYYSFQDTNNLYFV
MDYVPGGDLMALLIKRGIFEDNLARFYIGELVLAIESVHKLGFIHRDIKPDNVLIDRYGHIKLTDFGLCTGFHWTHDS
KYYQPEQALENHSRQFSMEPEGGWDSLVEEGDCGCKSSERLDNDLYEPLQRRNMRRHMRCQAHSLVGTPNYIA
PEVLMRIPYSQQCDWWSVGVILYEMLIGHPPFMARTPAEIQLKIINWKETLTIRKKLPRHSENLILQLCSAPENRIGR
NGAHEIKNHPYFDNFNFLSIHEEKAPFVPIINHPTDTSNFDPVPESKSNEFDIGDVSSQDVDDKLGPGAYAFYEFTFR
HFFDDGGFANPVAKKIEQNIKPNTVSPAKRSATTTSNSISIPNKVSVPNSDANKSKLPVFV

>Hvul_SAV

MFKKKDIIKTINSDIPARFVKKDGVAEDNMVGAIQTPTRKQKTPIPFRKLNFPPNDIPILRYPKDNKIPSDEISESYISS
NCHNVVHQKNIRHRFSPSFLLLRKKKHPSVNNCDLNGIIKEEDMTDIVCYKDVAEHESSKSITMSQLDDTQLHVMD
LEACEREYKARMEYIMKNYRHPPPYQSKKQDKPKIPAADAPLISKLLKETQLKDNTSMNNYWQSNLTLDNDIPQVK
KKLSVSDKLVKRTREQINLAHNNNNNNNYSNNNINQVSYFNVVDNMQRFSKDRDTMSAVYGDQYNHNEATIRG
CSSVPNLSIQYENSLESIINAQRVQQPRAHLEPGELELLISHYRKSSLDILAPDSANNYFTTDSANNHFTRDSTNNYFT
PYLKESPSYVPPSAYLNAEIPDWLQVYAKASPDLDKYLKWEMFRYPELDCWQTMLKRLYRKEVEQVVLWYEEYRIA
LQQEVERRSISFKKTHV

>Hvul_YAP

MDMNSTQRQGNFVLHVRQDSDTDLEQLFKNSVSTNKDIPRSKPFRDRKLPASFFRPPPSLETDQTAPIHTRARSLP
SNIGQIAQDQVILQQQQLQQQHPQNNFLLTPSHQRTQSYGTLESNYLPSGCEMRTTASGLKYYINHQNQSTSWQ
DPRKAQSMTVLPANPQNLLMDDLPEGWERAVTAEGEVYFINHQTKTTSWFDPRLNRPNNNLLLGGTNIQYYQQ
EKRHRQQQIQNQLLEREFFIHQRMNGQHTDSVLNNNSLINNLVREKYTAYMNSSVLGRGSSVDSGLDGMESYLTS
TSTDGLNDMDTADVDRNNQFDKNTSMEQGICFNNRLPEFFDSLQASNVDLDILEDGSELSSDLEAINTEALNDVD
MILSPNNKPNAYMTWL

>Hvul_TEAD

MAENCRDPSTHVSNTDPEQMASDAEGVWSPDIEQSFQEALAIYPPCGRRKIILSDEGKMYGRNELIARYIKLRTGK
TRSRKQVSSHIQVLARRKDPHVKDKAGIHPMNSMTSPQIVSVSAIHSKLGLQGVDSVAVKREMNLSPPLGYWAPG

LPQPGLPIPPPPIGFPYTSAGAYYANAITHATSISQSGNIIRSSNAPPGSSSSPTAHHMTSSLPHGSSNPHVNHSSSW
QSRVSTTQMPLRLIDFSAYIDQQRLEQPETYHKHLFVHIGSQRSFEDPNLEAIDIRQIYDKFPEKKGGLKEFYDKGPQ
HLFFLVKFWADLNTSIPDDAGSFYGVSTTYESSENMTVTCSTKVCSFGKQVVEKVETEYPRYENGRFVYRIQRSPMC
EYMINFIRKLKHLPEKFMMNSVLENFTILQVVSNRDTQETLLCLAFVFEISSSEHGAQHHIFKLVRD

5.4 SUMMARY OF RAW DATA PRODUCED FROM ILLUMINA RNA SEQUENCING

5.4.1 Raw data statistics

The total number of bases, reads, GC (%), Q20 (%), and Q30 (%) are calculated for the 16 samples.For example, in D0_A, 50,055,544 reads are produced, and total read bases are 7.6G bp. The GC content (%) is 37.477% and Q30 is 95.269%.

Table 5.2: Raw data Stats

Sample ID	Total read bases (bp)	Total reads	GC(%)	AT(%)	Q20(%)	Q30(%)
D0_A	7,558,387,144	50,055,544	37.477	62.52	98.530	95.269
D0_B	7,554,244,610	50,028,110	37.433	62.57	98.461	95.077
V0_A	6,187,809,974	40,978,874	37.907	62.09	98.408	95.042
V0_B	6,466,805,426	42,826,526	38.371	61.63	98.308	94.927
D2_A	6,490,129,792	42,980,992	37.933	62.07	98.335	94.937
D2_B	8,266,392,924	54,744,324	39.318	60.68	98.175	94.685
V2_A	6,529,259,630	43,240,130	38.132	61.87	98.486	95.251
V2_B	8,253,888,010	54,661,510	39.710	60.29	97.848	94.197
D8_A	6,879,628,252	45,560,452	37.800	62.2	98.544	95.317
D8_B	7,011,746,910	46,435,410	37.881	62.12	98.453	95.182
V8_A	6,686,713,370	44,282,870	37.978	62.02	98.287	94.700
V8_B	6,076,829,806	40,243,906	37.929	62.07	98.419	95.147
D24_A	8,359,712,132	55,362,332	37.869	62.13	98.239	94.667
D24_B	6,248,051,122	41,377,822	38.229	61.77	98.252	94.858
V24_A	6,353,637,268	42,077,068	38.415	61.59	98.565	95.463
V24_B	6,283,855,034	41,614,934	38.285	61.72	98.251	94.780

- Sample ID : Sample name. D- DMSO, V-Vp, 0- 0 hpa, 2- 2 hps, 8- 8 hpa, 24- 24 hpa, A/B- Biological Replicate A or Biological Replicate B.
- Total read bases : Total number of bases sequenced.
- Total reads : Total number of reads. For Illumina paired-end sequencing, this value refers to the sum of read 1 and read 2.
- GC(%) : GC content.
- AT(%) : AT content.
- Q20(%) : Ratio of bases that have phred quality score of over 20.
- Q30(%) : Ratio of bases that have phred quality score of over 30.

5.4.2 Total Read Bases

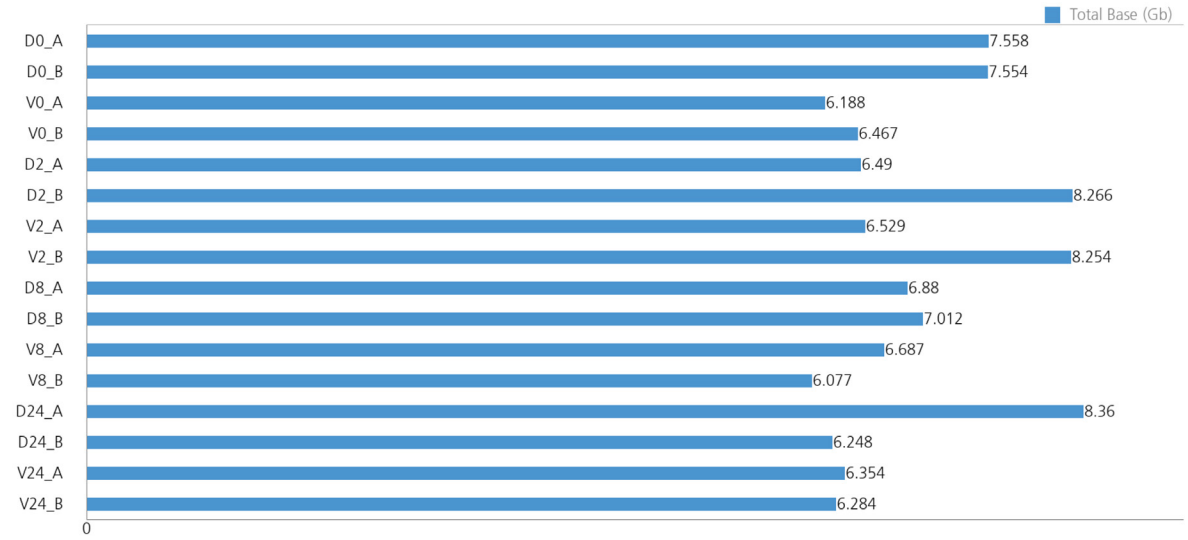

Figure 5.1: Throughput of Raw data

5.4.3 Total Reads

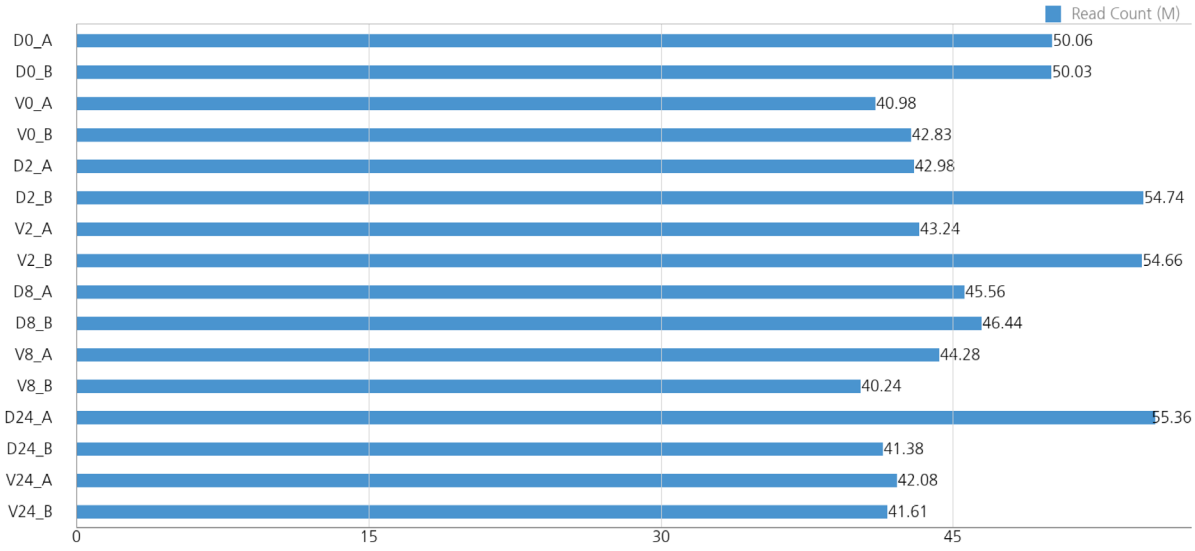

Figure 5.2: Total read count of Raw data

5.4.4 GC/AT Content

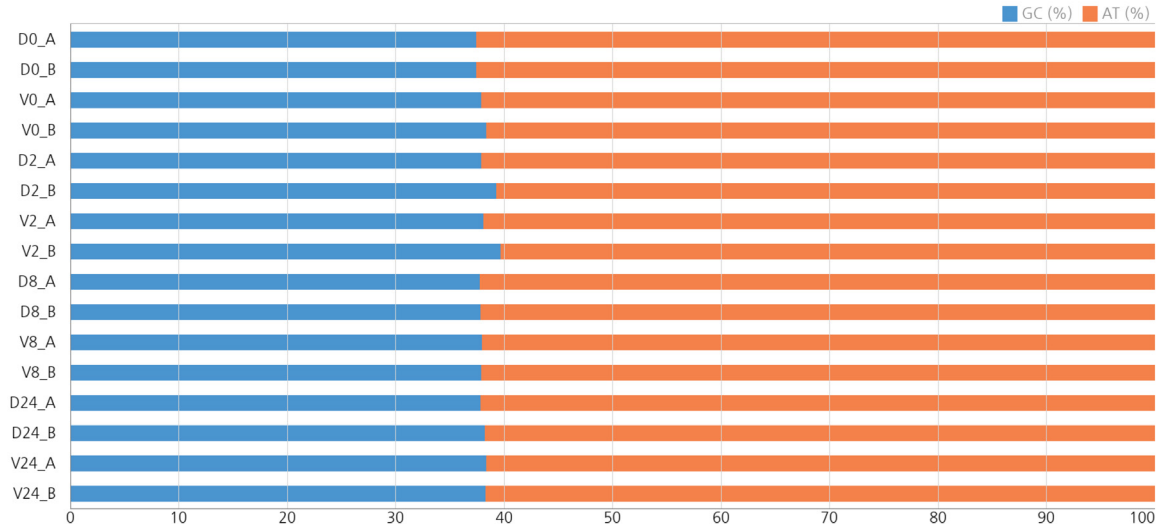

Figure 5.3: GC/AT Content of Raw data

5.4.5 Q20/Q30 (%)

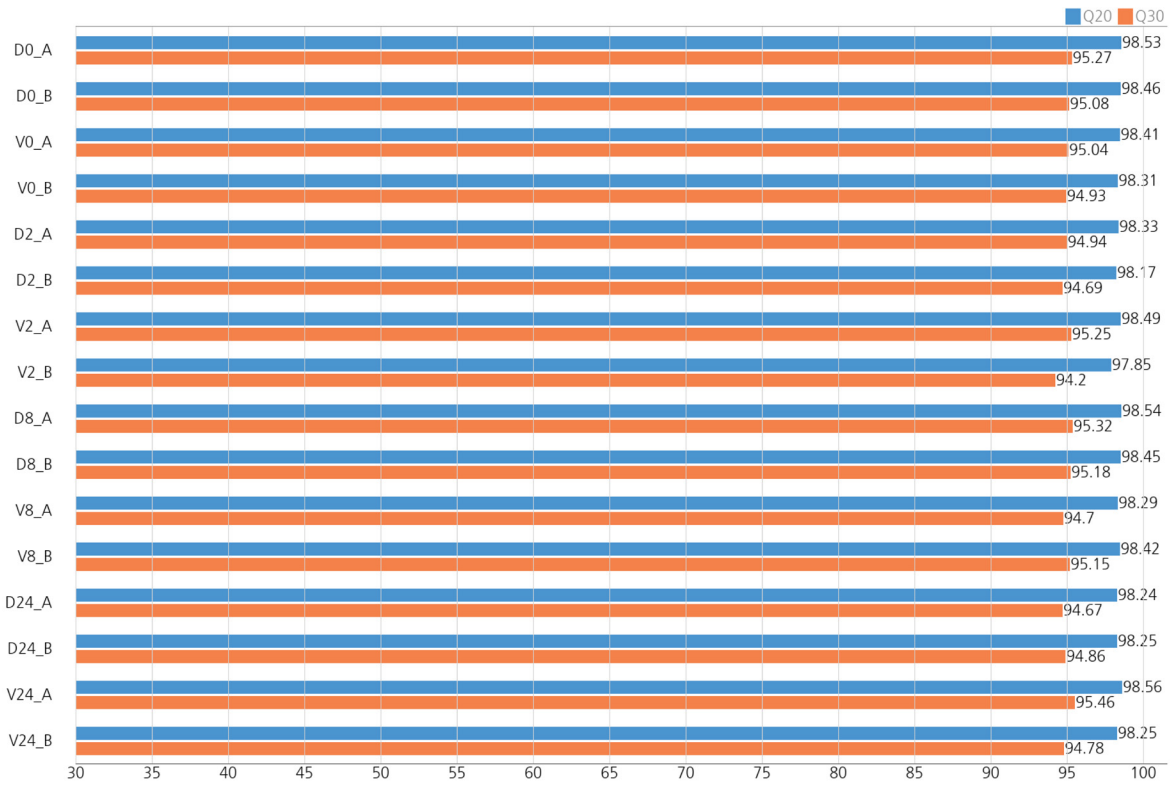

Figure 5.4: Q20/Q30 scores of Raw data